Title
Regulation of Transcriptional Interference by the Swi/Snf Complex

Author
Morse, Kaitlin

Publication Date
2023

Peer reviewed|Thesis/dissertation

Regulation of Transcriptional Interference by the Swi/Snf Complex

By

Kaitlin Morse

Dissertation submitted in partial satisfaction of the

requirements for the degree of

Doctor of Philosophy

in

Molecular and Cell Biology

in the

Graduate Division

of the

University of California, Berkeley

Committee in charge:

Associate Professor Elçin Ünal, Chair
Professor Gary Karpen
Assistant Professor James Nuñez
Professor Arash Komeili

Summer 2023

Regulation of Transcriptional Interference by the Swi/Snf Complex

Kaitlin Morse

Abstract

Regulation of Transcriptional Interference by the Swi/Snf Complex

by

Kaitlin Morse

Doctor of Philosophy in Molecular and Cell Biology

University of California, Berkeley

Associate Professor Elçin Ünal, Chair

Alternative transcription start sites can affect transcript isoform diversity and translation levels. In a recently described form of gene regulation, coordinated transcriptional and translational interference results in transcript isoform-dependent changes in protein expression. Specifically, a long undecoded transcript isoform (LUTI) is transcribed from a gene-distal promoter, interfering with expression of the gene-proximal promoter. Though it contains the coding sequence of the downstream gene, translation of the LUTI is restricted by uORFs present in its 5′ leader sequence. While transcriptional and chromatin features associated with LUTI expression have been described, the mechanism underlying LUTI-based transcriptional interference is not well understood. Using an unbiased genetic approach followed by integrated genomic analysis, we uncovered that the Swi/Snf chromatin remodeling complex is required for co-transcriptional nucleosome remodeling that leads to LUTI-based repression. We identified 12 genes with tandem promoters that rely on Swi/Snf function for transcriptional interference during protein folding stress, including LUTI-regulated genes.

We further explored Swi/Snf repressive activity by performing kinetic and molecular assays for the LUTI-regulated gene histidine triad nucleotide-binding 1 (*HNT1*), revealing that Swi/Snf recruitment and repressive function at the *HNT1* locus depends on transcription initiation and elongation of $HNT1^{LUTI}$. This prompted our further investigation into a role for Swi/Snf in transcription elongation, leading to the finding that Swi/Snf performs co-transcriptional nucleosome remodeling at its target loci independently of its canonical role in transcriptional activation. We conclude this co-transcriptional remodeling function by Swi/Snf may function to promote transcription elongation at canonical gene targets but serves a repressive function at target genes with tandem promoters and transcriptional readthrough. To our knowledge, this is the first evidence of Swi/Snf's direct involvement in gene repression via a *cis* transcriptional interference mechanism.

To Walter

Contents

List of Figures

List of Tables

Acknowledgements

I sincerely thank my advisor, Elçin Ünal, for her superb mentorship throughout my Ph.D. In addition to her attentive guidance with this project, she has led by example as a thoughtful and confident scientist, passing on these invaluable qualities throughout my training. Her excitement for science and nonstop determination has often inspired me to reach beyond what I thought I was capable of, even during challenging times in graduate school and life. I feel incredibly lucky to have the support of a mentor who truly invests in her students, from building a solid thesis project to preparing for next steps after graduation.

I also thank Gloria Brar for her advice and mentorship. Her expertise in gene regulation and the unfolded protein response helped immensely in the shaping and execution of my project. Furthermore, I could not have prepared and submitted the final manuscript for publication in Elçin's absence on maternity leave without Gloria's help and this is something I am especially thankful for. I would also like to thank Jeremy Thorner and Doug Koshland for their helpful advice and sincere interest in my project.

I am incredibly grateful to all members of the Brar and Ünal labs who I have been fortunate to befriend and learn from over the years. In particular, I could always rely on advice from my fellow gene regulation enthusiasts: Tina, Andrea, Amanda, and Emily. I would like to give a special mention to my best friend and bay mate Amanda Su. Amanda is both a wonderful person and inspiring scientist. She is extremely humble, despite overcoming more challenges than anyone I have known and maintaining her fantastic sense of humor all the while. I will miss having frequent opportunities to go for hikes, boba dates, and comedy show excursions, though I know we will always be friends.

I would like to thank the members of my thesis committee Gary Karpen, Arash Komeili, and James Nuñez for their thoughtful advice. They have always encouraged a high standard of work, demonstrated a strong interest in the project, and offered outside perspectives that have been pivotal to our investigations. Thanks also to Minghao Chia and Cal Milano for their technical support with sequencing projects.

Finally, I want to thank my family, who have always supported my ambitions and celebrated victories, big and small. My parents made sacrifices and worked hard to ensure I had this opportunity, for which I am eternally grateful. Last but not least, thanks to my supportive, hard-working, hilarious, and loving husband Walter for taking the leap six years ago to move across the country for my graduate program and being my rock every day since. I love you all.

Chapter 1 – Introduction

1.1 Eukaryotic gene regulation

Cells respond to internal and external signals by regulating gene expression. Gene regulation is essential for maintaining cellular homeostasis, enabling adaptation to stress, and controlling cell identity and differentiation. During development, cellular differentiation is the process cells undergo to acquire specialized functions. Even the simple, unicellular eukaryote *Saccharomyces cerevisiae* undergoes differentiation during its sexual life cycle to convert a diploid mother cell to four haploid gametes. In more complex organisms, differentiation is required to form specialized tissues and organs. Gene regulatory networks orchestrate these processes by activating or repressing specific sets of genes. For instance, in embryonic development, the activation of master regulatory homeobox (Hox) genes determines body segment identity along the anterior-posterior axis (Mallo and Alonso, 2013). Similarly, in adult tissues, the expression of tissue-specific genes is tightly regulated to maintain cell identity and function. As such, dysregulation of gene expression programs can lead to developmental disease or cancer.

In addition to development, gene regulation is critical for cells to properly respond to external stressors. A notable example is the activation of heat shock genes in response to elevated temperatures. This highly conserved stress response leads to increased expression of chaperones, which protect cells from protein misfolding and aggregation (Morimoto, 1998), and simultaneous downregulation of genes involved in proliferation (Lindquist, 1986). This balance of up- and down-regulation of distinct sets of genes helps redirect cellular resources towards stress mitigation. Understanding the diverse mechanisms of gene regulation and their impact on cellular function provides insights into both normal development and disease pathogenesis.

Gene expression has long been studied though the framework of the central dogma of biology, which describes the flow of genetic information from DNA to RNA to protein. In its simplest form, this encompasses the processes of transcription and translation, which are fundamental to the survival of all living organisms. However, as this chapter will explore, additional layers of gene regulation further complicate the path from DNA to protein. For example, in metazoans alternative splicing of transcripts is a common route to differentially regulate protein function or localization among different cell types (Marasco and Kornblihtt, 2023). Additionally, alternative transcription and translation events are prevalent in metazoans and simple eukaryotes such as yeast, which can contribute to greater diversity in protein products for a given gene or affect transcript and protein stability (Arribere and Gilbert, 2013; Chia et al., 2021; Eisenberg et al., 2020; Wang et al., 2016; Morris and Geballe, 2000). In this chapter, I will focus primarily on the first level of gene regulation, transcription, with an emphasis on noncanonical and cryptic transcription.

General mechanisms in eukaryotic transcription

Gene expression is initiated by transcription factors (TFs) and co-activators, which associate with promoters and enhancers to determine the timing, location, and amount of mRNA transcribed by RNA polymerase II (Pol II). Eukaryotic transcription begins with assembly of the preinitiation complex (PIC), comprised of Pol II and general transcription factors (GTFs), at the core promoter region of genes (Kornberg, 2007; Petrenko et al., 2019). While GTFs are sufficient for promoter recognition, regulated transcription and interaction between enhancers and promoters requires the Mediator complex. Comprised of 20 subunits in yeast, Mediator can act as both a coactivator and corepressor through its role in enhancer/promoter communication (Kornberg, 2007). Access for this general transcriptional machinery at promoters is regulated by ATP-dependent chromatin remodeling enzymes and general regulatory factors (GRFs) (Rando and Winston, 2012), which control nucleosome occupancy at transcription start sites (TSSs). Regulation of transcription initiation becomes even more complex through the activities of sequence-specific TFs, which regulate PIC formation at distinct promoters based on their abundance, localization, and function.

A classic example highlighting the interplay between TFs, Mediator, and chromatin remodelers to regulate transcription initiation is at *GAL* gene promoters in yeast. In the absence of galactose, the Gal4 TF is sequestered in the cytoplasm by the protein Gal80 (Traven et al., 2006). However, when galactose is present, it binds to Gal4, causing a conformational change that disrupts the Gal4-Gal80 interaction. This releases Gal4, allowing it to enter the nucleus and activate *GAL* gene expression. Upon activation, Gal4 binds to upstream activation sequences (UAS) in the *GAL* gene promoters, recruiting coactivators such as Mediator and the SAGA complex (Larschan and Winston, 2001). SAGA acetylates histones, resulting in recruitment of the Swi/Snf complex to *GAL* promoters where it increases promoter accessibility through nucleosome remodeling (Traven et al., 2006; Yudkovsky et al., 1999). The Mediator complex then acts as a bridge between Gal4 and the general transcription machinery, facilitating transcription initiation.

Shortly after initiation, transcription undergoes an unstable transition phase known as promoter escape. During promoter escape, Pol II pauses after synthesizing a short nascent RNA that hybridizes with the DNA template (Core and Adelman, 2019). At this point, Pol II is still associated with GTFs, resulting in the formation of an energetically unfavorable extended transcription bubble. In successful promoter escape, bubble collapse results in re-annealing of the DNA-DNA hybrid and pushes Pol II forward, disrupting Pol II/GTF contacts and promoting transcription elongation (Core and Adelman, 2019). Interestingly, most promoters in yeast are bi-directional, though divergent transcripts arising from Pol II escape occurring in the “wrong” direction are rapidly degraded by Nrd1-exosome-TRAMP complexes (Neil et al., 2009).

During elongation, Pol II is subject to dynamic post-translational modifications at the C-terminal domain on its largest subunit Rpb1 (Buratowski, 2009). Early in the elongation phase, serine 5 of the CTD (Ser5P) is phosphorylated by TFIIH, which further aids in promoter escape by disrupting Pol II/Mediator interactions (Buratowski, 2009; Core

and Adelman, 2019). Additionally, Ser5P recruits mRNA capping machinery and the Set1 histone 3 lysine 4 (H3K4) methyltransferase complex (also known as COMPASS, yeast homolog of the mammalian SET1 and MLL complexes) (Buratowski, 2009). In later stages of elongation, phosphorylation on serine 2 of the Pol II CTD (Ser2P) recruits the histone 3 lysine 36 methyltransferase Set2 (SETD2 in mammals) (Buratowski, 2009). CTD phosphorylation and these downstream histone methylation pathways recruit several other factors that aid in transcription elongation and prevent cryptic transcription (further details below). When Pol II backtracks during elongation, either due to nucleosome barriers or DNA secondary structure, the elongation factor TFIIS recognizes arrested Pol II and resolves the transcriptional block by stimulating cleavage of the nascent transcript at the 3′ end, restoring proper alignment of the nascent 3′ end within the Pol II active site (Core and Adelman, 2019; Malagon et al., 2004).

CTD Ser2P is also linked to transcriptional termination. Pcf11, a polyadenylation factor, preferentially binds Ser2P and promotes recruitment of polyadenylation and termination machinery (Buratowski, 2009). As Pol II transcribes past the polyadenylation signal, termination machinery stimulates cleavage and release of the mRNA. This cleavage event exposes a free 5′ RNA end still attached to Pol II, which is then degraded by the Rat1 (mammalian Xrn2) exonuclease, facilitating release of Pol II from the template (Kim et al., 2004).

These conserved stages of transcription are critical for expression of protein-coding genes. Interestingly, recent studies highlighting the pervasiveness of transcription outside of canonical genes demonstrate how the act of transcription itself can influence expression of genes within a transcriptional neighborhood (Kim et al., 2016; Nevers et al., 2018; Shuman, 2020). An estimated 70-90% of the human genome is transcribed into noncoding RNAs (ncRNAs) (Villegas and Zaphiropoulos, 2015). While many instances of ncRNA transcription likely represent transcriptional noise, certain long non-coding RNAs (lncRNAs) and antisense RNAs (asRNAs) have been linked to diverse cellular functions including maintenance of embryonic pluripotency, epigenetic imprinting, and cellular differentiation (Villegas and Zaphiropoulos, 2015).

lncRNAs are often transcribed and processed using mechanisms identical to those used for protein-coding mRNAs (Villegas and Zaphiropoulos, 2015). As such, general transcriptional mechanisms are thought be co-opted during lncRNA expression to influence expression of neighboring genes. In particular, epigenetic changes have been implicated in lncRNA- and asRNA-mediated silencing of gene expression in a phenomenon known as transcriptional interference (Batista and Chang, 2013; Hainer et al., 2011; Kim et al., 2016; Villegas and Zaphiropoulos, 2015; Werven et al., 2012). Below, I discuss forms of epigenetic regulation for both canonical and alternative transcription through two prevalent routes: histone modification and nucleosome positioning.

Regulation of transcription through chromatin modifications

In eukaryotes, nuclear DNA is organized into chromatin, consisting of interspaced compact structures called nucleosomes. A nucleosome consists of ~150 base pairs (bp)

of DNA wrapped around a histone octamer, which contains two of each subunits for H2A, H2B, H3, and H4. While organization of DNA into nucleosomes is important for efficient packaging of genetic material during cellular division, chromatin organization also plays a pivotal role in regulation of transcription. Post-translational modifications of histone tails, including acetylation, methylation, phosphorylation, and ubiquitination, regulate gene expression by modulating chromatin structure and accessibility as well as recruitment of *trans* regulatory factors such as TFs and chromatin remodeling enzymes. Specific histone modifications are associated with distinct transcriptional states, which may differ according to species-, cellular-, or chromatin-specific contexts. Below, I discuss two modifications in depth, acetylation and methylation, that are related to the findings presented in Chapters 2 and 3.

Histone acetylation:

Acetylation of histone lysine residues at promoter regions is generally associated with gene activation, while deacetylation is linked to gene repression. Histone acetyltransferases (HATs) catalyze the addition of acetyl groups, while histone deacetylases (HDACs) remove them, dynamically regulating transcriptional activity (Verdone, 2006). The conserved HAT Gcn5, which is a component of the SAGA complex, plays a central role in gene activation by acetylating histones at specific promoters. For example, Gcn5-mediated acetylation of histone H3 at lysine 9 (H3K9ac) in yeast *GAL* gene promoters induces their transcriptional activation (Rando and Winston, 2012). Conversely, histone deacetylation mediated by the Rpd3S HDAC leads to gene repression (Kim et al., 2016).

The molecular basis of transcriptional regulation through histone acetylation lies within the negatively-charged DNA backbone, which has a higher affinity for positively charged lysine residues. Acetylation of histone lysine residues neutralizes the charge on the histone tail and relaxes the DNA-histone interaction, making the DNA more accessible to transcriptional machinery (Verdone, 2006). In contrast, deacetylated histones more tightly wrap DNA rendering it inaccessible. In addition to regulating DNA/histone contact, histone acetylation status can influence the recruitment of nucleosome remodeling enzymes to further regulate transcription. For example, Swi/Snf family remodelers (see below) are recruited to acetylated histones through their bromodomains (Hassan et al., 2006). It is thought that recruitment by Swi/Snf or the related RSC remodeler to acetylated histones at promoter regions leads to gene activation by increasing accessibility at the nucleosome depleted region (NDR) through nucleosome remodeling activity (Bai and Morozov, 2010; Chandy et al., 2006).

Histone methylation:

Methylation of histone lysine residues is associated with gene activation or repression in a manner dependent on histone residue, degree of methylation, or species-specific function. During transcription elongation, Pol II CTD phosphorylation recruits histone methyltransferases (HMTs) (Buratowski, 2009). Specific histone methylation

marks regulate transcription through recruitment of HDACs, histone chaperones, and nucleosome remodeling enzymes, which play pivotal roles in transcription elongation.

In yeast and human cells, histone H3 lysine 36 (H3K36) methylation is associated with repression of cryptic transcription (Carrozza et al., 2005; Kim et al., 2016), a phenomenon in which promoters within transcribed regions become active. The Set2 methyltransferase (SETD2 in mammals) catalyzes the trimethylation of H3K36 (H3K36me3), predominantly enriched within actively transcribed gene bodies (Rando and Winston, 2012). The H3K36me3 modification recruits regulatory factors involved in transcription elongation and RNA processing, which in turn promote efficient transcription elongation and restrict aberrant transcription initiation within gene bodies (Carrozza et al., 2005; Gopalakrishnan et al., 2019). In particular, the H3K36me3 modification recruits the Rpd3S HDAC, which aids in suppressing spurious transcription initiation for genes with cryptic intragenic promoters, such as *STE11* and *FLO8* in yeast (Carrozza et al., 2005).

While many histone modifications and their associated functions are conserved across species, such as the H3K36me3 pathway, there are notable differences between yeast and human cells. For example, in yeast, H3K4me2 by COMPASS , like H3K36me3, is primarily associated with repressing cryptic transcription through HDAC recruitment at 5′ ends of transcribed regions (Kim et al., 2012). However, H3K4me3 by COMPASS in yeast is a mark correlated with histone acetylation at active promoters (Cruz et al., 2018). In humans, H3K4 methylation is exclusively associated with gene activation, with mono-, di-, and trimethylation at H3K4 being found at promoters and enhancers of actively transcribed genes (Hyun et al., 2017).

Interestingly, recent studies have highlighted the critical role of long non-coding RNAs (lncRNAs) in regulating histone methylation to influence transcription of neighboring genes (Kim et al., 2016; Moretto et al., 2018). For instance, the lncRNA Xist interacts with the polycomb repressive complex 2 (PRC2) in humans, leading to histone methylation and transcriptional repression across the entire X chromosome in a process known as X inactivation (Rinn and Chang, 2012). While Xist/PRC2 mediated silencing presents a dramatic example of long-range gene regulation by a lncRNA, lncRNAs have also been known to influence histone methylation to regulate gene expression on a more local scale. In yeast, for instance, a gene-distal promoter drives the expression of an intergenic non-coding transcription *IRT1* which results in downstream enrichment of H3K36me3 and repression of the gene *IME1* which regulates entry to meiosis (Moretto et al., 2018; Werven et al., 2012). These examples highlight that functions of histone methylation pathways extend beyond preventing transcription from cryptic promoters within coding regions and can also play regulatory roles at canonical gene promoters.

Nucleosome Positioning:

As mentioned above, histone acetylation at gene promoters results in recruitment of ATP-dependent nucleosome remodeling enzymes. Eukaryotic promoters consist of a nucleosome free region (NDR) flanked by two well-positioned nucleosomes: the -1 nucleosome upstream and +1 nucleosome downstream relative to the TSS. In yeast, RSC

and Swi/Snf remodel promoter-adjacent nucleosomes to facilitate transcriptional activation by creating an accessible NDR for TFs and the PIC to dock (Kubik et al., 2018; Rawal et al., 2018). While RSC associates with many more “housekeeping” genes during unstressed conditions compared to Swi/Snf, Swi/Snf specializes in regulating inducible gene expression (Rando and Winston, 2012). Humans, however, lack RSC complexes and instead have multiple Swi/Snf complexes with diverse functions that depend on tissue-specific subunit composition (Mathur and Roberts, 2018).

Swi/Snf and RSC are thought to primarily reposition nucleosomes through DNA translocation and nucleosome sliding along the DNA, although several studies have provided evidence supporting nucleosome eviction activity by these remodelers as well (Dechassa et al., 2010; Kassabov et al., 2003; Rawal et al., 2018; Schwabish and Struhl, 2007). The promoter-opening activity by RSC and Swi/Snf can be opposed by repressive ATP-dependent remodelers Ino80 and Isw2, which push the +1 nucleosome into the NDR (Kubik et al., 2019). As such, the interplay between these opposing types of remodelers is critical for proper TSS selection (Kubik et al., 2019).

During transcription elongation, several other ATP-dependent nucleosome remodelers and histone chaperones are recruited by Pol II CTD phosphorylation and histone methylation pathways. In addition to recruiting the Rpd3S HDAC, H3K36 methylation recruits the Chd1 and Isw1 nucleosome remodelers, which stabilize histones and regulate nucleosome spacing within the gene bodies (Hennig et al., 2012; Smolle et al., 2012). Activity by these remodelers has also been linked to repression of intragenic cryptic transcription (Hennig et al., 2012; Rando and Winston, 2012).

In addition to ATPase remodeling enzymes, histone chaperones play a role in chromatin structure and resetting during transcription elongation. The FACT complex partially disassembles the nucleosome during transcription by removing a single H2A/H2B dimer, allowing efficient Pol II traversal through the remaining histone hexamer (Kireeva et al., 2002; Venkatesh and Workman, 2015). Notably, exchange of H3 or H4 subunits is rare, and the H3K36me3-dependent stabilization of H3/H4 tetramers is thought to be important for maintaining chromatin architecture within gene bodies and prevention of spurious transcription (Smolle et al., 2012; Venkatesh and Workman, 2015).

Another histone exchange factor, the Paf1 complex, has been shown to regulate transcriptional interference of the *SER3* promoter in yeast during serine replete conditions. Similar to the case or *IRT1/IME1*, high serine levels trigger transcriptional activation of the upstream intergenic transcript *SRG1* (Laprade et al., 2004). *SRG1* transcription results in co-transcriptional deposition of nucleosomes by Paf1 and FACT over the *SER3* promoter and silencing of *SER3* expression (Hainer et al., 2011; Pruneski et al., 2011). Interestingly, this transcriptional interference pathway does not rely on histone modifications, exemplifying the locus specificity among lncRNA-based silencing pathways (Pruneski et al., 2011).

1.2 LUTI-based gene regulation reveals complexity in the mRNA-to-protein relationship

According to classical models of gene regulation, transcript levels directly correlate with protein synthesis. However, the high prevalence of non-coding transcription and variation in translation efficiency among transcript isoforms has unveiled deeper complexity in the mRNA-to-protein relationship (Brar et al., 2012; Chia et al., 2021; Hangauer et al., 2013; Jorgensen et al., 2020; Pelechano et al., 2013; Wang et al., 2016). For example, upstream open reading frame (uORF)-mediated translational regulation affects protein translation efficiency in organisms ranging from yeast to humans. uORFs are short open reading frames, generally not thought to encode functional peptides, encoded within 5′ leader sequences of certain transcripts.

Canonical translation initiation occurs when the scanning ribosomal pre-initiation complex, comprised of the small 40S ribosomal subunit and initiation factors, recognizes the first AUG codon within a transcript (Jackson et al., 2010). The large 60S subunit then joins the 40S to form a fully functional ribosome and initiation factors dissociate (Jackson et al., 2010). Upon termination at an in-frame stop codon, the ribosome dissociates from the mRNA and is recycled to begin a new initiation phase (Jackson et al., 2010; Morris and Geballe, 2000). Thus, accepted models for uORF-mediated translational repression propose that translation of uORFs prevents the ribosome from re-initiating at the downstream coding sequence (CDS) (Morris and Geballe, 2000; Silva et al., 2019). However, some studies have shown that reinitiation downstream at the CDS can occur in a manner that depends on nutrient availability and distance between the uORF and the CDS (Morris and Geballe, 2000).

Given that uORFs are encoded within the 5′ leader sequence of an mRNA, their impact on gene expression can be controlled through alternative transcription. Recently, an unconventional form of gene repression involving uORF-containing alternative transcripts was discovered in yeast. For genes regulated in this manner, transcription initiation from a gene-distal promoter drives expression of a 5′ extended mRNA that contains the entire CDS of the downstream gene (J. Chen et al., 2017; Cheng et al., 2018). However, uORF translation within the 5′ leader of the extended mRNA restricts translation of the CDS (Figure 1.1). Based on these features, the distal mRNA isoform has been termed the long undecoded transcript isoform (LUTI).

In addition to its translational repression, LUTI transcription often interferes in *cis* with transcription of the CDS-proximal promoter, which controls expression of the coding mRNA isoform (Chia et al., 2017; Tresenrider et al., 2021). While transcriptional interference and uORF-mediated repression have each previously been shown to regulate gene expression (Morris and Geballe, 2000; Shuman, 2020), LUTI-based regulation layers these two repressive mechanisms to finely and temporally tune protein synthesis. This coordinated transcriptional and translational interference by the LUTI reduces the pools of the coding mRNA in the cell by upregulating a coding-deficient mRNA isoform, ultimately resulting in decreased protein synthesis for the affected gene.

Thus, LUTIs help explain cases in which mRNA and protein levels are poorly correlated (Cheng et al., 2018).

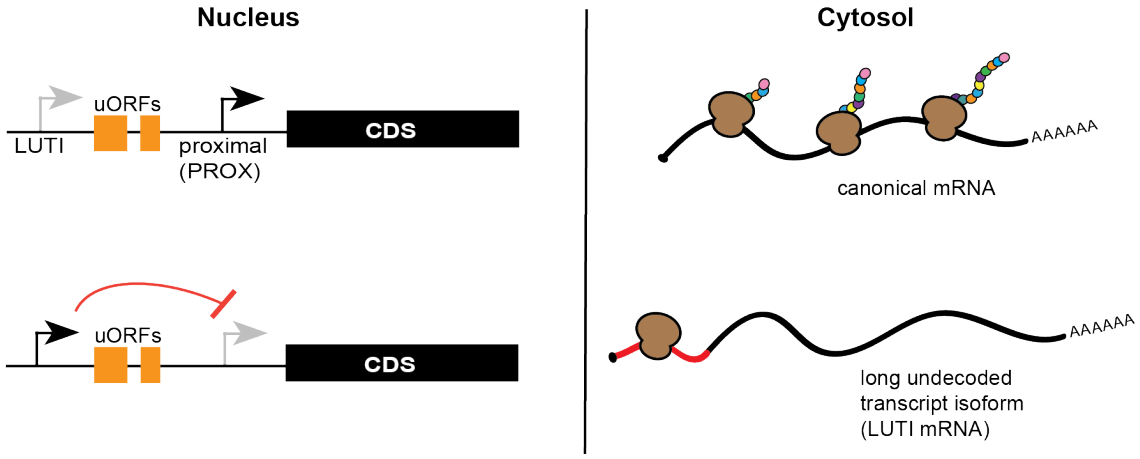

Figure 1.1: *Model for LUTI-based gene repression*
The CDS-proximal promoter drives expression of a canonical, well-translated mRNA. A CDS-distal promoter drives expression of a long, undecoded transcript isoform (LUTI). uORF translation within the 5′ extension of the LUTI restrict translation of the CDS. LUTIs have also been shown to interfere with PROX promoter initiation to limit levels of the coding mRNA isoform (Chia et al., 2017; Tresenrider et al., 2021).

Discovery of LUTI mRNAs

The first LUTI to be discovered regulates the gene *NDC80* in yeast. *NDC80* encodes a linchpin outer kinetochore subunit required for chromosome segregation during cell division. During vegetative growth, the transcriptional repressor Ume6 prevents initiation at the $NDC80^{LUTI}$ promoter, the canonical isoform is expressed, and Ndc80 protein is synthesized (Chen et al., 2017). In meiotic prophase, the master meiotic transcription factor Ime1 binds Ume6 to activate expression of the $NDC80^{LUTI}$, which results in enrichment of H3K4me2 and H3K36me3 at the $NDC80^{PROX}$ promoter and $NDC80^{PROX}$ repression (Chen et al., 2017; Chia et al., 2017). This temporal restriction of Ndc80 protein synthesis in meiotic prophase through LUTI expression is an important measure that ensures segregation of homologous chromosomes, rather than sister chromatids, in meiosis I (Chen et al., 2017). During meiotic divisions when full kinetochore assembly is necessary, nuclear Ime1 levels decline, the $NDC80^{LUTI}$ promoter becomes inactive, and a second meiotic transcription factor called Ndt80 activates $NDC80^{PROX}$ (Chen et al., 2017). $NDC80^{LUTI}$-based gene regulation thus employs developmentally-regulated transcription factors to toggle between a repressive and coding transcript, allowing for proper timing and levels of gene expression throughout differentiation.

Genome-wide approaches to identify LUTIs have employed integrated analysis of mRNA-seq, ribosome profiling, and quantitative mass spectrometry (Cheng et al., 2018). Identification of cases whereby mRNA and protein levels are poorly correlated and verification of uORF translation based on ribosome profiling revealed that at least 380 yeast genes (~8% of the measurable proteome) have a corresponding LUTI that is expressed during meiosis (Cheng et al., 2018). Cellular stress also induces activation of

LUTIs by the unfolded protein response (UPR) TF Hac1 and during zinc starvation by the zinc-responsive TF Zap1 (Van Dalfsen et al., 2018; Taggart et al., 2017). Importantly, the observation that the human proto-oncogene *MDM2* is subject to LUTI-based interference has revealed this form of gene repression is broadly conserved (Hollerer et al., 2019).

Case studies, in addition to that of Ndc80, have revealed that diverse gene targets are subject to LUTI-based repression, including the genes encoding the superoxide dismutase enzyme Sod1 (Vander Wende et al., 2023), the transcription factor Swi4 (Su et al., 2023), and the purine hydrolase enzyme Hnt1 (Van Dalfsen et al., 2018; Tatip et al., 2020). These studies have indicated functional roles for select LUTIs, notably revealing the LUTI-based downregulation of Swi4 is required for proper meiotic entry (Su et al., 2023), though additional work is needed to determine function for other LUTIs.

Why LUTI-based gene repression?

The pervasiveness of LUTI-based gene regulation and evidence that some LUTIs are functional components of biological processes indicate LUTI-based repression is evolutionarily advantageous. For proper *NDC80* regulation, the toggling between the LUTI and PROX isoforms is mediated by sequence-specific TF binding to the two promoters at different stages in meiosis. Other LUTIs identified are also targets of developmental- or stress-dependent TFs. While activation of gene expression by TFs has long been recognized as a key driver in development or stress response, less is known about how transcription factor-driven waves of gene activation are coordinated with gene repression. LUTIs reveal one route through which cells can simultaneously increase gene expression through TF activation of canonical targets while decreasing protein synthesis through TF activation of LUTI targets.

Cis-regulatory sequences that serve as binding sites for TFs can evolve at a faster rate than the coding regions for TF genes, which affect entire gene networks and are therefore under greater selective pressure. Thus, evolution of a LUTI promoter would be theoretically similar to the evolution of a binding site for a transcriptional repressor, an established mode of gene repression. In fact, among a set of 61 LUTIs that are activated by the Ume6/Ime1 co-activator complex, over half (33) of the LUTI promoters had a consensus Ume6 binding site that was conserved among related yeast species (Tresenrider et al., 2021). LUTI-based transcriptional interference presents the added benefit of being a tunable system, with higher LUTI expression leading to stronger repression (Chia et al., 2017; Tresenrider et al., 2021). This allows flexibility in the degree of repression, rather than a simple on/off switch.

Though higher LUTI expression is associated with more potent repression of the proximal promoter, the underlying mechanism for LUTI-based transcriptional interference is not clear. Variability in the degree of interference among different LUTI-regulated genes suggests *trans*-acting factors regulate repression by the LUTI, possibly through co-transcriptional chromatin modifications as has been described for several lncRNA pathways. In Chapter 2, I will describe an unbiased genetic approach we undertook to identify *trans*-acting regulators of LUTI-based interference. This led to the discovery of a

previously unknown role by the Swi/Snf complex in transcriptional interference. In Chapter 3, I will reveal evidence that Swi/Snf directly performs transcriptional interference at proximal promoters for select LUTI-regulated genes and other alternative transcripts. This activity by Swi/Snf occurs through co-transcriptional nucleosome remodeling, a general Swi/Snf function that is often masked by its roles in promoter activation. Overall, our work introduces this highly conserved chromatin remodeling complex as a new player within the broad array of transcriptional interference pathways. Furthermore, our findings indicate Swi/Snf's establishment of transcriptional interference occurs through two discrete steps: activation of gene distal promoters and repression of downstream proximal promoters. This dual role for Swi/Snf in gene activation and repression within the same genomic locus is unique from previously described transcriptional interference pathways involving factors thought to act solely in transcription elongation mechanisms.

Chapter 2 – Forward genetics to identify regulators of LUTI-based transcriptional interference

2.1 Introduction

A key component of LUTI-based gene repression is *cis*-mediated silencing of a canonical gene promoter by transcription of the LUTI. While numerous examples exist in which *cis*-acting noncoding RNAs regulate the expression of neighboring genes (Bird et al., 2006; Garg et al., 2018; J. H. Kim et al., 2016; Laprade et al., 2004; Werven et al., 2012), LUTI-based regulation distinctly involves the expression of an interfering mRNA transcript carrying a full CDS that is translationally repressed. In this regard, LUTI-based repression is counterintuitive from classical views of gene regulation as it involves TF activation of poorly translated mRNA isoforms, which ultimately leads to gene repression. Consequently, a single TF can coordinately activate or repress protein synthesis for distinct sets of genes, depending on whether it binds to a canonical or a LUTI promoter, respectively.

Despite robust identification and characterization of LUTI-regulated genes, the mechanism underlying LUTI-based transcriptional interference is not well understood. In fact, transcript isoform profiling revealed that the degree of proximal promoter repression during LUTI expression is variable, indicating LUTI-mediated transcriptional repression is differentially regulated among affected loci (Tresenrider et al., 2021). Through characterization of transcriptional and translational regulation for set of 74 LUTIs activated in early meiosis, it was found that while uORF-based translational repression is ubiquitous, LUTI transcription interferes with proximal promoter activation in about half of all cases (Tresenrider et al., 2021).

The distinction between LUTI expression (i.e. translational interference alone) and LUTI-based gene repression (i.e. integrated translational *and* transcriptional interference) is important, as proximal promoter repression is needed to reduce the pools of coding transcript in the cell and ultimately reduce protein levels. Set1- and Set2-mediated histone methylation (H3K4me2 and H3K36me3, respectively) were previously found to be required for $NDC80^{LUTI}$-based transcriptional interference of $NDC80^{PROX}$ (Chia et al., 2017). Additionally, LUTI-induced nucleosome remodeling by unknown factors was observed at the $NDC80^{PROX}$ promoter (Chia et al., 2017).

These observations from the *NDC80* case study led to systematic genome-wide characterization of the association between these chromatin changes and LUTI-based transcriptional interference for the 74 early meiotic LUTIs. Among the chromatin changes measured, increased H3K36me3 and changes in nucleosome positioning at the proximal

promoter were found to be the strongest predictors of transcriptionally-interfering LUTIs (Tresenrider et al., 2021). However, detangling causality from correlation for these chromatin and transcriptional features requires more in-depth functional analysis. Additionally, factors required for the LUTI-induced nucleosome remodeling remain unknown, prompting an unbiased search for regulators of LUTI-based transcriptional interference. In this study, we used a genetic selection approach to identify new regulatory factors required for LUTI-based transcriptional interference in budding yeast. This strategy led us to uncover a novel repressive function of the Swi/Snf chromatin remodeling complex in establishing transcriptional interference.

The Swi/Snf complex is a highly conserved, twelve-subunit ATP-dependent nucleosome remodeling complex that activates the expression of diverse sets of genes in various contexts (Dutta et al., 2014; Rando and Winston, 2012; Rawal et al., 2018; Sahu et al., 2021; Shivaswamy and Iyer, 2008). We show that in addition to its canonical function in gene activation, the Swi/Snf complex is required for LUTI-based gene repression. In contrast to previous findings that Swi/Snf can indirectly participate in transcriptional interference by activating transcription of an upstream intergenic promoter (Martens et al., 2005), our investigation uncovered unique Swi/Snf mutations that impact LUTI-based transcriptional interference without impacting LUTI expression. These findings support a direct role by Swi/Snf in transcriptional repression, highlighting the diverse functions capable by this conserved chromatin remodeler.

2.2 Results

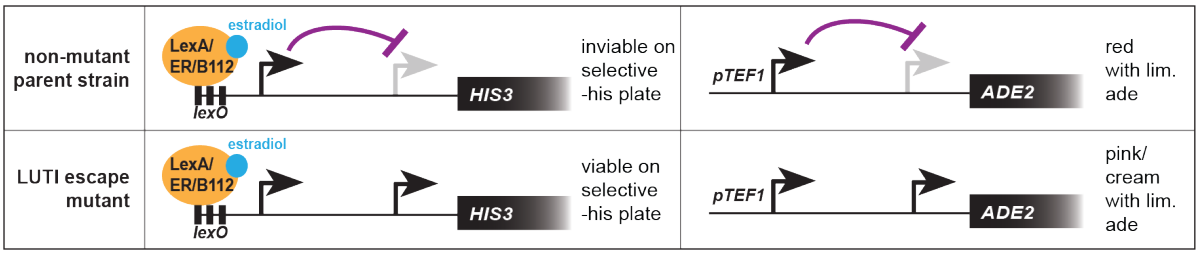

Figure 2.1: *Schematic of HIS3^{LUTI} and ADE2^{LUTI} reporters used to select for LUTI escape mutants*
In control cells harboring the reporters (UB22912), expression of *HIS3^{LUTI}* or *ADE2^{LUTI}* silences expression of the protein-coding, proximal promoter-derived transcript, thereby rendering cells auxotrophic for histidine and adenine. In spontaneous LUTI escape mutants, cells that fail to silence *HIS3* expression can be selected based on their ability to grow in media lacking histidine, whereas cells that fail to silence *ADE2* expression can be screened based on their ability to metabolize red-pigmented purine precursors.

A genetic approach to identify mutants defective in LUTI-based gene repression

To identify regulatory factors required for LUTI-based gene repression, we undertook a genetic approach. To create a reporter for LUTI regulation, we fused the 5′ leader sequence of a well-characterized LUTI, *NDC80^{LUTI}* (J. Chen et al., 2017; Chia et al., 2017), to the CDS for the histidine biosynthesis gene *HIS3.* To enable inducible

expression of the *HIS3*^{LUTI} reporter, we replaced the native *NDC80*^{LUTI} promoter with a *lexO* promoter, which can be induced by a β-estradiol activatable heterologous transcription factor (LexA-ER-B112) (Ottoz et al., 2014) (Figure 2.1). We plated cells on media lacking histidine supplemented with β-estradiol to induce *HIS3*^{LUTI} and 3-amino-1,2,4-triazole (3-AT) to completely inhibit low levels of His3 activity (refer to Appendix B for further details). These conditions should prevent the growth of cells where LUTI-based repression is intact (Figures 2.1 and 2.2A). However, disruption of the LUTI-based repression arising from spontaneous mutations should yield viable colonies under the same conditions due to loss of transcriptional and/or translational interference of *HIS3*. In fact, after three days of growth under selection, we observed viable colonies on the selective plates, which we termed "LUTI escape mutants."

Mutants that we wished to filter out from our analysis were those that failed to express the LUTI in the first place, such as mutations that disrupt transcriptional activation that is dependent on the *lexO*/LexA-ER-B112 inducible system. Accordingly, we performed secondary screening on each mutant using an independent reporter. For this, we used a constitutive, highly expressed *TEF1* promoter to drive LUTI expression and replaced the *HIS3* CDS with the CDS for the adenine biosynthesis gene *ADE2* (Figure 2.1). In this case, cells that properly silenced *ADE2* expression turned red on media with limited adenine due to their accumulation of red-pigmented purine precursors, whereas LUTI escape mutants appeared pink or cream-colored due to their failure to repress *ADE2* (Figure 2.2B).

Swi/Snf mutations underly LUTI escape phenotypes

To identify the causative mutations behind the LUTI escape phenotypes, we then sequenced the genomes of cells exhibiting both *HIS3*^{LUTI} and *ADE2*^{LUTI} escape phenotypes. Mutations of interest were first identified computationally by variant calling and filtering to remove mutations present in the parental control strain or those not representing at least 95% of all sequencing reads (refer to Appendix B for additional details). All mutations of interest were then validated by performing segregant analysis after backcrossing to the nonmutant control strain. In total, we identified and validated eleven unique mutations conferring LUTI escape phenotypes. Strikingly, all identified mutations fell within genes encoding subunits of the Swi/Snf chromatin remodeling complex (Table 2.1, Figure 2.2D). Our selection-based strategy uncovered mutations in six of the eight subunits that are specific to the Swi/Snf complex and are not members of other chromatin remodeling complexes (Olave et al., 2002; Peil et al., 2022; Turegun et al., 2018), with five of the identified mutations falling within the gene encoding the catalytic subunit, *SNF2* (Table 2.1).

Gene	Mutation	Disruption of *HIS3*^{LUTI}-based repression (growth) †	Disruption of *ADE2*^{LUTI}-based repression (color) ††	LUTI escape Phenotype	Conserved?†††
SNF2	Frameshift at His 412	++	pink	recessive	yes
SNF2	Frameshift at Lys 651	+	cream	recessive	yes
SNF2	Gln 928 > Lys	++	cream	dominant negative	yes
SNF2	Trp 935 > Arg	++	pink	recessive	yes
SNF2	Glu 973 > Stop	+	cream	recessive	yes
SNF5	Gln 225 > Stop	++	pink	recessive	yes
SNF5	Gln 267 > Stop	+	pink	recessive	yes
SNF12	Gln 226 > Stop	+	cream	recessive	yes
SWI1	Ser 764 > Stop	++	pink	recessive	no
SWI3	Glu 815 > Stop	++	pink	recessive	no
SNF6	Arg 135 > Stop	+	cream	recessive	no

Table 2.1: *Genotypes and phenotypes of mutants uncovered from LUTI escape selection strategy to identify regulators of LUTI-based interference*

† Growth was scored on media lacking histidine with 25 nM β-estradiol and 200 μM 3-amino-1,2,4-triazole (3-AT). The parent control strain used for genetic selection fails to grow in these conditions.

†† Color was scored on yeast extract peptone with 2% dextrose (YPD) media with limiting adenine. The parent control strain used for screening is red in these conditions.

††† Conservation determined by whether the mutation affects a conserved residue (in the case of missense mutations) or region (in the case of nonsense or frameshift mutations) of the human protein homolog.

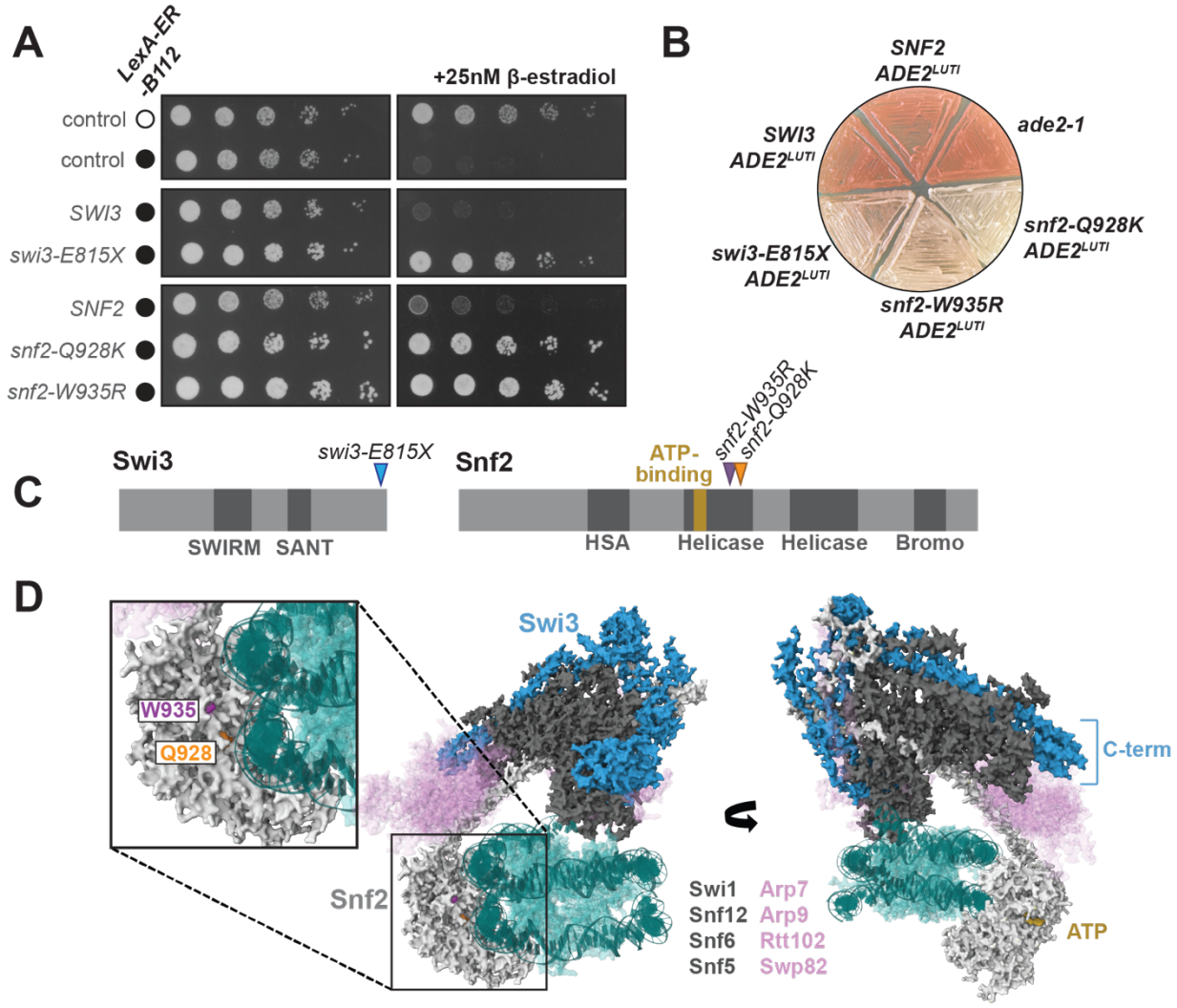

Figure 2.2: *Mutations in the Swi/Snf complex disrupt LUTI-based transcriptional interference*
(A) *HIS3*^{LUTI} serial dilution and spotting growth assay. Cells were plated on synthetic complete media lacking histidine with 200 μM 3-AT (left) or 200 μM 3-AT and 25 nM β-estradiol (right) and grown for 72 h at 30°C before imaging. Strains (from top to bottom): UB29385, UB29188, UB29791, UB24301, UB28911, UB28919, UB28925. **(B)** *ADE2*^{LUTI} color assay. Cells were streaked onto a YPD plate lacking supplemental adenine and grown for 24 h at 30°C before imaging. Strains: *ade2-1* (UB7), *SNF2 ADE2*^{LUTI} (UB30034), *SWI3 ADE2*^{LUTI} (UB30190), *swi3-E815X ADE2*^{LUTI} (UB23545), *snf2-W935R ADE2*^{LUTI} (UB28923), and *snf2-Q928K ADE2*^{LUTI} (UB30185). **(C)** Schematic of primary protein structure for Swi3 (left) and Snf2 (right), with LUTI escape mutations *swi3-E815X, snf2-W935R*, and *snf2-Q928K* mapped onto the structure (arrows). **(D)** Cryo-EM structure of the yeast Swi/Snf complex bound to a nucleosome (teal), published by (Han et al., 2020) and rendered in MolStar (Sehnal et al., 2021). The Swi3 dimer is portrayed in blue, Snf2 in light gray, and other subunits with gene mutations recovered in the LUTI escape screen (Swi1, Snf12, Snf6, and Snf5) in dark gray. Other subunits (Arp7, Arp9, Rtt102, and Swp82) are portrayed in light pink. Snf11 was not resolved on this structure. The Snf2 residues W935 (purple) and Q928 (orange), which are affected by the *snf2-W935R* and *snf2-Q928K* mutations, are highlighted. The C-terminus of Swi3, which is affected by the *swi3-E815X* mutation, is highlighted however the specific region truncated by the *swi3-E815X* mutation is not resolved on this structure.

We did not identify mutations in *SWP82* or *SNF11*, which also encode subunits specific to the Swi/Snf complex. We investigated whether deletion of these genes would disrupt LUTI-based repression and found that the *swp82Δ* mutation did not confer a LUTI escape phenotype for the $HIS3^{LUTI}$ or $ADE2^{LUTI}$ reporters (Figures 2.3A and 2.3B). This may be due to a limited role for *SWP82* in Swi/Snf function as judged by the lack of a growth defect in the null mutant (Figure 2.3C). Furthermore, *swp82Δ* was previously shown to confer milder gene expression defects compared to other null mutants of Swi/Snf (Dutta et al., 2017). *snf11Δ* cells did exhibit subtle LUTI escape phenotypes (Figures 2.3A and 2.3B). Snf11 is only 169 amino acids long and may have eluded our selection approach, which relied on spontaneous mutations, due to its small size.

We sought to determine whether LUTI escape phenotypes in different Swi/Snf mutants were due to lack of a direct repressive activity at the proximal promoter versus lack of LUTI expression (indirect repression). As such, we performed RT-qPCR on wild type and mutant cells harboring the *lex*-inducible $HIS3^{LUTI}$ reporter. The *swi3-E815X* and *snf2-W935R* mutants expressed the $HIS3^{LUTI}$ to high levels, indicating they are specifically defective for transcriptional interference rather than LUTI initiation (Figure 2.3D). However, we were surprised at the lack of $HIS3^{LUTI}$ induction in the *snf2-Q928K* mutant, given it was selected along with the other LUTI escape mutants based on conferring phenotypes with independent LUTI promoters. Given that the *snf2Δ* and *swi3Δ* also strongly affected *lexO* induction (Figure 2.3D), we conclude that the *snf2-Q928K* mutant behaves like a null phenotype in this case and its $HIS3^{LUTI}$ escape phenotype is a result of decreased transcription through the proximal promoter. Unlike the *snf2Δ* and *swi3Δ*, *snf11Δ* cells did express $HIS3^{LUTI}$ upon induction with β-estradiol (Figure 2.3D), indicating its LUTI escape phenotype is a result of decreased repressive function, like the *swi3-E815X* and *snf2-W935R* mutants, rather than reduced expression of the LUTI.

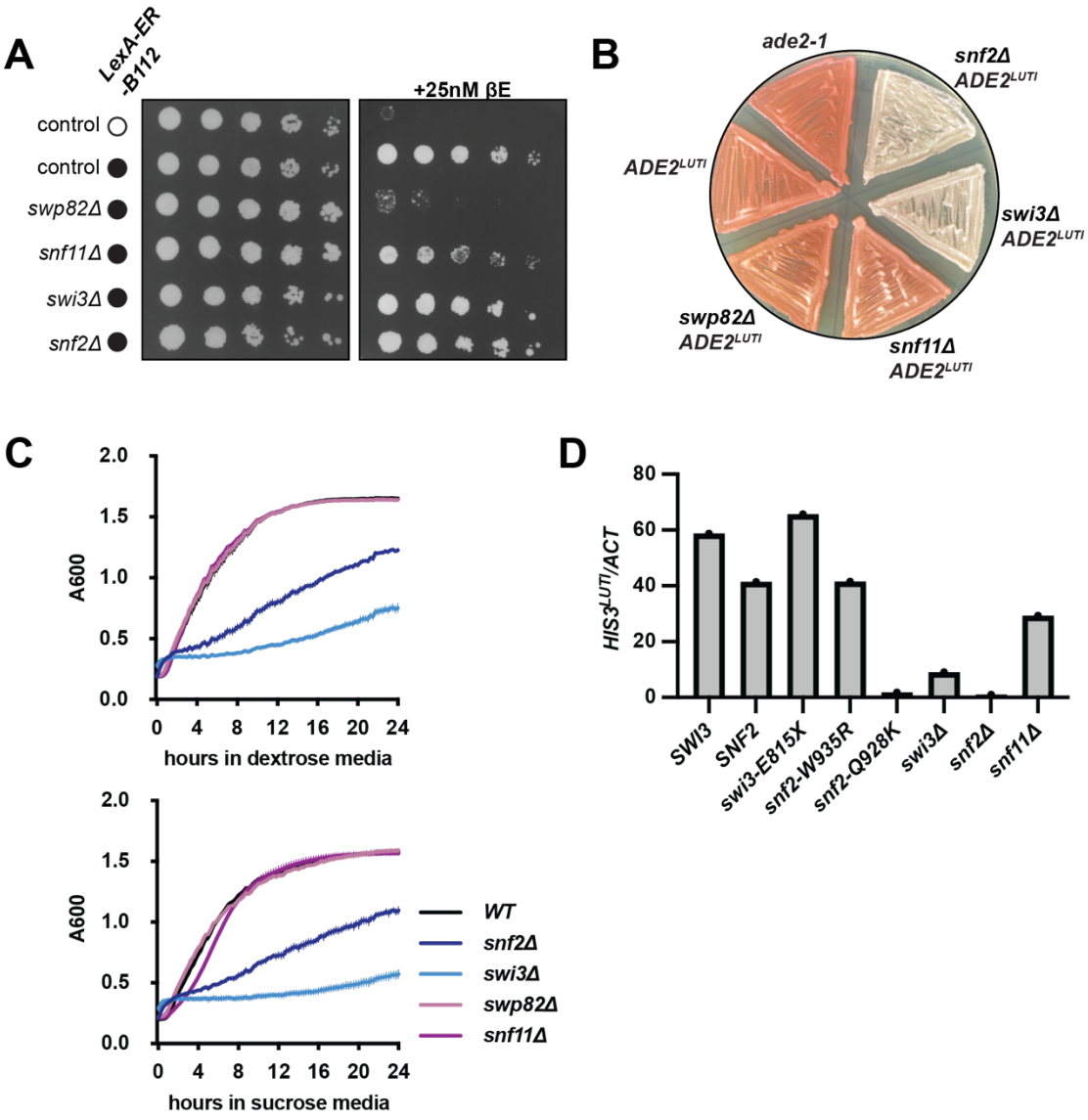

Figure 2.3: *Roles in LUTI-based regulation vary among different Swi/Snf subunits*
(A) *HIS3*^{LUTI} serial dilution and spotting growth assay. Cells were plated on synthetic complete media lacking histidine with 200 μM 3-AT (left) or 200 μM 3-AT and 25 nM β-estradiol (right) and grown for 72 h at 30°C before imaging. Strains (from top to bottom): UB17314, UB13670, UB33427, UB33424, UB33482, and UB34040. **(B)** *ADE2*^{LUTI} color assay. Cells were streaked onto a YPD plate lacking supplemental adenine and grown for 24 h at 30°C before imaging. Strains: *ade2-1* (UB7), *ADE2*^{LUTI} (UB21565), *swp82Δ ADE2*^{LUTI} (UB30456), *snf11Δ ADE2*^{LUTI} (UB30507), *swi3Δ ADE2*^{LUTI} (UB27673), and *snf2Δ ADE2*^{LUTI} (UB27669). **(C)** Growth curves for cells grown in rich media with 2% dextrose (YPD, left) or 2% sucrose (right). Absorbance readings at 600 nm collected every 15 minutes for 24 h is plotted for the following strains: WT (UB4784), *swp82Δ* (UB31746), *snf11Δ* (UB31807), *snf2Δ* (UB20060), and *swi3Δ* (UB27896). **(D)** RT-qPCR measuring levels of *lexO-HIS3*^{LUTI} levels after induction with 25 nM β-estradiol for two hours. Strains, left to right: UB29790, UB36205, UB24303, UB29164, UB28916, UB33482, UB34040, UB33424.

It was surprising that we only recovered mutations in the subunits of Swi/Snf and no other chromatin remodelers. In fact, Chd1 and Isw-family chromatin remodelers have

known functions in co-transcriptional nucleosome remodeling (Hennig et al., 2012; Rando and Winston, 2012; Smolle et al., 2012). To assess their involvement in LUTI-based repression, we deleted catalytic subunits from each complex. We found that deletion of *ISW1, ISW2,* or *CHD1*, alone or in combination, did not disrupt *HIS3*^{LUTI} or *ADE2*^{LUTI}-based repression (Figures 2.4A and 2.4B). This finding suggests that the Swi/Snf complex plays a specific role in LUTI-based gene repression for the *HIS3*^{LUTI} and *ADE2*^{LUTI} reporter genes.

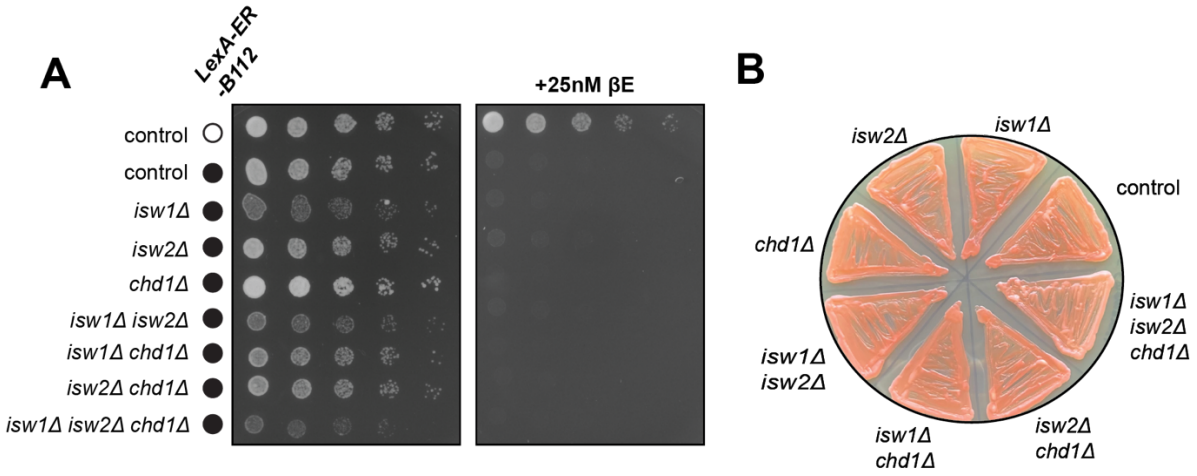

Figure 2.4: *Candidate-based screening for LUTI escape phenotypes*
(A) *HIS3*^{LUTI} serial dilution and spotting growth assay. Cells were plated on synthetic complete media lacking histidine with 200 μM 3-AT (left) or 200 μM 3-AT and 25 nM β-estradiol (right) and grown for 72 h at 30°C before imaging. Strains (from top to bottom): UB24051, UB22912, UB24057, UB23996, UB24000, UB29782, UB29784, UB23999, and UB30085. **(B)** *ADE2*^{LUTI} color assay. Cells were streaked onto a YPD plate lacking supplemental adenine and grown for 24 h at 30°C before imaging. Strains, all harboring *ADE2*^{LUTI}: control (UB22912), *isw1Δ* (UB24057), *isw2Δ* (UB23996), *chd1Δ* (UB24000), *isw1Δ isw2Δ* (UB29782), *isw1Δ chd1Δ* (UB29784), *isw2Δ chd1Δ* (UB23999), and *isw1Δ isw2Δ chd1Δ* (UB30085).

LUTI escape mutants confer partial loss of Swi/Snf function

All LUTI escape mutants conferred recessive phenotypes except for *snf2-Q928K* (Table 2.1), which displayed a partial dominant phenotype (Table 2.1 and Figure 2.5A). We chose to use this mutant along with *snf2-W935R* and *swi3-E815X*, a nonsense mutant affecting the structural subunit Swi3, to further investigate the role of Swi/Snf chromatin remodeling in transcriptional interference (Figures 2.2C and 2.2D). These three mutants were selected for further characterization based on their minimal growth defects compared to *snf2Δ* or *swi3Δ* and strong LUTI escape phenotypes (Figures 2.2A and 2.2B). For each gene, we constructed strains lacking the endogenous allele and harboring a transgenic rescue construct at the *LEU2* locus containing either the wild-type allele of the gene as a control or the LUTI escape allele, under the native gene promoter.

Because null mutations in *SNF2* or *SWI3* are extremely pleiotropic (Dutta et al., 2017), we wondered whether the LUTI escape mutants broadly share phenotypes with their respective null mutants or if they instead affect specific functions of the Swi/Snf

complex. To address this question, we first examined a well-characterized Swi/Snf loss-of-function phenotype: inability to ferment sucrose (Neigeborn and Carlson, 1984). As expected, *snf2Δ* and *swi3Δ* mutants grew poorly in sucrose media (Figure 2.5B). In contrast, the *swi3-E815X* mutant grew at a rate identical to wild-type cells, while the *snf2-W935R* and *snf2-Q928K* mutants only exhibited slight growth defects (Figure 2.5B).

The Swi/Snf complex is also necessary for transcription of the gene *HO,* which encodes the endonuclease required for mating type switching (Stern et al., 1984). Although the strains used in this study are heterothallic due to a protein coding mutation in the *HO* gene, the *HO* locus is still transcribed in wild type cells. As expected, the *snf2Δ* and *swi3Δ* mutants failed to properly express *HO* mRNA, exhibiting 43- and 69-fold lower *HO* mRNA levels, respectively, compared to wild type controls (Student's t test, two-tailed, p = 0.0005 [*snf2Δ*], p = 0.0015 [*swi3Δ*]). While the *swi3-E815X* mutant did not strongly affect *HO* transcription (1.6-fold lower than wild type, p = 0.0543), *snf2-W935R* mutants displayed an intermediate phenotype (7-fold lower than wild type, p = 0.0011) and *snf2-Q928K* cells exhibited similar low *HO* mRNA levels (43-fold lower than wild type, p = 0.0015) as the null mutants (Figure 2.5C).

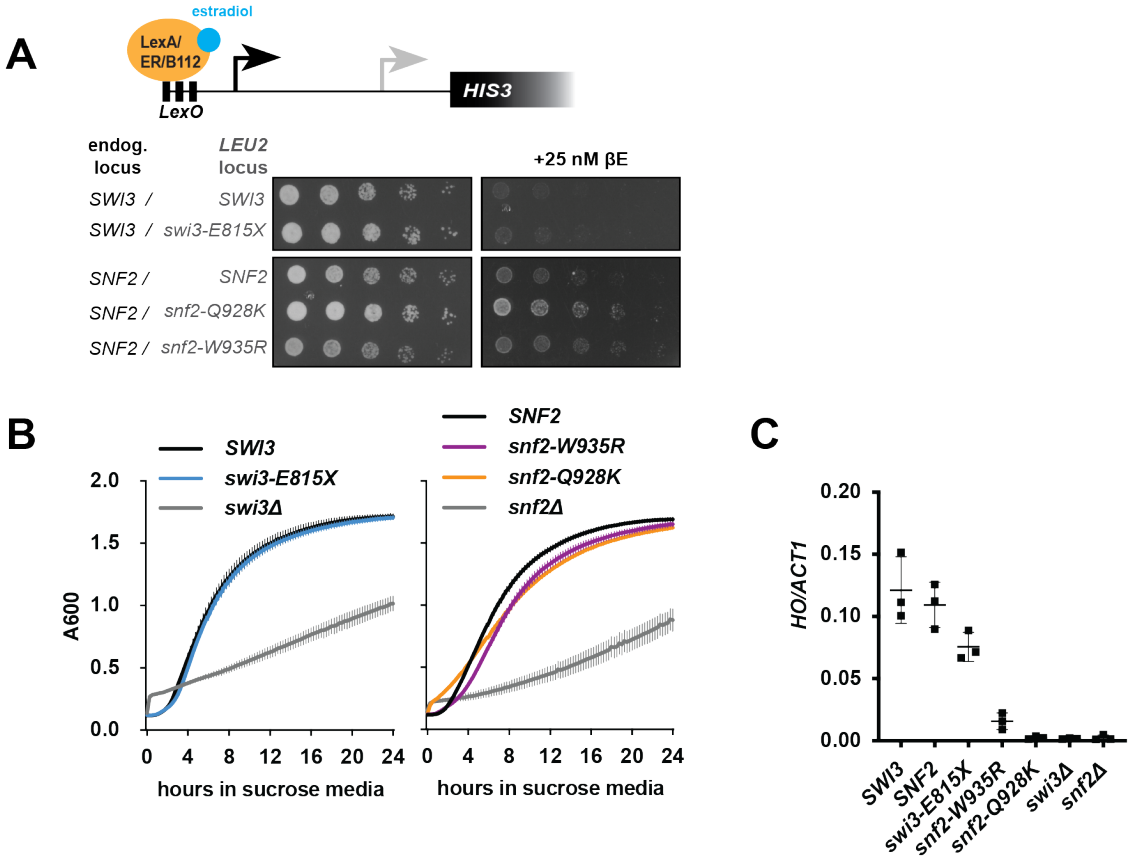

Figure 2.5: *LUTI escape mutations confer partial loss of Swi/Snf function*
(A) *HIS3*^{LUTI} serial dilution and spotting growth assay in haploid cells harboring transgenic alleles at the *LEU2* locus for *SWI3* (UB29792), *swi3-E815X* (UB29694), *SNF2* (UB28907), *snf2-Q928K* (UB29170), or

snf2-W935R (UB29166). (**B)** Growth curves for cells grown in rich media with 2% sucrose. Absorbance readings at 600 nm collected at 15-minute intervals for 24 h is plotted for *SWI3* (UB19205, left, black), *swi3-E815X* (UB19209, left, blue), *swi3Δ* (UB27896, left, gray), *SNF2* (UB28914, right, black), *snf2-Q935R* (UB28922, right, purple), *snf2-Q928K* (UB28915, right, orange), and *snf2Δ* (UB29781, right, gray). **(C)** RT-qPCR measuring relative abundance of *HO* mRNA in *SWI3* and *SNF2* mutants compared to their controls (n = 3). Strains (left to right): UB19205, UB28914, UB19209, UB28922, UB28915, UB27896, UB29781. Student's t test was performed on each mutant-to-wild type comparison (two-tailed, p = 0.0543 [*swi3-E815X*], p = 0.0011 [*snf2-W935R*], p = 0.0005 [snf2-*Q928K*], p = 0.0015 [*swi3Δ*], p = 0.0005 [*snf2Δ*]).

To better understand how the LUTI escape mutants affect gene expression at a global scale, we next performed mRNA-seq on *swi3-E815X*, *snf2-W935R,* and *snf2-Q928K* mutants along with the respective wild-type control and null mutant. While the *snf2Δ* and *swi3Δ* mutants displayed widespread changes in gene expression compared to wild-type cells (Spearman's rank correlation coefficient, ρ = 0.883 [*snf2Δ*], ρ = 0.892 [*swi3Δ*]), the LUTI escape mutants affected only a limited number of genes (Figure 2.6). Hierarchical clustering further revealed that *swi3-E815X* and *snf2-W935R* mutants were grouped with the wild-type controls and displayed gene expression profiles nearly matching that of wild-type cells (ρ = 0.98 [*swi3*-E815X], ρ = 0.97 [*snf2-W935R*]; Figure 2.6). In contrast, the *snf2-Q928K* mutant displayed an intermediate gene expression profile, with some genes matching the null phenotype and some matching wild-type gene expression (ρ = 0.947 [*snf2-Q928K* vs. wild type], ρ = 0.95 [*snf2-Q928K* vs. *snf2Δ*]; Figure 2.6). These findings confirm that the *snf2-Q928K* mutant displays more severe and pleiotropic loss-of-function phenotypes compared to *snf2-W935R* and *swi3-E815X*.

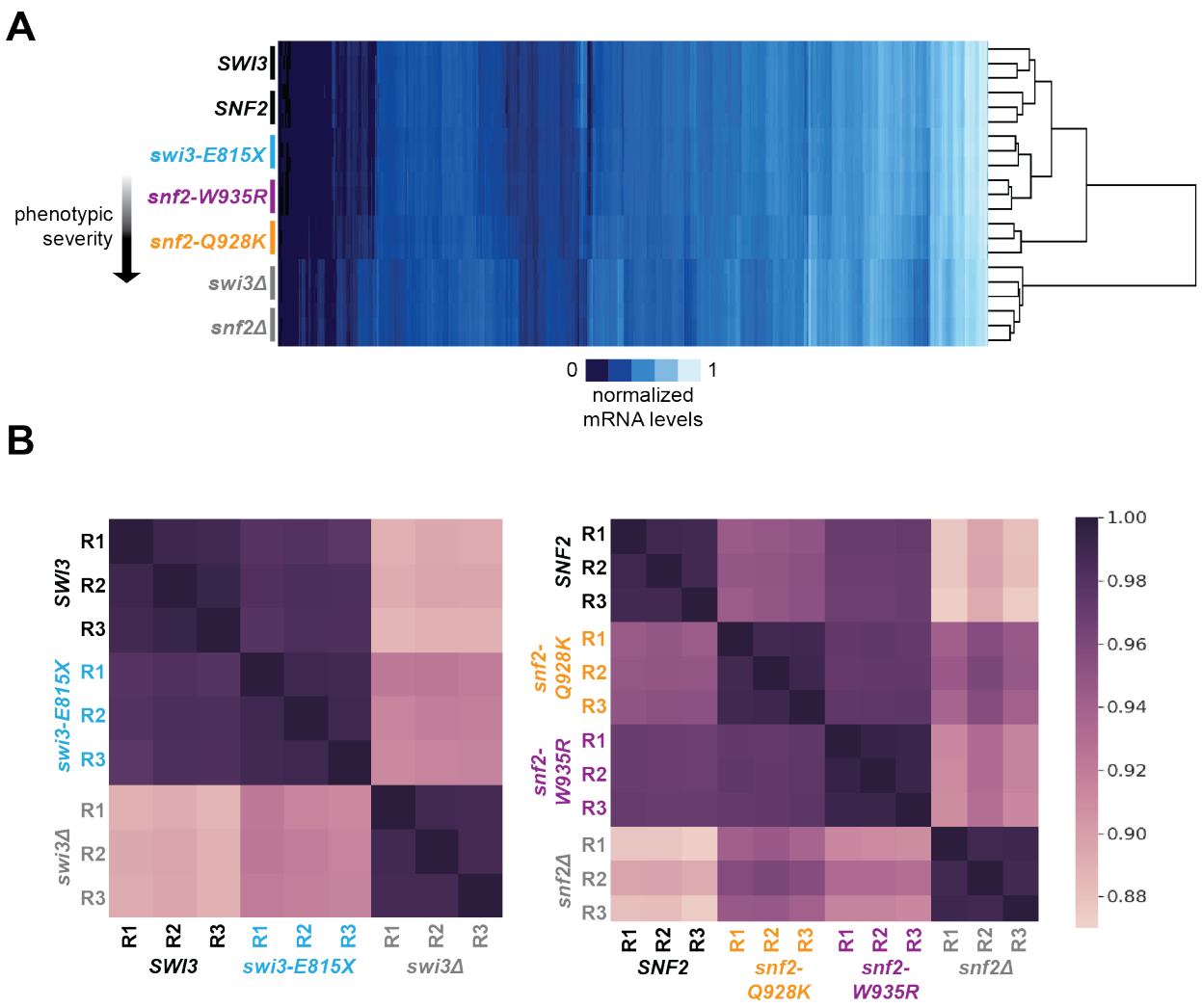

Figure 2.6: *Global mRNA expression profiles among LUTI escape mutants reveal spectrum of phenotypic severity*
(A) Heatmap of hierarchical clustering performed on genes (x-axis, Euclidian-distance similarity metric) and strains in biological triplicate (y-axis, centered correlation similarity metric) produced from mRNA sequencing TPM values. Strains (top to bottom): UB19205, UB28914, UB19209, UB28922, UB28915, UB27896, UB29781. All three LUTI escape mutants cluster more closely with wild-type controls than the null mutants, however the *snf2-Q928K* mutant has a gene expression profile that is more divergent from wild type than the *swi3-E815X* or *snf2-W935R* mutants. **(B)** Heatmaps generated using Spearman's rank correlation coefficient values from mRNA sequencing data.

The Swi/Snf complex has been previously implicated in transcriptional interference of the serine biosynthesis gene *SER3*. In serine-rich conditions, Swi/Snf activates an upstream intergenic non-coding RNA called *SRG1*, which reads through the *SER3* promoter resulting in increased nucleosome occupancy and repression of *SER3* (Figure 2.7A) (Hainer et al., 2011; Martens et al., 2005; Martens and Winston, 2002). In YPD, a serine-rich media, both *snf2Δ* and *swi3Δ* cells exhibited lower levels of *SRG1* transcript compared to wild-type cells (Figure 2.7B), leading to significant upregulation of *SER3* (p=

0.0058 [*snf2Δ*], p= 0.0018 [*swi3Δ*], Figure 2.7C). The *snf2-Q928K* mutant downregulated *SRG1* transcript to the same degree as *snf2Δ* cells (Figure 2.7A) and upregulated *SER3* ~40-fold relative to wild type (Figure 2.7B), whereas the *swi3-E815X* and *snf2-W935R* mutants regulated this locus normally. Thus *snf2-W935R* and *swi3-E815X* mutants appear to display defects related to transcriptional interference at specific loci. Altogether, we conclude that each LUTI escape mutation disrupts Swi/Snf function, but to varying degrees, with *snf2-Q928K* exhibiting more severe transcriptional defects than *snf2-W935R*, and *snf2-W935R* exhibiting slightly more defects than *swi3-E815X* (Figure 2.6A).

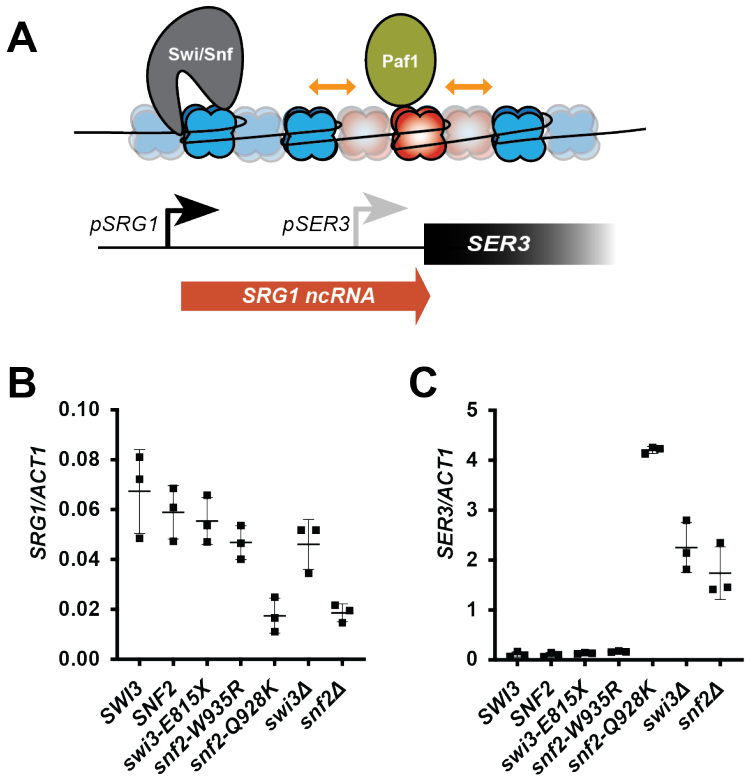

Figure 2.7: *LUTI escape mutants do not directly impact SRG1-mediated transcriptional interference at the SER3 promoter*
(A) Schematic of transcriptional interference mechanism at the *SER3* locus during serine replete conditions. Swi/Snf activates the promoter for the noncoding RNA *SRG1. SRG1* transcription reads through the *SER3* promoter, terminating at the beginning of the *SER3* CDS. *SRG1* transcription induces co-transcriptional nucleosome remodeling by the Paf1 complex, resulting in increased nucleosome occupancy at the *SER3* promoter and repression of *SER3* transcription. **(B)** RT-qPCR measuring relative abundance of *SRG1* (left) and *SER3* (right) mRNA in Swi/Snf mutants compared to wild-type cells (n = 3). Student's t test was performed on each mutant-to-wild type comparison (two-tailed, p = 0.3490 [*swi3-E815X*], p = 0.1718 [*snf2-W935R*], p = 0.0050 [snf2-*Q928K*], p = 0.1331 [*swi3Δ*], p = 0.0035 [*snf2Δ*]). Strains (from left to right): UB19205, UB28914, UB19209, UB28922, UB28915, UB27896, UB29781. **(C)** Same as (B), but for *SER3*. Student's t test was performed on each mutant-to-wild type comparison (two-tailed, p = 0.4956 [*swi3-E815X*], p = 0.0871 [*snf2-W935R*], p < 0.0001 [snf2-*Q928K*], p = 0.0018 [*swi3Δ*], p = 0.0058 [*snf2Δ*]).

2.3 Discussion

We undertook two genetic strategies to identify regulators of LUTI-based transcriptional interference: candidate screening of deletion mutants and unbiased selection of LUTI escape mutants. Deletion of chromatin remodeling genes with previously reported roles in co-transcriptional nucleosome remodeling (*ISW1*, *ISW2*, and *CHD1*) did not impact LUTI-based repression with our reporter system. However, unbiased selection of LUTI escape mutants led to our surprising discovery that the Swi/Snf complex is required for the transcriptional interference induced by LUTI reporter alleles.

Further characterization of Swi/Snf mutants revealed LUTI escape phenotypes are variable among mutations affecting different subunits and even among different mutations within the same subunit, indicating Swi/Snf repressive activity may be specifically impacted by mutations we uncovered from LUTI escape selection. In support of this notion, comparison of LUTI escape alleles to null alleles revealed very few transcriptional defects in the *swi3-E815X* or *snf2-W935R* mutants. Defects specific to transcriptional interference cannot be reliably measured by conventional mRNA-seq (see Chapter 3), though the results presented in this chapter eliminate the possibility that these LUTI escape alleles strongly impact Swi/Snf's canonical transcriptional activation function. These findings introduce the possibility that Swi/Snf performs a previously unknown function in transcriptional interference at select loci, broadening our understanding of this conserved chromatin remodeler.

Swi/Snf regulation of transcriptional interference may be specific to certain loci

Swi/Snf's role in LUTI-based transcriptional interference is reminiscent of the transcriptional interference case involving *SRG1*-mediated repression of *SER3* in serine-rich conditions. However, we observed key differences regarding the involvement of Swi/Snf for these two interference pathways. First, the LUTI escape mutants *swi3-E815X* and *snf2-W935R* specifically impair *HIS3* gene repression without compromising $HIS3^{LUTI}$ induction. These results combined with the result that *snf2Δ* and *swi3Δ* mutants fail to express the $HIS3^{LUTI}$ indicate Swi/Snf performs two functions in LUTI-based regulation: activation of the LUTI and repression of the proximal promoter. Furthermore, our results demonstrate that these functions can be uncoupled from one another in the mutant backgrounds *swi3-E815X* and *snf2-W935R*. In contrast to these dual roles in LUTI regulation, Swi/Snf's role in *SER3* repression appears to be limited to a single role: activation of *SRG1. SRG1* activation then leads to *SER3* repression through activity by other elongation factors, the Paf1 complex and Spt proteins (Hainer et al., 2011; Pruneski et al., 2011).

Second, LUTIs are full-length mRNA isoforms that contain the entire coding sequence and terminate at the canonical termination sequence for the genes they regulate. *SRG1*, on the other hand, is a short intergenic transcript that terminates after reading through the *SER3* promoter. Although general transcription elongation machinery is expected to play a role in both pathways, there may be specialized pathways devoted to isoform-dependent versus intergenic transcriptional interference. Future work to further

define the specific contexts among transcriptional interference pathways might include interrogating roles for distance between transcription start sites (TSSs), length of the two transcripts involved, and expression levels (see Chapter 3 for additional details).

LUTI escape mutants differentially impact Swi/Snf function

Our characterization uncovered striking phenotypic differences between the two missense mutations within the helicase domain of Snf2, *snf2-W935R* and *snf2-Q928K*. How might these LUTI escape mutations impact Swi/Snf remodeling function? Mapping these conserved residues on the cryo-EM structure of the Swi/Snf complex bound to a nucleosome revealed that the Q928 residue of Snf2 directly contacts nucleosomal DNA, whereas the W935 residue resides in a nearby pocket of Snf2 that does not directly contact DNA or histones (Figure 2.2D). This structural information, combined with our findings that the *snf2-Q928K* impairs Swi/Snf function more severely than *snf2-W935R*, suggests the glutamine residue at position 928 is critical for Snf2 remodeling function. Several cancer-associated mutations in humans also affect residues in the nucleosome binding region of the *SNF2* homolog *BRG1* (K. Chen et al., 2023), indicating this binding interface is functionally conserved.

Current models for Swi/Snf nucleosome remodeling propose ATP hydrolysis by Snf2 promotes DNA translocation and nucleosome sliding (Bowman, 2010; K. Chen et al., 2023; M. Li et al., 2019). Both the *snf2-W935R* and *snf2-Q928K* mutations result in a neutral-to-positive charge substitution, which may impair Snf2's ability to translocate nucleosomal DNA due to an increased affinity for the negatively charged DNA backbone. Another possibility is that missense mutations at nucleosome-binding sites in Snf2 lead to structural changes that impair its ATPase activity. In support of this notion, a *snf2-W935A* mutant was previously shown to reduce ATPase activity to 80% that of wild-type levels (Smith and Peterson, 2005). Although the Q928 residue has not been interrogated for a role in ATPase function, Snf2 mutations that eliminate ATPase activity result in dominant negative phenotypes (Richmond and Peterson, 1996), indicating the dominant negative phenotype for the *snf2-Q928K* allele uncovered in this study may stem from defects in ATP binding or hydrolysis.

The *swi3-E815X* mutation results in a truncation of Swi3 at its C-terminal coiled-coil domain. As Swi3 is thought to act as a scaffold for complex assembly (Han et al., 2020; Yang et al., 2007), defects in Swi/Snf remodeling could arise from structural changes in this mutant or reduced interactions between the complex with other transcription factors. It is possible the mutations confer structural changes that inhibit key interactions between the Swi/Snf complex and elongation factors. Additional work to investigate structural changes induced by LUTI escape mutations and physical interactions between Swi/Snf subunits with transcription elongation factors is required to assess how the LUTI escape mutations differentially impact Swi/Snf function in transcription initiation and transcriptional interference.

Concluding remarks

In summary, we uncovered a role for Swi/Snf, a conserved chromatin remodeling complex associated with gene activation, in transcriptional interference. Two LUTI escape mutants in particular, *swi3-E815X* and *snf2-W935R*, affect Swi/Snf's role in LUTI-based repression without affecting LUTI activation for a $HIS3^{LUTI}$ reporter gene. In addition to providing mutant contexts that seemingly separate Swi/Snf's gene activation function from a previously unknown role in transcriptional interference, these LUTI escape mutants provide the added benefit of exhibiting far less pleiotropy compared to their null counterparts. These features allow for further dissection of Swi/Snf-mediated transcriptional interference within a context where indirect effects on gene expression are minimal.

Chapter 3 – Swi/Snf regulation of transcriptional interference during protein-folding stress

3.1 Introduction

A natural context to investigate Swi/Snf regulation of transcript toggling: the unfolded protein response

Swi/Snf has been previously shown regulate the transcriptional interference of *SER3* indirectly through activation of the interfering transcript *SRG1* (Martens et al., 2005). However, direct interference through Swi/Snf chromatin remodeling at a silenced promoter has not previously been observed before. To explore this activity on a genome-wide scale, we turned to a cellular context during which transcript isoform toggling is widespread: the unfolded protein response (UPR) (Van Dalfsen et al. 2018). The UPR can be induced with addition of protein-folding inhibitors such as dithiothreitol (DTT) or tunicamycin. Induction of the UPR in yeast involves ER sensing of stress by Ire, which catalyzes cytosolic splicing of *HAC1* mRNA (Rüegsegger et al., 2001). Once spliced, *HAC1* (mammalian *XBP1* homolog) is translated to produce the transcription factor Hac1, which activates hundreds of transcriptional targets to mitigate cellular stress (Cox and Walter, 1996; Van Dalfsen et al., 2018; Xia, 2019).

Previously, it was shown that in addition to activating canonical transcriptional targets, Hac1 activates transcription of several LUTIs. Nineteen Hac1-dependent LUTI candidates were identified based on mRNA-sequencing and ribosome profiling data using a *hac1Δ* mutant compared to wild type (Van Dalfsen et al., 2018). Among these LUTI candidates, 15 were confirmed as Hac1-dependent LUTIs based on the same methods using a conditional depletion allele, *HAC1-AID*, to limit indirect effects in the pleiotropic *hac1Δ* background. Given this precedent for the occurrence of transcript toggling during protein-folding stress, we decided to use the UPR as a cellular context to further investigate LUTI escape phenotypes in Swi/Snf mutants.

Tools to profile transcript isoforms allow for quantification of current LUTI-regulated transcripts and identification of novel LUTIs

While previous work to identify UPR-induced LUTIs focused on those that were regulated by the conserved UPR transcription factor Hac1, we were not limited in this study to only Hac1-induced alternative transcripts. As such, we performed techniques that would allow for both the identification of new alternative interfering transcripts, including LUTIs, and quantification of distinct transcript isoforms in mutant and wild-type cells. Modified mRNA-sequencing pipelines that enrich for 5′ ends of transcripts, such as

transcript leader sequencing (TL-seq), have been recently used alongside long-read sequencing (Nanopore direct mRNA-seq) to identify and characterize alternative transcript isoforms (Chia et al., 2021; Tresenrider et al., 2022). Nanopore direct mRNA-seq provides the advantage over conventional mRNA-seq or TL-seq of visualizing full, intact mRNA molecules, allowing for the distinguishment between upstream intergenic transcripts versus full-length transcript isoforms for a given gene. However, direct mRNA-sequencing technology is currently fairly low-throughput, with a single sequencing run generating about five million reads. Furthermore, a strong 3′ bias among Nanopore RNA reads, presumably due to (1) issues with low processivity during reverse and transcription and/or (2) clogging of pores as the RNA is threaded through in the 3′ to 5′ direction, make quantification of direct mRNA-seq data unreliable. Therefore, to quantitatively measure transcription originating from different TSSs, we turned towards TL-seq and relied on Nanopore direct mRNA-seq to validate the presence of readthrough transcripts at genes of interest.

These methods led us to uncover 12 genes, including three LUTIs, with a DTT-induced distal TSS (TSS^{DIST}) that require Swi/Snf for repression of the downstream proximal TSS (TSS^{PROX}). Among these genes, we observed an increase in Snf2 binding at the regulatory region between the two TSSs and Swi/Snf-dependent changes in nucleosome positioning around the TSS^{PROX} upon stress induction. Based on results from the TL-sequencing, we further dissected the mechanism for Swi/Snf-mediated transcriptional interference for the well-characterized LUTI-regulated gene *HNT1*, leading to the finding that Swi/Snf repressive function at the $HNT1^{PROX}$ TSS depends on both initiation of $HNT1^{LUTI}$ and transcription elongation of $HNT1^{LUTI}$ through downstream chromatin.

Finally, we reexamined mRNA-sequencing data from unstressed cells gathered in Chapter 2 and integrate those expression data with chromatin data collected in this study. Our results reveal that Swi/Snf performs nucleosome remodeling downstream of the active transcription start site (TSS) for its target loci. When the Swi/Snf complex is recruited to distal promoter targets, this downstream remodeling activity interferes with CDS-proximal promoters, leading to gene repression for select LUTI-regulated genes. In addition to furthering our understanding of LUTI-based transcriptional interference, our results clarify a long-standing question in the chromatin remodeling field by providing conclusive evidence that the Swi/Snf complex can directly repress transcription *in vivo* through its nucleosome remodeling activity.

3.2 Results

Swi/Snf regulates DTT-induced alternative transcript isoform expression

In order to quantify differences in transcript isoform expression for genes with alternative transcription start sites (TSSs), we performed transcript leader sequencing (TL-seq) (Arribere and Gilbert, 2013) in wild type and LUTI escape mutants that were either untreated or treated with dithiothreitol (DTT) to induce the UPR. To restrict our analysis to loci in which the distal TSS (TSS^{DIST}) drives readthrough transcription across

the CDS-proximal TSS (TSS^{PROX}), rather than cases of intergenic transcription that terminates upstream of the proximal promoter, we also performed Nanopore direct mRNA-sequencing (direct mRNA-seq) in wild-type cells to visualize full-length mRNA isoforms. Finally, we excluded indirect gene targets that do not exhibit Snf2 binding with DTT treatment by performing Snf2 chromatin immunoprecipitation followed by whole genome sequencing (ChIP-seq) (Figure 3.1A).

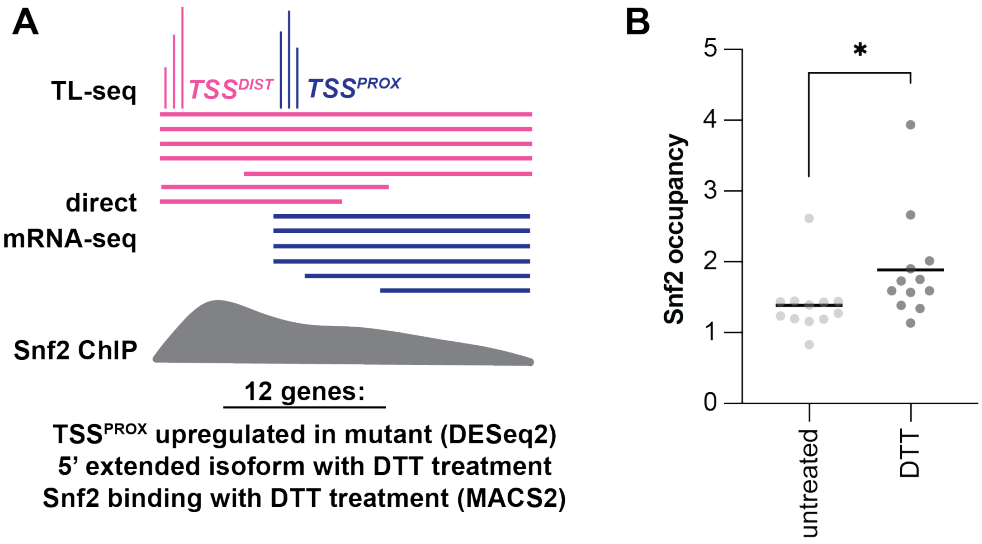

Figure 3.1: *Identification of alternative transcripts regulated by Swi/Snf*
(A) Schematic of the strategy to identify Swi/Snf-regulated genes that exhibit transcript toggling upon UPR induction by treatment with 5 mM DTT for 1 h. Twelve genes were identified that (1) exhibited significant upregulation in one or more Swi/Snf mutant of the TSS^{PROX} (DESeq2, $p < 0.05$), were (2) subject to transcriptional readthrough from an upstream distal promoter and (3) have a Snf2 ChIP peak that was called by MACS2. **(B)** Snf2 ChIP-seq signals plotted for the 12 genes identified by the strategy outlined in (A). The average Snf2 binding levels in wild-type cells (UB30387 and UB30070, n = 2 for each wild-type *SNF2* and *SWI3* control strain, see Appendix B for details) is 1.4-fold higher on average when cells are treated with DTT compared to the unstressed condition (paired t test, two-tailed, $p = 0.0423$).

We uncovered 12 TSS^{PROX} loci that fit the following criteria upon DTT treatment: (1) The TSS^{PROX} was significantly upregulated in one or more of the LUTI escape mutants (DESeq2, adjusted p-value > 0.05); (2) A TSS^{DIST}-driven readthrough transcript was expressed; and (3) Snf2 was enriched at the corresponding locus. Upon DTT-dependent induction of TSS^{DIST} transcription, Snf2 occupancy levels increased at the 5′ regulatory region by an average of 1.4-fold compared to unstressed conditions (paired t test, two-tailed, $p = 0.0423$; Figure 3.1B). Excitingly, the TSS^{PROX} for the previously characterized LUTI-regulated gene *HNT1* (Van Dalfsen et al. 2018) was significantly upregulated in all three LUTI escape mutants (Figures 3.2 B-D). Furthermore, analysis of a previously published ribosome profiling dataset (Van Dalfsen et al. 2018) revealed that *ADI1* and *ODC2* also exhibited uORF translation in the 5′ leader sequence of their distal mRNA isoform (Figure 3.3A). Deletion of the distal promoter for *ADI1* and *ODC2* resulted in increased abundance of the TSS^{PROX}-derived mRNA isoform and increased protein levels

(Figures 3.3B and 3.3C), revealing these are also LUTI-regulated genes subject to both transcriptional and translational interference upon DTT treatment.

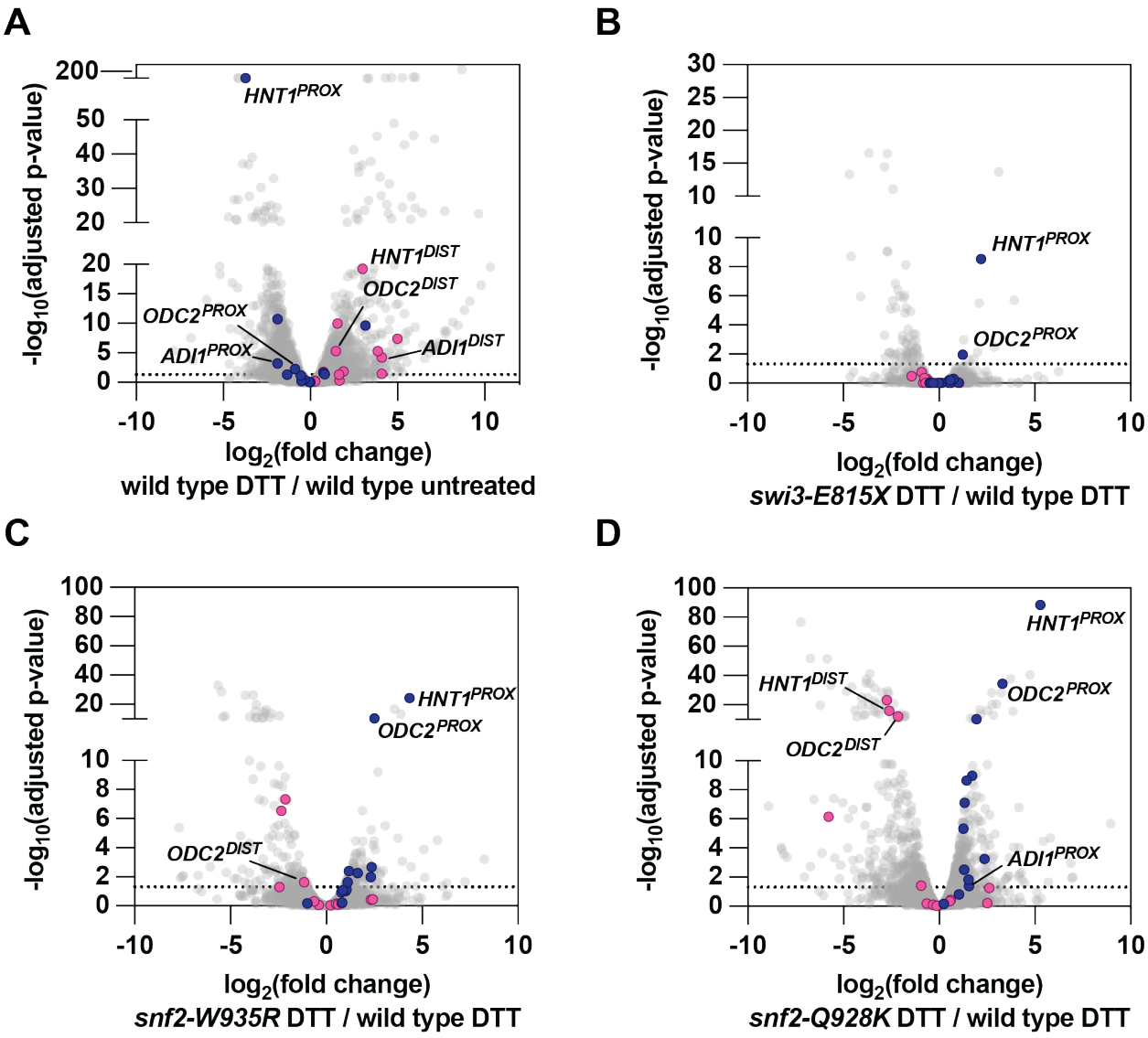

Figure 3.2: *Differential expression of alternative mRNA isoforms in Swi/Snf LUTI escape mutants*
(A) Volcano plot produced from the output of differential gene expression analysis (DESeq2) on TL-seq data for wild-type cells (UB19205 and UB28914, see Appendix B for details) that were untreated or treated with DTT (n = 4). Distal TSSs (pink) and proximal TSSs (dark blue) for genes that are Swi/Snf regulated and exhibit promoter toggling with stress induction are highlighted. **(B-D)** Same as (A), but comparing **(B)** DTT-treated *swi3-E815X* (UB19209) cells to DTT-treated *SWI3* (UB19205) cells (n = 2), **(C)** DTT-treated *snf2-W935R* (UB28922) cells to DTT-treated *SNF2* (UB28914) cells (n = 2), and **(D)** DTT-treated *snf2-Q928K* (UB28915) cells to DTT-treated *SNF2* (UB28914) cells (n = 2).

Gene	**WT PROX expression** untreated (TPM)	**WT PROX expression** DTT (TPM)	**WT DIST expression** untreated (TPM)	**WT DIST expression** DTT (TPM)	**DIST uORF translation?** From Van Dalfsen *et al*. 2018
ADI1	16.968	5.680	0.270	5.684	yes
COS10	4.557	49.754	0.158	3.394	no
ECM3	8.299	9.772	0.904	15.258	no
ERG27	706.594	837.564	0.188	7.602	no
FBA1	27089.810	26279.194	22.025	16.047	no
FLC1	3.996	3.544	146.525	526.781	no
HNT1	126.984	11.943	23.181	173.320	yes
IES6	63.197	52.341	0.149	0.625	no
ODC2	55.523	37.506	33.153	114.650	yes
PRY1	38.986	86.380	47.518	100.333	no
STM1	1984.210	664.437	1.287	4.885	no
YBR076C-A	20.828	9.554	7.268	11.092	no

Table 3.1: *Expression levels and uORF translation for Swi/Snf regulated alternative transcript isoforms induced with DTT*
(Columns 1-4) Quantification, in transcripts per million (TPM) of TL-seq reads for the 12 Swi/Snf-regulated alternative transcripts that are induced upon DTT treatment. The average of four wild-type replicates is displayed. **(Column 5)** Qualitative assessment of uORF translation based on visualization of genome-browser tracks from ribosome profiling data generated in Van Dalfsen *et al.* 2018.

For nine of the 12 genes, the distal mRNA isoform did not fit the criteria of a LUTI because it did not display evidence of lower translation efficiency compared to the proximal isoform (Table 3.1). However, these genes remain useful models to investigate Swi/Snf-dependent transcriptional interference, given that LUTI-based transcriptional interference and translational repression are not mechanistically coupled. For these non-LUTI cases, Swi/Snf may act to repress the TSS^{PROX} upon TSS^{DIST} activation, however there is no corresponding impact on protein levels. Indeed, when we deleted the distal promoter for *ERG27,* a gene that did not exhibit isoform-dependent protein level changes (Figure 3.3C), there was a subtle increase in $ERG27^{PROX}$ expression (Figure 3.3B). We conclude that the Swi/Snf complex represses transcription at select promoters that are subject to transcriptional readthrough upon DTT treatment, including LUTI-regulated promoters.

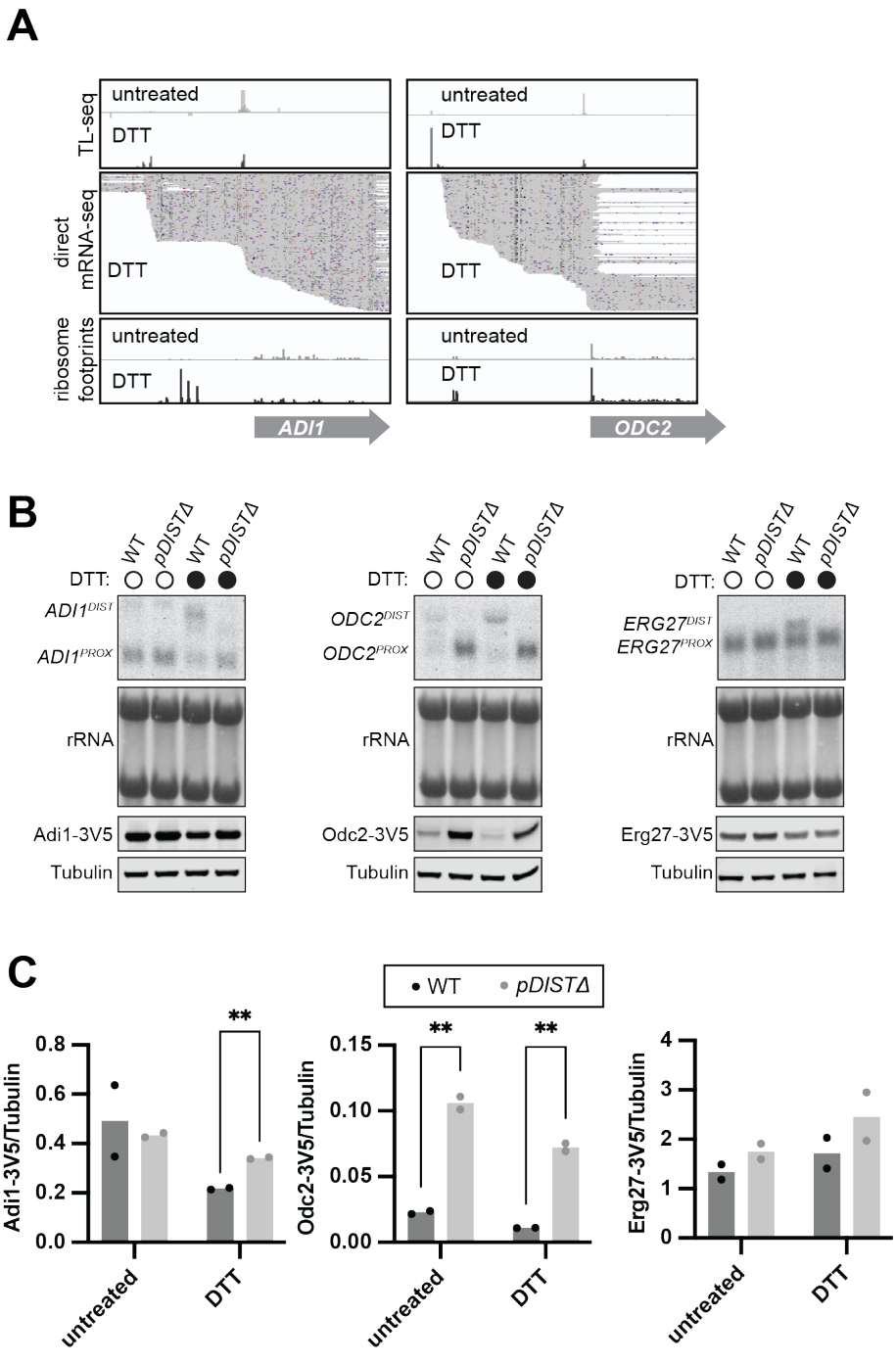

Figure 3.3: *Validation of interfering alternative transcript isoforms*
(A) RNA blot (top) and immunoblot (bottom). Both blots are specific for the V5 sequence that is C-terminally fused to *ADI1* (left), *ODC2* (middle), or *ERG27* alleles integrated at the *TRP1* locus. Transgenes either harbored the TSS^{DIST} and its promoter (WT) or lacked this sequence (*pDISTΔ*). Untreated control cells or cells treated with 5 mM DTT were collected one h post-induction. rRNA is detected on the RNA blot by methylene blue staining. For the immunoblot, alpha-tubulin is used as a loading control. One of two biological replicates is shown. Strains: *ADI1* (UB36511), $ADI1^{pDISTΔ}$ (UB36513), *ODC2* (UB36515), $ODC2^{pDISTΔ}$ (UB36521), *ERG27* (UB36594), and $ERG27^{pDISTΔ}$ (UB36596). **(B)** Genome browser snapshot. TL-Seq and direct mRNA-seq data from this study are overlaid with ribosome footprints from Van Dalfsen

et. al 2018 for the genes *ADI1* and *ODC2*. For *ODC2*, the distal isoform is expressed in the unstressed and DTT condition, but expressed increases with DTT treatment. For *ADI1,* the distal isoform is expressed exclusively in response to DTT treatment. In both cases, there is uORF translation within the 5′ leader sequence of the distal isoform. **(C)** Quantification of immunoblot portrayed in (B) for two biological replicates. Student's t test (two-tailed) revealed a significant increase in Odc2 protein levels upon deletion of the $ODC2^{DIST}$ promoter in both untreated and DTT-treated cells (p =0.0036 [untreated], p = 0.0023 [DTT]), whereas Adi1 protein levels were significantly increased with deletion of the $ADI1^{DIST}$ promoter in DTT-treated condition only (p = 0.7281 [untreated], p = 0.0016 [DTT]. Erg27 protein levels were not found to be significantly different with deletion of the $ERG27^{DIST}$ promoter in either condition (p = 0.1988 [untreated], p = 0.3291 [DTT]).

Among the LUTI escape mutants, the *snf2-Q928K* mutant displayed the most changes in genome-wide TSS expression levels relative to wild type (Figure 3.2D). This is consistent with mRNA-seq results which revealed this mutant was more pleiotropic compared to the *snf2-W935R* or *swi3-E815X* mutants. In *snf2-Q928K* cells, the TSS^{DIST} for five genes was downregulated (*HNT1, ODC2, PRY1, ERG27,* and *FLC1*), thus TSS^{PROX} upregulation for these genes likely results from reduced transcriptional readthrough in this mutant (Figure 3.3D). The *snf2-W935R* mutant also exhibited downregulation of the TSS^{DIST} for four genes (*ODC2, PRY1, ERG27,* and *FLC1*), albeit to a lesser extent than in *snf2-Q928K* cells, consistent with the *snf2-W935R* mutation conferring more mild loss of Swi/Snf function compared to the *snf2-Q928K* mutation (Figure 3.3C). Finally, the *swi3-E815X* mutant had the fewest changes in TSS expression compared to wild type, both globally and among the 12 transcriptional interference targets, exhibiting significant upregulation of the $ODC2^{PROX}$ and $HNT1^{PROX}$ isoforms and no significant changes for TSS^{DIST} levels (Figure 3.3B).

Gene	TSS^{DIST} consensus cluster?	Readthrough transcript?	Snf2 binding?
HNT1	Yes	Yes	Yes
SRM1	Yes	No	No
PRY1	Yes	Yes	No
PCM1	Yes	Yes	No
COX20	No	Yes	Yes
MSK1	No	No	No
SOM1	No	Yes	Yes
GTT1	No	Yes	No
IRC4	No	Yes	No
CRR1	No	No	No
HEM1	No	Yes	Yes
OXA1	No	Yes	No
NRG2	No	Yes	Yes
YPL067C	No	No	Yes
CTS1	No	No	No

YHB1	No	Yes	Yes
FLR1	No	No	No
SRL1	No	No	Yes
SET2	No	No	No

Table 3.2: *Screening of LUTI candidates from Van Dalfsen et al. 2018*
Summary of TL-seq, Nanopore direct mRNA-seq, and Snf2 ChIP-seq results among a list of previously published LUTIs in the SK1 strain background. Detection of 5′ extended isoforms from this list was determined based on (1) whether a consensus cluster was called by cageR analysis of TL-seq data and (2) whether a full-length readthrough mRNA isoform was visible in Nanopore direct mRNA-seq data. Snf2 binding was determined by whether a peak was called by MACS2 in the DTT condition.

In addition to our unbiased identification of Swi/Snf regulated TSSs, we also examined a list of 19 previously identified LUTIs induced during the UPR (Dalfsen et al., 2018). These LUTIs were originally identified in the SK1 strain background based on showing (1) increased expression of a 5′ extended mRNA based on mRNA-seq data and (2) decreased translation efficiency based on ribosome profiling data, each of which dependent on the UPR transcription factor Hac1. Our TL-seq analysis detected a TSS^{DIST} for only four of these 19 genes, although low levels of 5′ extended mRNA isoforms were visible for several more genes in our Nanopore direct RNA-seq data (Table 3.2, Figure 3.4). The lack of detection for distal TSSs among these LUTI candidates may be a result of low expression, as TL-seq is not as sensitive as mRNA sequencing for detecting low-abundant transcripts. Among the four genes with a TSS^{DIST} called by TL-seq, only *HNT1* also exhibited Snf2 binding with DTT treatment, indicating Swi/Snf does not regulate genes with dual promoters in a general manner during stress and instead exhibits target specificity among alternative transcripts.

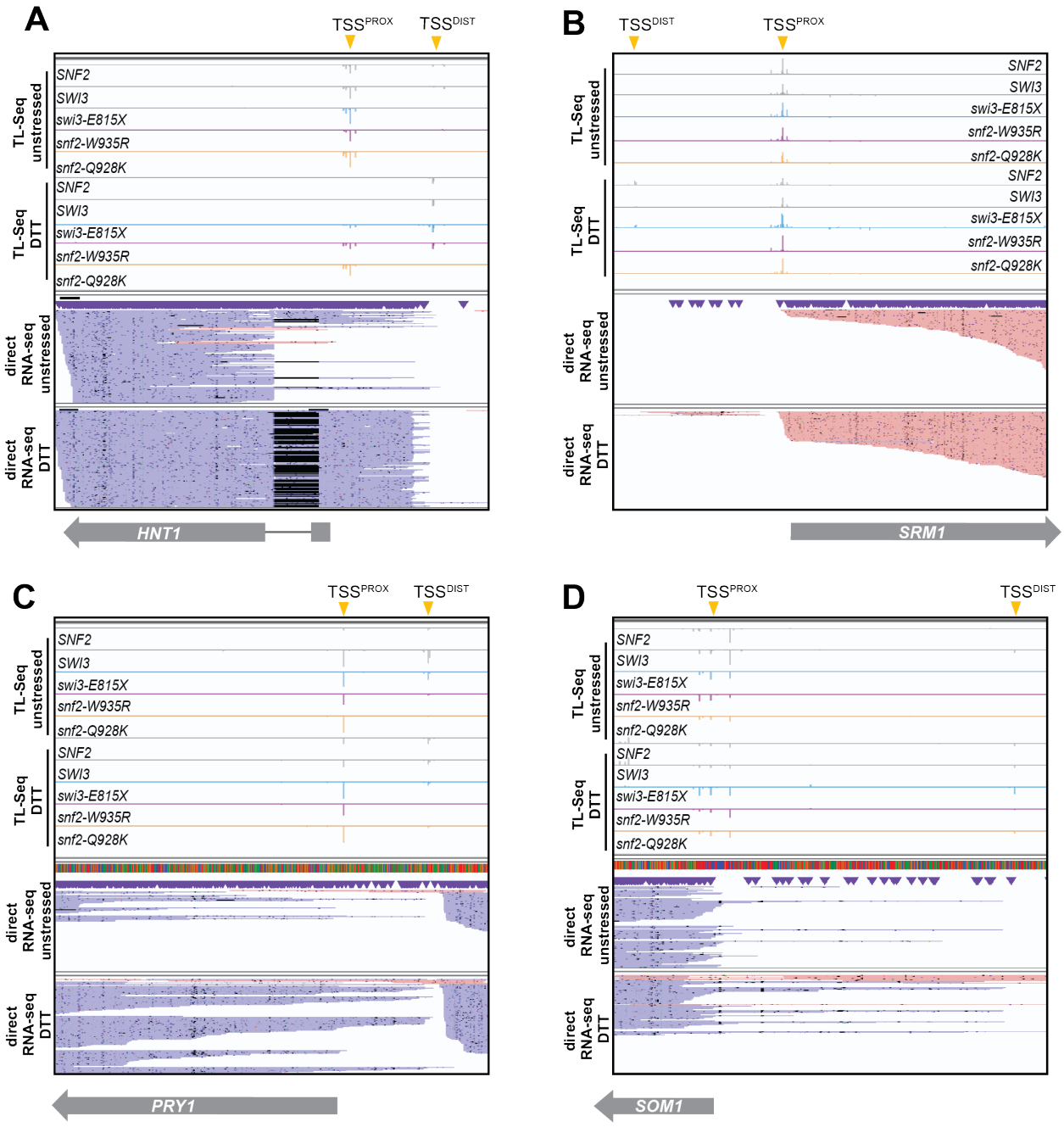

Figure 3.4: *TL-seq and direct mRNA-seq analysis of LUTI candidates from Van Dalfsen et al. 2018*
Genome browser snapshots portraying TL-seq and Nanopore direct mRNA-seq. TL-seq reads for *SNF2* (UB30387), *SWI3* (UB30070), *swi3-E815X* (UB30071), *snf2-W935R* (UB30391), and *snf2-Q928K* (UB30389) and direct mRNA-seq reads for *SWI3* (UB30070) are shown for cells that were untreated (top) or treated with 5 mM DTT (bottom). One of two biological replicates is portrayed, except for direct mRNA-sequencing for which only one replicate was performed. **(A)** The *HNT1* locus has a DTT-induced 5′ extended mRNA isoform that is anticorrelated with the canonical mRNA isoform driven by the proximal promoter. *HNT1*^{PROX} is upregulated in LUTI escape mutants. **(B)** TL-seq consensus clustering analysis called a distal promoter for the *SRM1* locus (Table 3.2), although Nanopore sequencing reveals this distal-driven transcript does not read through the TSS^{PROX}. **(C)** TL-seq consensus clustering analysis called a

distal promoter for the *PRY1* locus that is expressed in both unstressed and stressed conditions. Nanopore sequencing revealed a full-length 5′ extended mRNA isoform, although this locus is not bound by Snf2 (Table 3.2) indicating *PRY1*^{PROX} is not a Swi/Snf target. **(D)** A full-length readthrough mRNA isoform is detected for *SOM1* by Nanopore direct mRNA-seq, however TL-seq consensus clustering did not call a distal TSS (Table 3.2), perhaps due to low expression from the distal promoter.

Overall, TL-seq analyses reveal that the Swi/Snf complex regulates transcriptional interference in response to protein folding stress through two routes: activation of select distal promoters and repression of the downstream proximal promoters. It seems the *snf2-Q928K* mutation reduces canonical transcription initiation activity by the Swi/Snf complex, consistent with our previous finding that *SRG1* expression is reduced in this mutant. However, the *snf2-W935R* mutation only slightly reduces initiation of the TSS^{DIST} for some loci, yet still disrupts repressive activity by Swi/Snf at the TSS^{PROX}. The *swi3-E815X* mutation also reduces repressive activity by Swi/Snf at the TSS^{PROX} but to a lesser extent than the *snf2-W935R* mutant.

Swi/Snf is necessary for nucleosome remodeling at the TSS^{PROX} at select loci with dual promoters

To investigate whether transcriptional interference at loci affected by LUTI escape mutants is mediated by changes in chromatin structure, we performed micrococcal nuclease digestion and whole genome sequencing (MNase-seq). When we analyzed the nucleosome profiles for the LUTI-regulated gene *HNT1* in wild-type cells, we observed a shift from stable nucleosome positioning for the -1 and +1 nucleosomes surrounding the *HNT1*^{PROX} TSS to fuzzy positioning upon DTT treatment (Figure 3.5), indicating that *HNT1*^{LUTI} expression is associated with nucleosome remodeling downstream of the *HNT1*^{LUTI} TSS. In contrast, the +1 nucleosome relative to the *HNT1*^{PROX} TSS remained stably positioned in all three LUTI escape mutants (Figure 3.5), suggesting LUTI-coupled nucleosome remodeling is impaired in these mutants. The -1 nucleosome relative to the *HNT1*^{PROX} TSS, which spans the *HNT1*^{LUTI} TSS in untreated cells, also displayed a stronger MNase-seq signal in the *snf2-Q928K* and *snf2-W935R* mutants with DTT treatment, although its position was shifted compared to the untreated condition (Figure 3.5). Lack of remodeling for this nucleosome may preclude *HNT1*^{LUTI} expression during UPR induction in *snf2-Q928K* cells, as remodeling of the chromatin upstream of the *HNT1*^{LUTI} TSS is associated with high activation of *HNT1*^{LUTI} in wild-type cells.

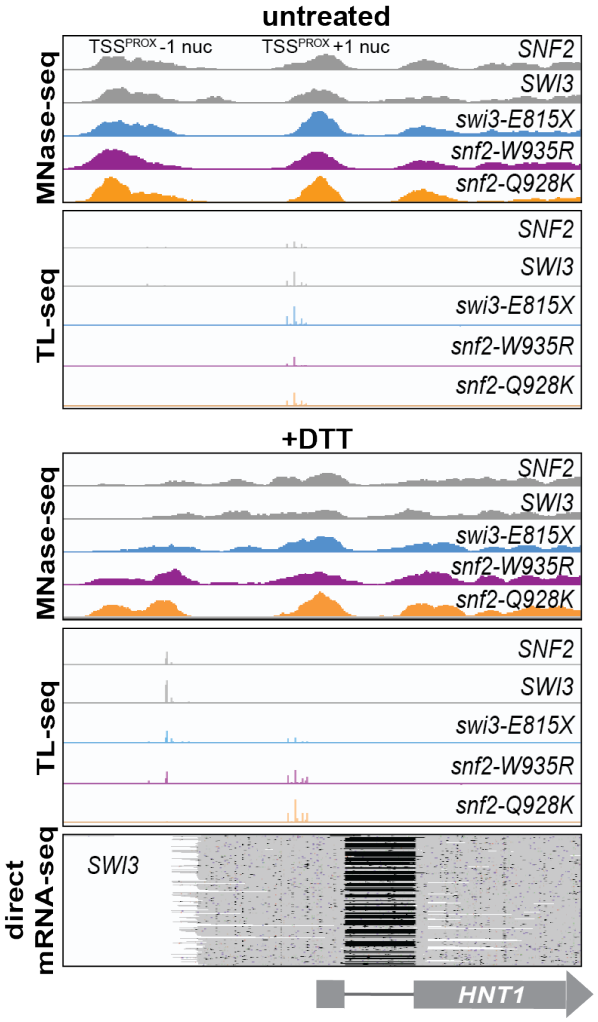

Figure 3.5: *Nucleosome repositioning at the HNT1 locus upon induction of HNT1^{LUTI} is reduced in Swi/Snf mutants*
Genome browser snapshots portraying MNase-seq, TL-seq, and Nanopore direct mRNA-seq for the *HNT1* locus for *SNF2* (UB30387), *SWI3* (UB30070), *swi3-E815X* (UB30071), *snf2-W935R* (UB30391), and *snf2-Q928K* (UB30389) cells that were untreated (top) or treated with 5 mM DTT (bottom). One of two biological replicates is portrayed, except for direct mRNA-sequencing for which only one replicate was performed.

We next investigated whether nucleosome positioning was also stabilized in the LUTI escape mutants for the other 11 TSS^{PROX} loci. We compared nucleosome fuzziness scores, a quantitative measurement for nucleosome positioning in which higher fuzziness corresponds to more poorly positioned nucleosomes, across wild-type and mutant cells. Both the -1 and +1 nucleosomes surrounding each TSS^{PROX} became more fuzzy in wild-type cells upon DTT treatment compared to unstressed conditions, indicating remodeling of these nucleosomes is associated with distal promoter expression (paired t test, two-tailed, p = 0.0462 [-1 nuc], p = 0.0729 [+1 nuc]; Figures 3.6B and 3.6C). For half of the 12 genes investigated, as with *HNT1*, the TSS^{PROX} -1 nucleosome is also the +1 nucleosome for the TSS^{DIST}. In these cases, remodeling of this nucleosome may be required to facilitate proper initiation of the distal isoform. Nucleosome fuzziness for the TSS^{PROX} -1 nucleosome was not significantly different in the *swi3-E815X* or *snf2-W935R* mutants compared to wild type (p = 0.1283 [*swi3-E815X*], p = 0.2043 [*snf2-W935R*]), but there was a significant decrease in fuzziness for the *snf2-Q928K* mutant (p = 0.0129; Figure 3.6C). Together, these results combined with our TL-seq results are consistent with a model in which *snf2-Q928K* cells are defective for transcription initiation, as opposed to *snf2-W935R* and *swi3-E815X* cells, which may be defective for nucleosome remodeling at positions downstream from the transcriptionally active TSS^{DIST}.

In response to protein folding stress, all three LUTI escape mutants exhibited reduced nucleosome fuzziness for the TSS^{PROX} +1 nucleosome compared to wild-type cells (p = 0.0470 [*swi3-E815X*], p = 0.0397 [*snf2-W935R*], p = 0.0040 [*snf2-Q928K*]; Figure 3.6C). Excitingly, these results align with the previous finding that increased TSS^{PROX} +1 nucleosome fuzziness was found to be correlated with more potent LUTI-

based transcriptional interference (Tresenrider et al., 2021). We also examined changes in nucleosome occupancy within the nucleosome depleted region (NDR) for the TSS^{PROX} and found that upon DTT treatment, nucleosome occupancy within the NDR increased on average by 1.9-fold compared to the unstressed condition ($p = 0.0445$; Figure 3.6D). Each LUTI escape mutant had lower nucleosome occupancy within the TSS^{PROX} NDR compared to wild-type cells upon DTT treatment (not significant, Figure 3.6D), indicating that increased expression of proximal mRNA isoforms in the mutants may result from increased promoter accessibility. Analyzing the binding profiles of Snf2 at the twelve genes with Swi/Snf-regulated alternative transcript isoforms revealed that the LUTI escape mutants still exhibit Snf2 binding at these target loci, although Snf2 enrichment in the *swi3-E815X* mutant was slightly reduced compared to wild type (Figure 3.6E). In fact, the *snf2-W935R* and *snf2-Q928K* mutants had increased levels of Snf2 binding, indicating these mutations impair nucleosome remodeling activity rather than recruitment of the complex.

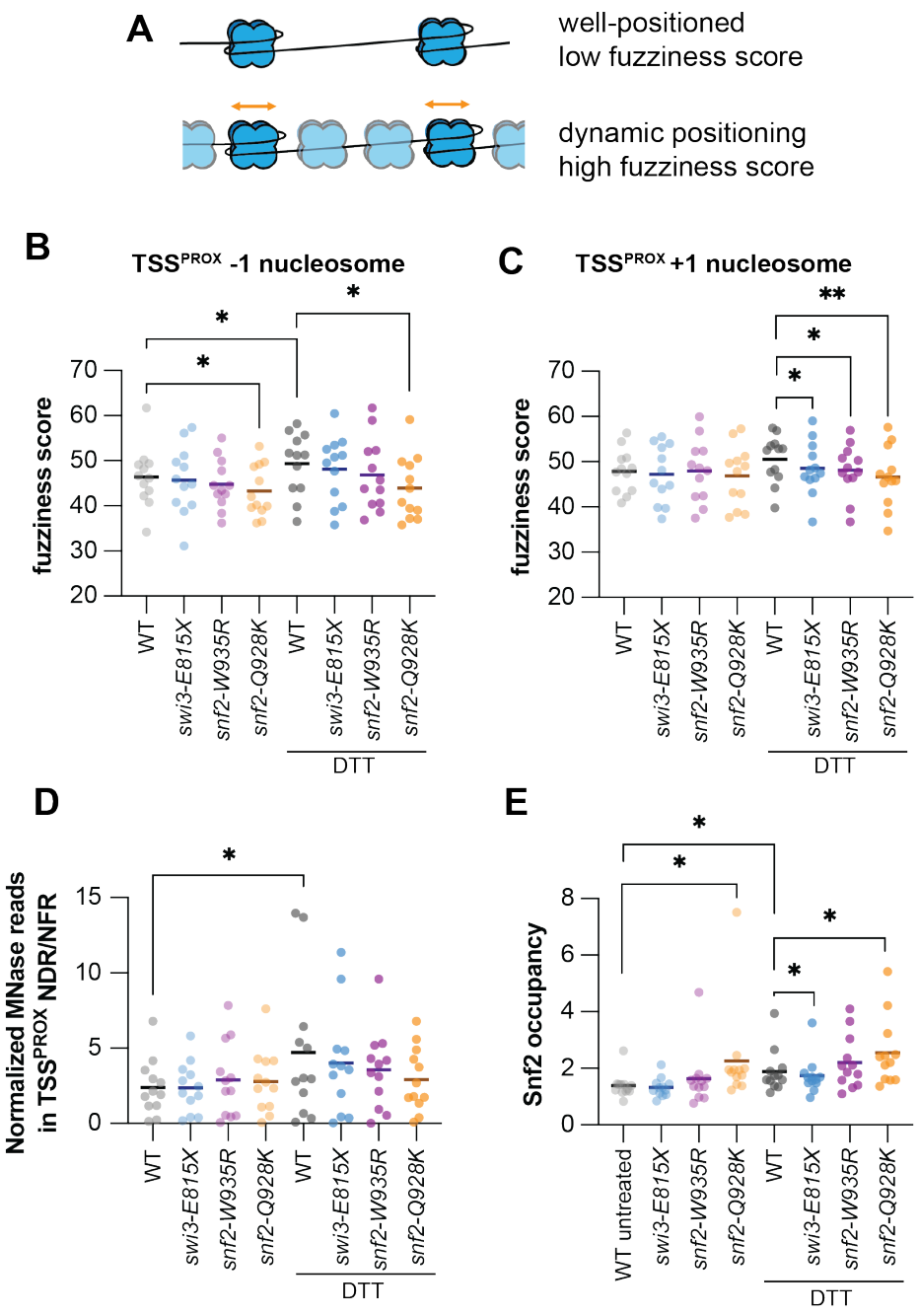

Figure 3.6: *Swi/Snf regulates nucleosome positioning at sites with alternative transcription during DTT-induced stress*

(A) schematic of nucleosome stability (top) versus nucleosome fuzziness (bottom). **(B) .** Nucleosome fuzziness scores output from DANPOS3 for the -1 nucleosome relative to the TSS^{PROX} in wild-type cells (n = 4, strains UB30387 and UB30070) and *swi3-E815X* (UB30071), *snf2-W935R* (UB30391), and *snf2-Q928K* (UB30389) mutants (n = 2) that were untreated or treated with 5 mM DTT. A paired t test was performed on wild type fuzziness scores comparing untreated to DTT-treated cells (two-tailed, p = 0.0462) and each mutant-to-wild type comparison in untreated conditions (p = 0.5938 [*swi3-E815X*], p = 0.2487 [*snf2-W935R*], p = 0.0371 [*snf2-Q928K*]) or with DTT treatment (p = 0.1283 [*swi3-E815X*], p = 0.2043 [*snf2-W935R*], p = 0.0129 [*snf2-Q928K*]). **(C)** Same as (B), but for the +1 nucleosome relative to the TSS^{PROX}. A paired t test was performed on wild type fuzziness scores comparing untreated to DTT-treated cells (two-

tailed, p = 0.0729) and each mutant-to-wild type comparison in untreated conditions (p = 0.4463 [*swi3-E815X*], p = 0.9578 [*snf2-W935R*], p = 0.4348 [*snf2-Q928K*]) or with DTT treatment (p = 0.0470 [*swi3-E815X*], p = 0.0397 [*snf2-W935R*], p = 0.0040 [*snf2-Q928K*]). **(D)** same as (B and C) except for the nucleosome free/nucleosome depleted regions at each PROX promoter. A paired t test was performed on wild-type nucleosome occupancy comparing untreated to DTT-treated cells (two-tailed, p = 0.0445) and each mutant-to-wild type comparison in untreated conditions (p = 0.9629 [*swi3-E815X*], p = 0.4263 [*snf2-W935R*], p = 0.5048 [*snf2-Q928K*]) or with 5 mM DTT treatment (p = 0.1441 [*swi3-E815X*], p = 0.2004 [*snf2-W935R*], p = 0.2293 [*snf2-Q928K*]). **(E)** Snf2 ChIP-seq signals for genes with Swi/Snf-regulated alternative transcripts. The average Snf2 binding levels are compared between wild type (n = 4) and LUTI escape mutants (n = 2) in the untreated condition (paired t test, two-tailed, p = 0.2263 [*swi3-E815X*], p = 0.1839 [*snf2-W935R*], p = 0.0385 [*snf2-Q928K*]) and DTT-treated conditions (p = 0.0398 [*swi3-E815X*], p = 0.0514 [*snf2-W935R*], p = 0.0300 [*snf2-Q928K*]). Strains: wild type (UB30387 and UB30070), *swi3-E815X* (UB30071), *snf2-W935R* (UB30391), and *snf2-Q928K* (UB30389).

Swi/Snf facilitates rapid and sustained repression of *HNT1*^{PROX} upon *HNT1*^{LUTI} induction

To further dissect the role of the Swi/Snf complex in transcriptional interference, we next examined the kinetics of *HNT1*^{PROX} repression and chromatin changes when *HNT1*^{LUTI} is induced. Wild-type cells induced *HNT1*^{LUTI} within 5 minutes of DTT treatment and expression of *HNT1*^{LUTI} further increased 3-fold by 30 minutes, at which time *HNT1*^{PROX} was almost completely silenced (Figures 3.7A and 3.7C). Snf2 was also recruited to the *HNT1* locus within 5 minutes of DTT treatment, and levels of Snf2 binding increased over time in a pattern that strikingly resembled the *HNT1*^{LUTI} expression pattern (Figures 3.7C and 3.7D), introducing the possibility that Snf2 recruitment is coupled to *HNT1*^{LUTI} transcription. Along with this rapid recruitment of the Swi/Snf complex following UPR induction, the -1 and +1 nucleosomes surrounding the *HNT1*^{PROX} TSS were also remodeled within 5 minutes of DTT treatment (Figure 3.7E).

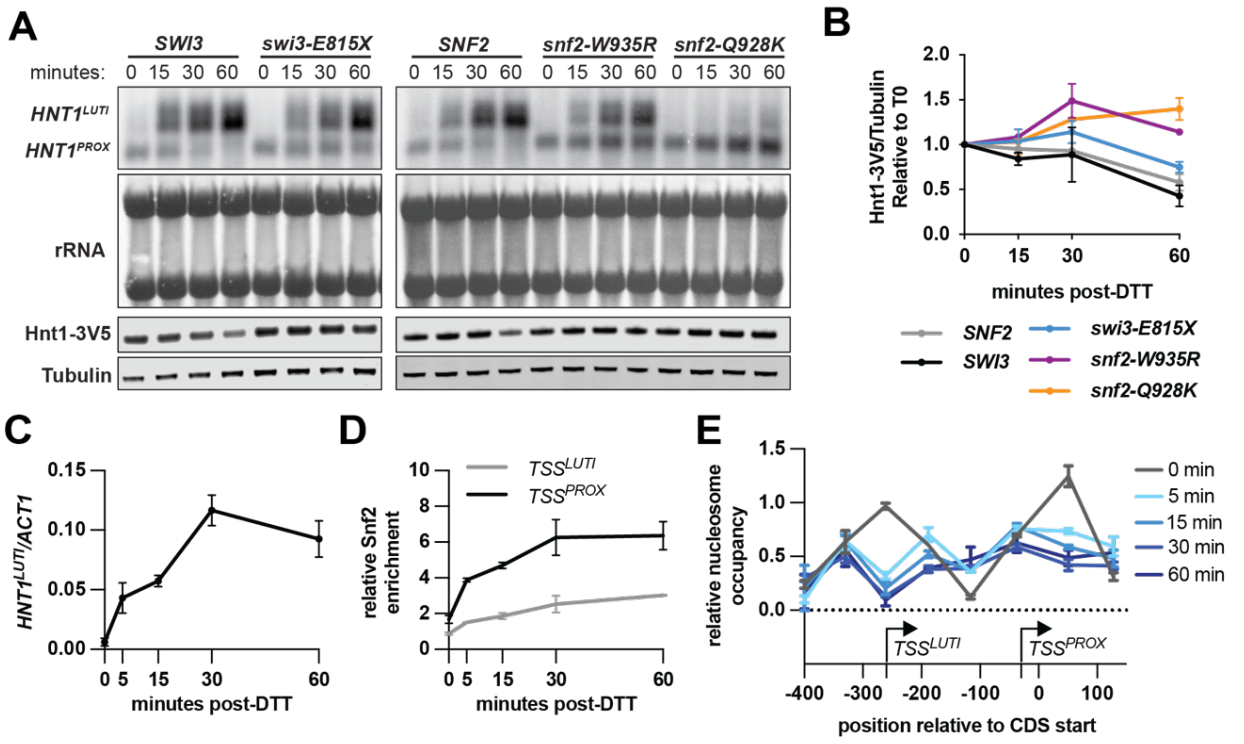

Figure 3.7: *Swi/Snf facilitates rapid and sustained repression of HNT1^{PROX} upon HNT1^{LUTI} induction*
(A) RNA blot probed for the *HNT1* CDS (top) and immunoblot against the V5 epitope in strains harboring an *HNT1-3V5* fusion allele (bottom). For the RNA blot, rRNA bands are detected by methylene blue staining. For the immunoblot, alpha-tubulin is used as a loading control. Cells were collected at 0, 15, 30, and 60 minutes after treatment with 5 mM DTT for RNA and protein extraction. Strains: *SWI3* (UB24251), *swi3-E815X* (UB24253), *SNF2* (UB30152), *snf2-W935R* (UB30156), and *snf2-Q928K* (UB30154). One of two biological replicates is shown. **(B)** Quantification of immunoblots portrayed in (A) for two biological replicates. **(C)** RT-qPCR measuring relative abundance of *HNT1^{LUTI}* mRNA in cells (UB29161) collected at 0, 5, 15, 30, and 60 minutes after DTT treatment (n = 2). **(D)** Snf2 ChIP-qPCR measuring relative occupancy of Snf2-3V5 (Swi/Snf) at the *HNT1^{LUTI}* TSS (black) or *HNT1^{PROX}* TSS (gray; n = 2). A primer pair directed against the heterochromatic HMR locus was used as an internal control. Cell collection was done in parallel with cells collected in (C) and (E). **(E)** MNase-qPCR measuring relative nucleosome occupancy at the *HNT1* 5′ regulatory region (n = 2). A primer pair directed against the *PHO5* promoter was used as an internal control.

Consistent with the TL-seq results, *snf2-W935R* and *swi3-E815X* cells induced *HNT1^{LUTI}* but failed to silence *HNT1^{PROX}*, exhibiting higher levels of the *HNT1^{PROX}* isoform visible as early as 15 minutes post-DTT treatment (Figure 3.7A). In contrast, *snf2-Q928K* cells failed to express *HNT1^{LUTI}* and exhibited dramatic upregulation of *HNT1^{PROX}* (Figure 3.7A). The high accumulation of *HNT1^{PROX}* in this mutant resembled the outcome of deleting the *HNT1^{LUTI}* promoter (Figure 3.8), suggesting that increased *HNT1^{PROX}* expression in *snf2-Q928K* cells was due solely to the lack of *HNT1^{LUTI}* expression.

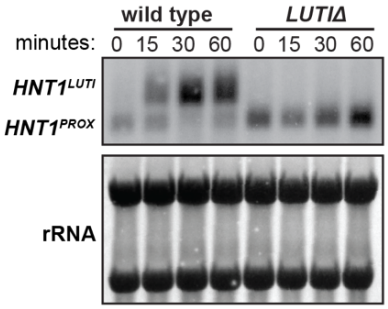

Figure 3.8: *Blocking HNT1^{LUTI} expression results in high accumulation of HNT1^{PROX} mRNA with UPR induction*
RNA blot probed for the *HNT1* CDS in wild type cells (UB32339) or cells lacking the *HNT1^{LUTI}* promoter (*LUTIΔ*, UB32342). Cells were collected at 0, 15, 30, and 60 minutes after treatment with 5 mM DTT for RNA extraction. rRNA bands were detected by methylene blue staining.

Importantly, the *snf2-Q928K* mutant properly activated the UPR response, as indicated by cytosolic splicing of the UPR transcription factor *HAC1* mRNA (Cox and Walter, 1996; Rüegsegger et al., 2001) (Figure 3.9). Activation of Hac1 splicing in the *snf2-Q928K* mutant suggests its transcriptional defects are specific to certain targets, including *HNT1*, and do not result from failure to respond to protein folding stress altogether. As expected, increased levels of the coding *HNT1^{PROX}* mRNA isoform in each of the Swi/Snf LUTI escape mutants resulted in increased Hnt1-3V5 protein levels (Figures 3.7A and 3.7B).

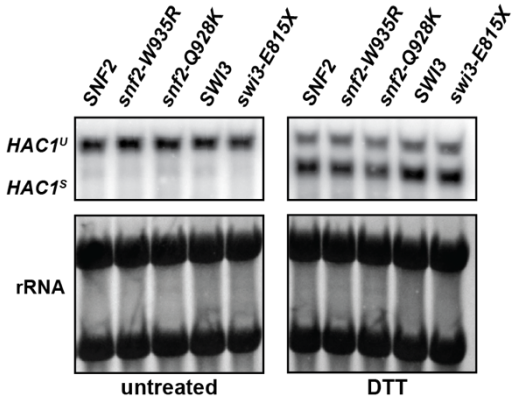

Figure 3.9: *LUTI escape mutants properly activate the UPR*
RNA blot probed for the *HAC1* CDS in cells that were untreated or treated with DTT for 1 h. Strains: *SNF2* (UB30152), *snf2-W935R* (UB30156), *snf2-Q928K* (UB30154), *SWI3* (UB24251), and *swi3-E815X* (UB24253).

Previous work revealed that histone 3 lysine 4 dimethylation (H3K4me2) and lysine 36 trimethylation (H3K36me3) methylation by the histone methyltransferases Set1 and Set2, respectively, along with histone deacetylase machinery recruited by each methylation pathway, is necessary for the LUTI-based repression of certain genes (Chia et al., 2017; Tresenrider et al., 2021). To investigate whether these pathways also affect LUTI-based repression of *HNT1*, we assayed *HNT1* transcript isoform levels in *set2Δ set3Δ* cells, which lack both of these histone methylation/deacetylation pathways. Although we observed increased H3K36me3 levels at the *HNT1^{PROX}* TSS upon *HNT1^{LUTI}* induction (Figure 3.10C), this histone modifier mutant had no effect on *HNT1* regulation (Figures 3.10A and 3.10B), indicating histone methylation and Swi/Snf remodeling act in separate, parallel pathways to achieve LUTI-based gene repression for different gene targets.

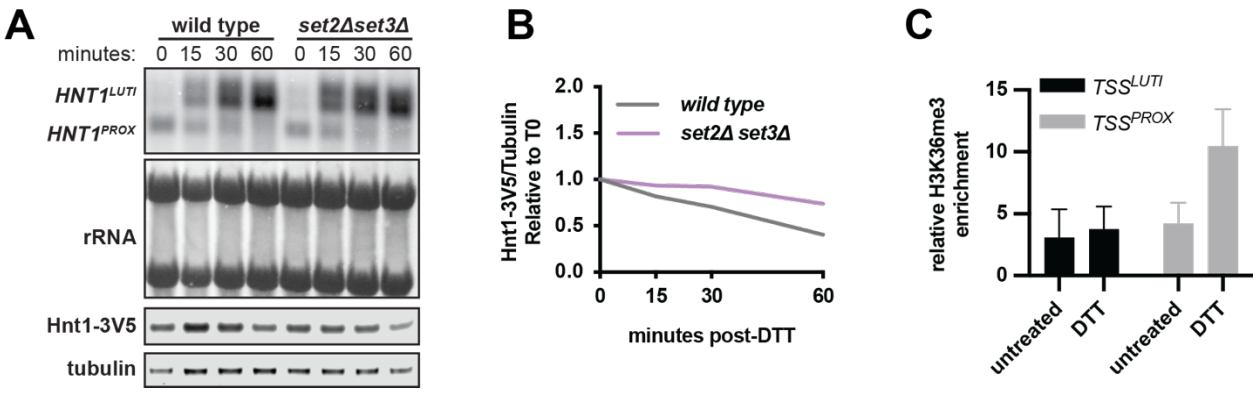

Figure 3.10: *H3K36me3 and H3K4me2 pathways do not impact HNT1 regulation*
(A) RNA blot probed for the *HNT1* CDS (top) and immunoblot against the V5 epitope in strains harboring an *HNT1-3V5* fusion allele (bottom). For the RNA blot, rRNA bands are detected by methylene blue staining. For the immunoblot, alpha-tubulin is used as a loading control. Cells were collected at 0, 15, 30, and 60 minutes after treatment with 5 mM DTT for RNA and protein extraction. Strains: UB4784 (WT) and UB24198 (*set2Δ set3Δ*)**. (B)** Quantification of immunoblots portrayed in (A) for one biological replicate. (C) Histone ChIP-qPCR measuring enrichment of H3K36me3 at the *HNT1* locus in unstressed and DTT-treated cells for two biological replicates collected with and without 5 mM DTT treatment for 1 h. A primer pair directed against the heterochromatic HMR locus was used as an internal control.

Chromatin changes at the *HNT1* locus depend on transcription initiation and elongation of $HNT1^{LUTI}$

We next sought to investigate whether Snf2 recruitment and nucleosome remodeling at the *HNT1* locus is dependent on transcription initiation of $HNT1^{LUTI}$, its elongation through downstream chromatin, or both its initiation and elongation. We engineered two LUTI perturbation mutants: one lacking the $HNT1^{LUTI}$ promoter (*LUTIΔ*) and the other containing an insertion of a strong transcriptional terminator sequence (*CYC1t)* between the $HNT1^{LUTI}$ and $HNT1^{PROX}$ TSSs (Figure 3.10A). Both perturbations eliminated full-length $HNT1^{LUTI}$ expression (Figure 3.11B).

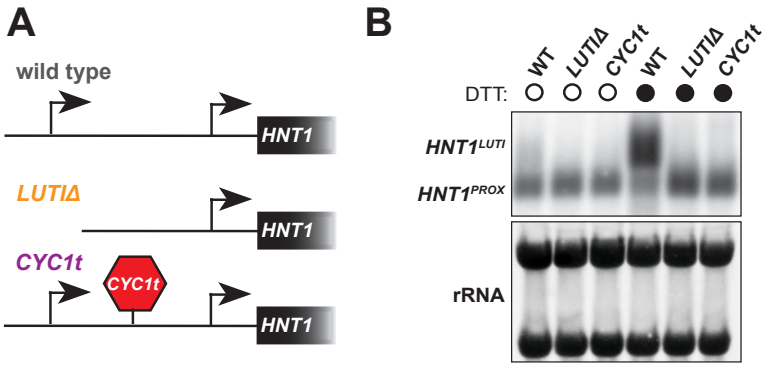

Figure 3.11: *Cis regulatory mutations to block HNT1^{LUTI} expression*
(A) Schematic of *cis* regulatory *HNT1* mutant alleles. **(B)** RNA blot probed for the *HNT1* CDS with RNA collected from wild-type (UB32339), *HNT1^{LUTIΔ}* (UB32342), and *HNT1$^{LUTI\text{-}CYC1t}$* (UB36048) cells that were untreated or treated with 5 mM DTT for 30 min.

As the *HNT1^{LUTI}* TSS chromatin is deleted in the *LUTIΔ* mutant, the signal for Snf2 binding was reduced to background levels in *LUTIΔ* cells at this position (Figure 3.12A). Snf2 binding at the *HNT1^{LUTI}* TSS was unaffected by *CYC1t* insertion, suggesting *HNT1^{LUTI}* initiation is sufficient for Swi/Snf recruitment upon DTT treatment (Figure 3.12A). Interestingly, binding of Snf2 at the *HNT1^{PROX}* TSS was reduced in both *LUTIΔ* and *CYC1t* mutants compared to wild-type cells upon UPR induction (Two-way ANOVA, p = 0.0093 [*LUTIΔ*], p = 0.0254 [*CYC1t*]; Figure 3.12B). To assay nucleosome remodeling in the LUTI perturbation mutants, we restricted our analysis to positions with shared sequence identity among all three strains, which encompasses the *HNT1^{PROX}* +1 nucleosome. In contrast to wild-type cells, this nucleosome was not remodeled in *LUTIΔ* or *CYC1t* cells with UPR induction (Figure 3.12C).

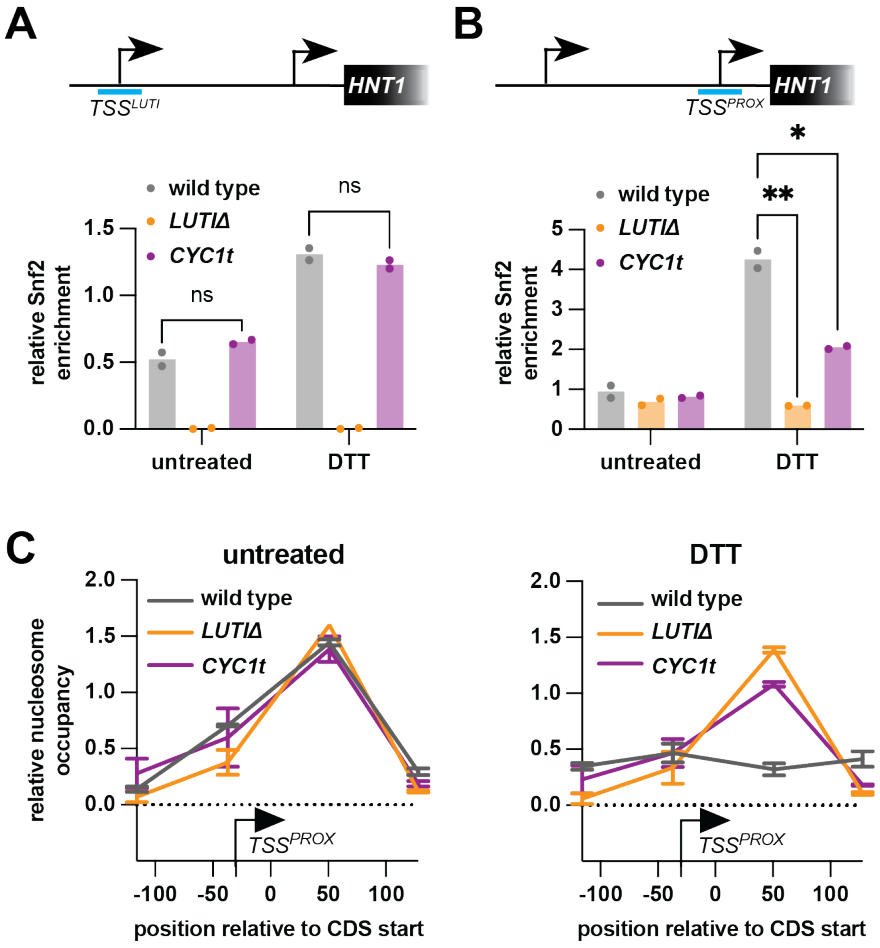

Figure 3.12: *Chromatin changes at HNT1 depend on transcription initiation and elongation of HNT1^{LUTI}*
(A) Snf2 ChIP-qPCR measuring relative occupancy of Snf2 at the *HNT1^{LUTI}* TSS (n = 2). Cells were collected in parallel with cells collected in (B), (D), and (E). **(B)** Snf2 ChIP-qPCR measuring relative occupancy of Snf2 at the *HNT1^{PROX}* TSS (n = 2). There is significantly decreased Snf2 binding in DTT-treated *HNT^{LUTIΔ}* cells (two-way ANOVA, p = 0.0093) and *HNT1$^{LUTI\text{-}CYC1t}$* cells (two-way ANOVA, p = 0.0254) compared to wild type. Differences between the *HNT^{LUTIΔ}* and *HNT1$^{LUTI\text{-}CYC1t}$* cells were not statistically significant (two-way ANOVA, p = 0.0254). **(C)** MNase-qPCR measuring relative occupancy for the *HNT1^{PROX}* +1 nucleosome.

Altogether, these results revealed that *HNT1^{LUTI}* initiation is sufficient for Swi/Snf recruitment to the *HNT1* locus, but downstream Swi/Snf occupancy and nucleosome remodeling at the *HNT1^{PROX}* promoter requires productive elongation of *HNT1^{LUTI}*. Importantly, the lack of Snf2 binding and nucleosome remodeling at the *HNT1^{PROX}* TSS in the *CYC1t* mutant implies remodeling of the *HNT1^{PROX}* +1 nucleosome in wild-type cells is an active process by the Swi/Snf complex rather than a result of cascading effects from upstream remodeling at the *HNT1^{LUTI}* promoter.

Swi/Snf regulates gene-body nucleosome occupancy for its canonical gene targets

We wondered whether Swi/Snf-dependent transcriptional interference stems from a general function of the Swi/Snf complex in nucleosome remodeling during transcription elongation. Previous studies have implicated the Swi/Snf complex in transcription elongation (Schwabish and Struhl, 2007; Shivaswamy and Iyer, 2008), however in these cases mutant analysis was performed using *snf2Δ* cells which exhibit severe transcriptional defects, making it difficult to uncouple transcription initiation from elongation phenotypes at target loci. The *swi3-E815X* and *snf2-W935R* mutants, which exhibit few changes in global transcript levels (Chapter 2), present a unique opportunity to investigate Swi/Snf regulation of chromatin at its gene targets in a context where transcription levels are largely unperturbed.

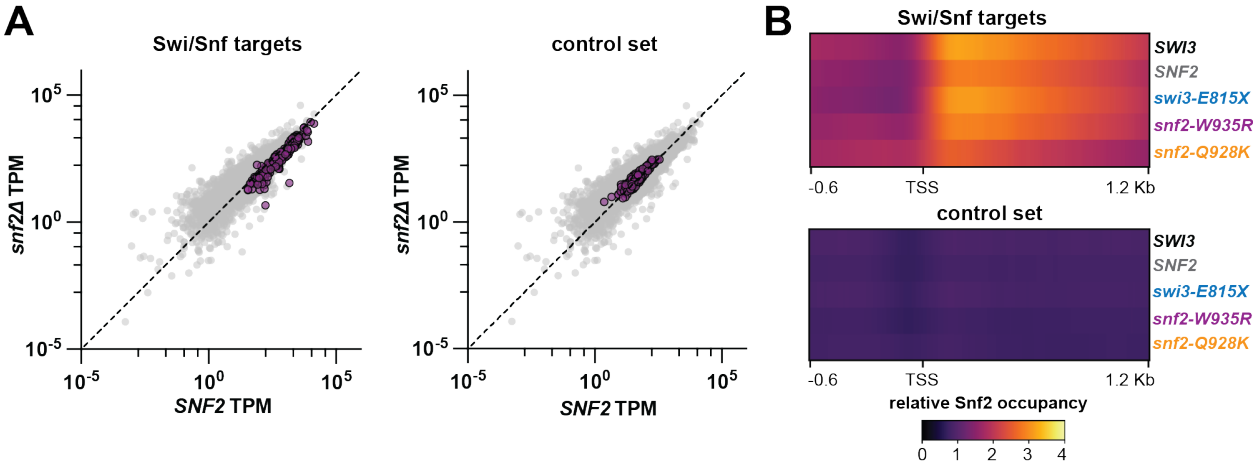

Figure 3.13: *Identification of Swi/Snf canonical targets in unstressed cells*
(A) Scatterplots comparing mRNA abundances (TPM) between *snf2Δ* (UB29781) and *SNF2* (UB28914) cells. Genes that are Swi/Snf-regulated (left, n = 250) or genes from a non-regulated control set (right, n = 250) are highlighted in purple. **(B)** Heatmaps portraying normalized Snf2 occupancy generated from Snf2 ChIP-seq data for genes that are Swi/Snf-regulated (top) or the non-regulated control set (bottom). Strains: *SWI3* (UB30070), *SNF2* (UB30387), *swi3-E815X* (UB30071), *snf2-W935R* (UB30391), and *snf2-Q928K* (UB30389).

First, we generated a list of genes that were significantly downregulated in *snf2Δ* cells compared to wild type under normal, unstressed conditions (DESeq2, adjusted p-value < 0.05). From this list, we next eliminated genes that were not bound by Snf2 based on ChIP-seq data, as these are not direct Swi/Snf targets. Finally, we eliminated genes that were also differentially regulated in either *swi3-E815X* or *snf2-W935R* mutants (Figure 3.14). We did not remove genes affected by the *snf2-Q928K* mutant, as this mutant confers more severe loss of Swi/Snf function, resembling null transcriptional phenotypes for many loci (Chapter 2, Figure 3.14). This yielded a list of 250 Swi/Snf targets (Figure 3.13A). As a control set, we generated a random set of 250 genes whose transcription was not significantly affected by any of the Swi/Snf mutants (DESeq2 adjusted p-value > 0.05) and were not bound by Snf2 (Figures 3.13A and 3.14B).

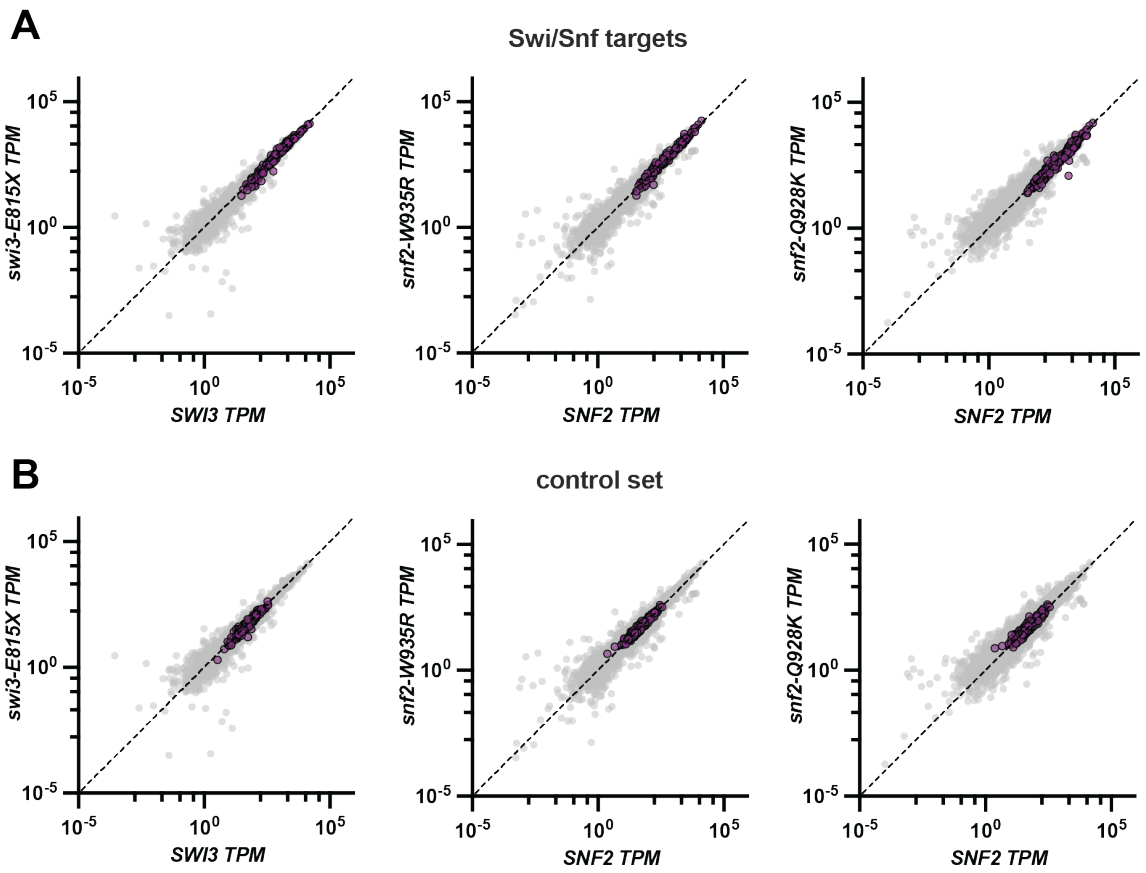

Figure 3.14: *Swi/Snf targets chosen do not exhibit altered transcript levels in swi3-E815X or snf2-W935R mutants*
(A) Scatterplot with TPM values, plotted on logarithmic scale, depicting expression of Swi/Snf target genes (n = 250) Left: *swi3-E815X* mutant (UB19209) compared to *SWI3* control cells (UB19205). Middle: *snf2-W35R* mutant (UB28922) compared to *SNF2* control cells (UB28914). Right: *snf2-Q928K* mutant (UB28915) compared to *SNF2* control cells (UB28914). One of three biological replicates is shown. **(B)** Same as (A), but for non-Swi/Snf regulated control genes (n = 250).

We next compared average Swi/Snf occupancy and nucleosome profiles for these two sets of genes between wild type and LUTI escape mutants. Importantly, Snf2 ChIP-Seq and MNase-Seq experiments were performed with spike-in control cells from a divergent strain of *S. cerevisiae*, enabling us to compare between samples after scaling read coverage with the calculated normalization factor (Vale-Silva et al., 2019) (Table 3.3). As expected, LUTI escape mutants did not exhibit Snf2 binding or nucleosome profile differences for the control set of genes, apart from increased occupancy of the -1 and +1 nucleosome in *snf2-Q928K* cells that may be due to the higher degree of pleiotropy in this mutant (Figures 3.13B and 3.14A). The *swi3-E815X* and *snf2-W935R* mutants exhibited normal binding of Snf2 for Swi/Snf targets, with average Snf2 occupancy peaking at the region encompassing +1, +2, and +3 nucleosomes (Figures 3.13B and 3.14A). The *snf2-Q928K* mutant, however, exhibited slightly lower Snf2 occupancy at positions downstream of the TSS (Figure 3.13B).

Sample	SNP-ChIP R1	SNP-ChIP R2	SNP-MNase R1	SNP-MNase R2
SNF2 untreated	1.000000	1.000000	1.000000	1.000000
SNF2 DTT	0.956971	0.948967	0.975196	1.011362
snf2-W935R untreated	1.054977	0.973205	1.001119	1.036597
snf2-W935R DTT	1.077176	0.978632	1.007814	1.052789
snf2-Q928K untreated	1.087979	0.978393	1.046129	1.097865
snf2-Q928K DTT	1.139370	1.005207	1.021932	1.064902
SWI3 untreated	1.040968	1.084763	0.974123	0.984093
SWI3 DTT	0.988442	1.030440	0.990765	1.005636
swi3-E815X untreated	1.015006	1.005317	0.991758	1.069252
swi3-E815X DTT	0.997280	0.979123	1.001634	1.078848

Table 3.3: *List of normalization factors from SNP-ChIP and SNP-MNase experiments*
Normalization factors calculated from the protocol described in Vale-Silva *et al.* 2019 used to scale read covered for ChIP-seq and MNase-seq experiments. All samples were normalized to the *SNF2* wild type untreated strain within each replicate. Numbers close to 1 indicate there are no major global differences in nuclear Snf2 (for ChIP) or nucleosome occupancy (for MNase) between samples.

On average, the *snf2-Q928K* mutant also exhibited increased nucleosome occupancy within the NDR and at downstream nucleosomes for Swi/Snf target genes (Figure 3.15A and 3.16B). Interestingly, the *swi3-E815X* and *snf2-W935R* mutants did

not impact the chromatin at the TSS or +1 nucleosome as strongly as the *snf2-Q928K* mutant but did exhibit increased nucleosome occupancy for gene-body nucleosomes, especially for the +2 nucleosome (Figures 3.15A-C). In general, positions further downstream from the +2 nucleosome are decreasingly impacted by Swi/Snf mutations with greater distance, and at the +5 nucleosome the differences between mutants and wild type are largely resolved (Figure 3.15A and 3.15C).

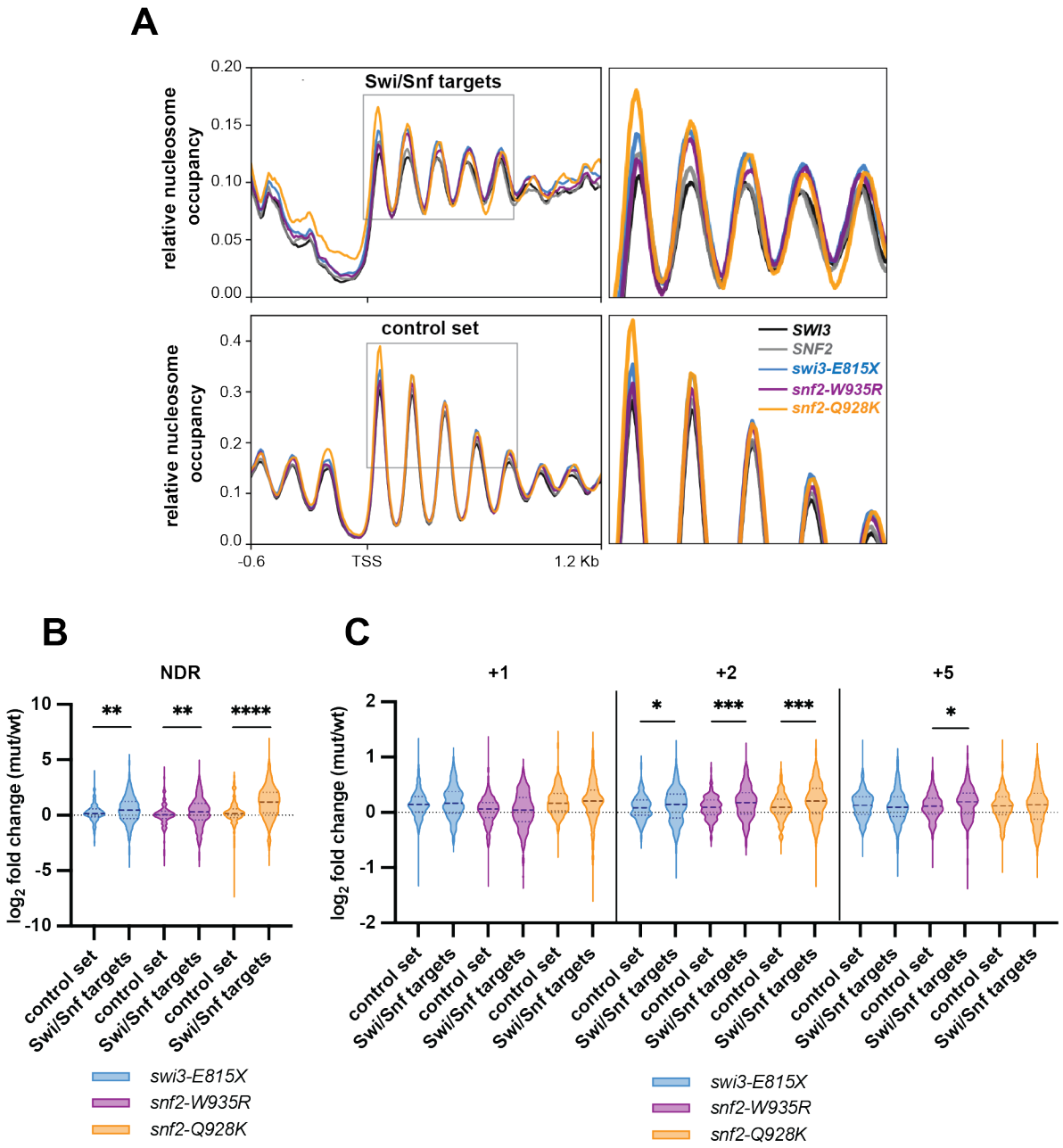

Figure 3.15: *Swi/Snf regulates gene-body nucleosome occupancy for its canonical gene targets*
(A) Metagene plots created from MNase-seq data for genes that are Swi/Snf regulated (top) or the non-regulated control set (bottom). Strains: *SWI3* (UB30070), *SNF2* (UB30387), *swi3-E815X* (UB30071), *snf2-*

W935R (UB30391), and *snf2-Q928K* (UB30389). **(B)** Quantification of nucleosome occupancy within the NDR for non-regulated control genes and Swi/Snf targets. Log_2(fold change) in occupancy was calculated from MNase-seq read depth after spike-in normalization for *swi3-E815X* (n = 2, UB30071), *snf2-W935R* (n = 2, UB30391), and *snf2-Q928K* (n = 2, UB30389) mutants relative to wildtype (n = 4, UB30070 and UB30387). Occupancy differences between control genes and Swi/Snf target genes is analyzed by Mann-Whitney U test (two tailed, p = 0.0018 [*swi3-E815X*], p = 0.0081 [*snf2-W935R*], p < 0.0001 [*snf2-Q928K*]. **(C)** Same as (B), but for the +1, +2, and + 5 nucleosomes. Differences are analyzed by Mann-Whitney U test (two tailed, p = 0.2054 [*swi3-E815X*, +1], p = 0.9986 [*snf2-W935R*, +1], p = 0.6092 [*snf2-Q928K*, +1], p = 0.0425 [*swi3-E815X, +2*], p = 0.0006 [*snf2-W935R*, +2], p = 0.0001 [*snf2-Q928K*, +2], p = 0.1654 [*swi3-E815X*, +5], p = 0.0112 [*snf2-W935R*, +5], p = 0.7697 [*snf2-Q928K*, +5]).

Based on the observation that the *swi3-E815X* and *snf2-W935R* mutants impact chromatin within a limited range of the active TSS for Swi/Snf-regulated genes, we wondered whether Swi/Snf regulation of LUTI-based repression depends on distance between the two TSSs. To test this, we assayed repression by the $SOD1^{LUTI}$, which has an abnormally long 5′ extension of nearly 2 kilobases (Vander Wende et al., 2023), in these LUTI escape mutants. We engineered alleles of $SOD1^{LUTI}$, varying the distance between the two promoters by integrating a *lex*-inducible promoter at different positions upstream of the TSS^{PROX}, with 1700 base pairs (bp) upstream being the wild-type length (Figure 3.16A). Both the *swi3-E815X* and *snf2-W935R* mutants seemed to most severely impact repression by the shortest $SOD1^{LUTI}$ (330 bp), although the *swi3-E815X* mutant exhibited a moderate LUTI escape phenotype for the medium (860 bp) and long (1700) $SOD1^{LUTI}$ (Figures 3.16A and 3.16B).

Because the $SOD1^{LUTI(330)}$ lacks DNA sequence present in the $SOD1^{LUTI(860)}$, we cannot conclude whether stronger mutant phenotypes are due to shorter length between TSSs or altered TF binding sites. Therefore, we engineered another short $SOD1^{LUTI(550)}$ that contains only the sequence within $SOD1^{LUTI(860)}$ that is missing in $SOD1^{LUTI(330)}$, except for the ~100 bp upstream of the TSS^{PROX} which we left unchanged in attempt to maintain integrity of the proximal promoter (Figure 3.16A). Unfortunately, this perturbation severely reduced $SOD1^{PROX}$ expression in uninduced conditions (Figure 3.16B and 3.16C), indicating key elements of the proximal promoter were removed in this strain despite attempts to maintain its full function. Based on the limitations with these experiments, we cannot eliminate the possibility that sequence context plays a role in Swi/Snf repression of $SOD1^{PROX}$. Additionally, altering the lengths of the $SOD1^{LUTI}$ impacted its expression levels, with shorter extension lengths being associated with higher $SOD1^{LUTI}$ expression (Figures 3.16B and 3.16C), introducing another variable that may contribute to Swi/Snf function at this locus. Altogether, it cannot be concluded whether Swi/Snf LUTI escape phenotypes are specific to genes with shorter distances between the TSSs, as these experiments introduce several factors that could influence repression by Swi/Snf at LUTI-regulated genes.

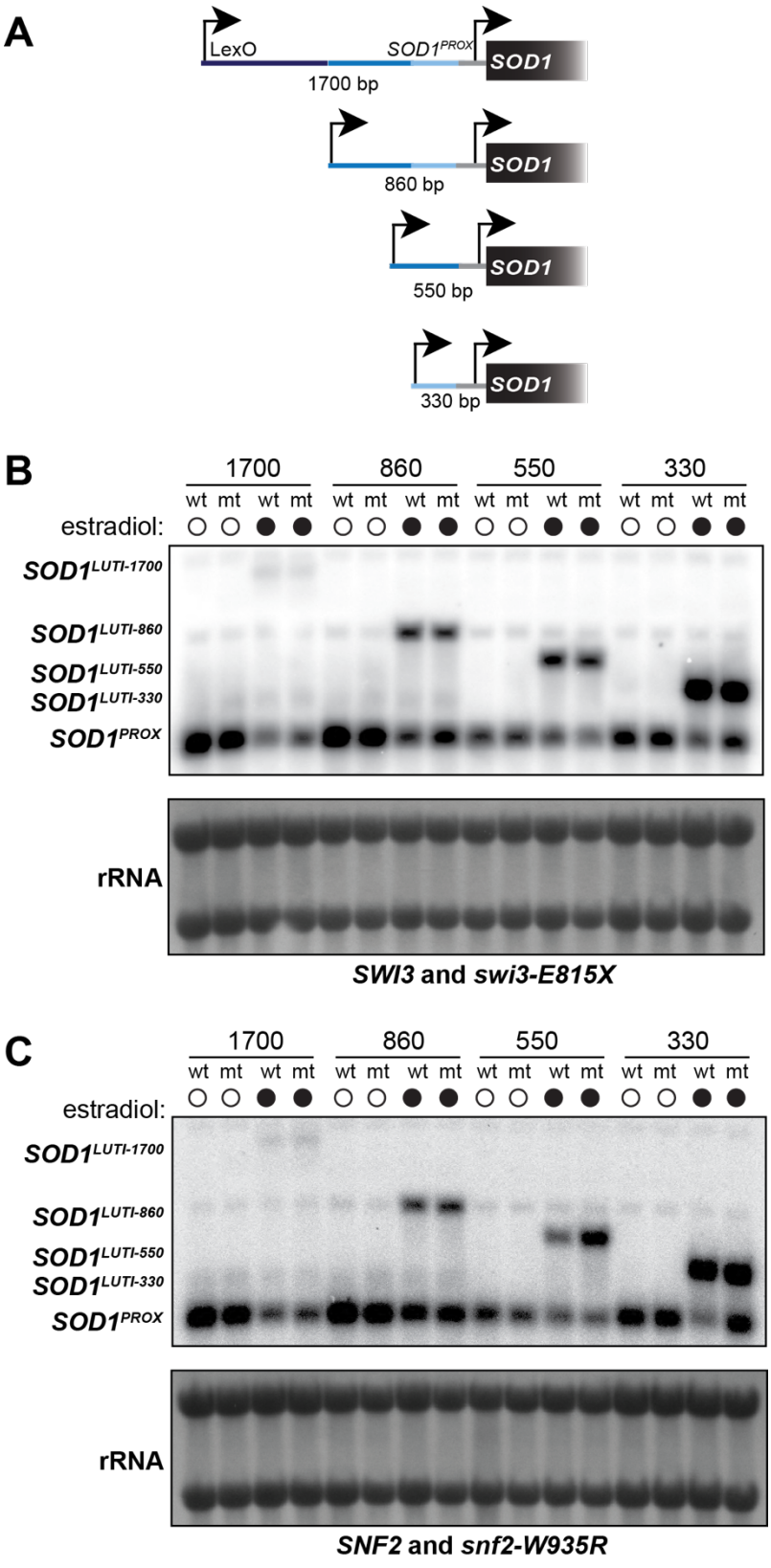
A
LexO
SOD1PROX
SOD1
1700 bp
SOD1
860 bp
SOD1
550 bp
SOD1
330 bp
B
1700
860
550
330
wt mt wt mt wt mt wt mt wt mt wt mt wt mt wt mt
estradiol:
SOD1LUTI-1700
SOD1LUTI-860
SOD1LUTI-550
SOD1LUTI-330
SOD1PROX
rRNA
SWI3 and swi3-E815X
C
1700
860
550
330
wt mt wt mt wt mt wt mt wt mt wt mt wt mt wt mt
estradiol:
SOD1LUTI-1700
SOD1LUTI-860
SOD1LUTI-550
SOD1LUTI-330
SOD1PROX
rRNA
SNF2 and snf2-W935R

Figure 3.16: *Investigating TSS distance-dependent activity by Swi/Snf*
(A) schematic of *lex*-inducible *SOD1*^{LUTI} alleles generated. **(B)** RNA blot probed for the *SOD1* CDS in *SWI3* control (UB36454 [1700], UB36456 [860], UB36989 [560], and UB36457 [330]) or *swi3-E815X* (UB36458 [1700], UB36460 [860], UB36976 [560], and UB36462 [330]) cells treated or untreated with 15 nM β-estradiol for 2 h. **(C)** Same as (B), but for *SNF2* control (UB36684 [1700], UB36686 [860], UB36973 [560], and UB36688 [330]) and *snf2-W935R* (UB36633 [1700], UB36635 [860], UB36974 [560], and UB36637 [330]) cells.

Given their effects on gene-body nucleosomes, we wondered whether the *swi3-E815X* and *snf2-W935R* mutations confer specific defects in co-transcriptional nucleosome remodeling for Swi/Snf targets. While these mutants do not impair transcription elongation to a degree that impacts transcript levels (Figure 3.14), it is possible that the activity of other transcription elongation factors compensates for loss of Swi/Snf function to promote normal elongation by Pol II. To address this possibility, we assayed synthetic phenotypes for LUTI escape mutants combined with deletion of *DST1,* a gene encoding the general elongation factor TFIIS which alleviates Pol II stalling and is commonly synthetic lethal with deletion of other elongation factors (Costa and Arndt, 2000; Davie and Kane, 2000; Malagon et al., 2004).

Consistent with previous observations that *snf2Δ dst1Δ* cells are inviable (Davie and Kane, 2000; Schwabish and Struhl, 2007), the *dst1Δ* combined with the *snf2-Q928K* mutation resulted in a profound growth defect (Figure 3.17). The *swi3-E815X* and *snf2-W935R* mutants also displayed growth defects when combined with *dst1Δ* (Figure 3.17), in contrast to their minimal effects on Swi/Snf loss-of-function phenotypes that are dependent on Swi/Snf's gene activation function (Chapter 2). From these results, we concluded that the *swi3-E815X* and *snf2-W935R* mutants confer broad defects in co-transcriptional remodeling. Furthermore, these LUTI escape mutants allow for canonical Swi/Snf function in transcriptional activation to be uncoupled from an understudied role for Swi/Snf in transcription elongation.

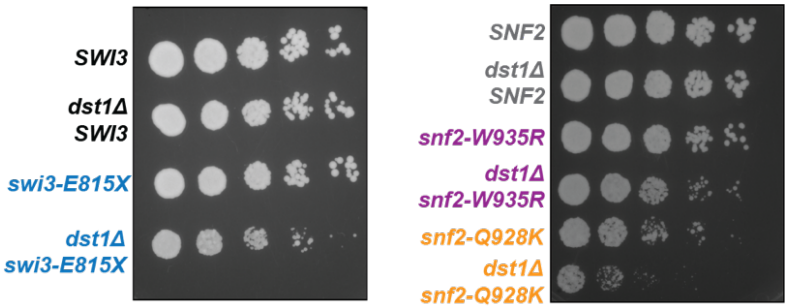

Figure 3.17: *Swi/Snf LUTI escape mutants exhibit synthetic growth defects with deletion of an elongation factor*
Serial dilution and plating growth assay on YPD media. Strains: *SWI3* (UB19205), *SWI3 dst1Δ* (UB36182), *swi3-E815X* (UB19209), *swi3-E815X dst1Δ* (UB28096), *SNF2* (UB28914), *SNF2 dst1Δ* (UB36185), *snf2-W935R* (UB28922), *snf2-W935R dst1Δ* (UB36186), *snf2-Q928K* (UB28915), and *snf2-Q928K dst1Δ* (UB36188).

3.3 Discussion

The Swi/Snf complex is a highly conserved chromatin remodeler that has been extensively studied for its role in transcriptional activation. Mutations in Swi/Snf subunits are found in ~20% of all human tumors, making the complex one of the most commonly affected in cancer (Kadoch and Crabtree, 2015). Interestingly, a few studies have provided evidence in support of Swi/Snf acting in gene repression (Choi et al., 2015; Martens and Winston, 2002; Menon et al., 2019; Murphy et al., 1999; Zhu et al., 2013), however, it has remained unclear whether Swi/Snf-dependent transcriptional repression occurs directly or indirectly as a result of transcription initiation defects at nearby loci or decreased expression of other transcriptional regulators.

In this study, we have demonstrated a direct role of the Swi/Snf complex in transcriptional repression. This occurs by co-transcriptional nucleosome remodeling by Swi/Snf downstream of distal TSSs expressing non-canonical transcripts including LUTIs. Consequently, the nucleosome depleted region of the CDS-proximal promoter, which resides downstream of the distal TSS becomes nucleosome occupied, thereby resulting in the repression of the protein-coding transcript isoform (Figure 3.18, top). LUTI escape mutants *swi3-E815X* and *snf2-W935R* have minimal effects on Swi/Snf's ability to facilitate transcription initiation at its target loci. Instead, these mutations specifically disrupt nucleosome remodeling at positions downstream of the active TSS, resulting in the repression of the TSS^{PROX} for Swi/Snf's TSS^{DIST} targets (Figure 3.18, middle). With more severe loss of Swi/Snf function, as in null or *snf2-Q928K* mutants, remodeling at the active TSS is reduced, leading to impaired transcription initiation. In these cases, transcriptional interference at the TSS^{PROX} for Swi/Snf's TSS^{DIST} targets is reduced indirectly, as a result of lower TSS^{DIST} transcription (Figure 3.18, bottom).

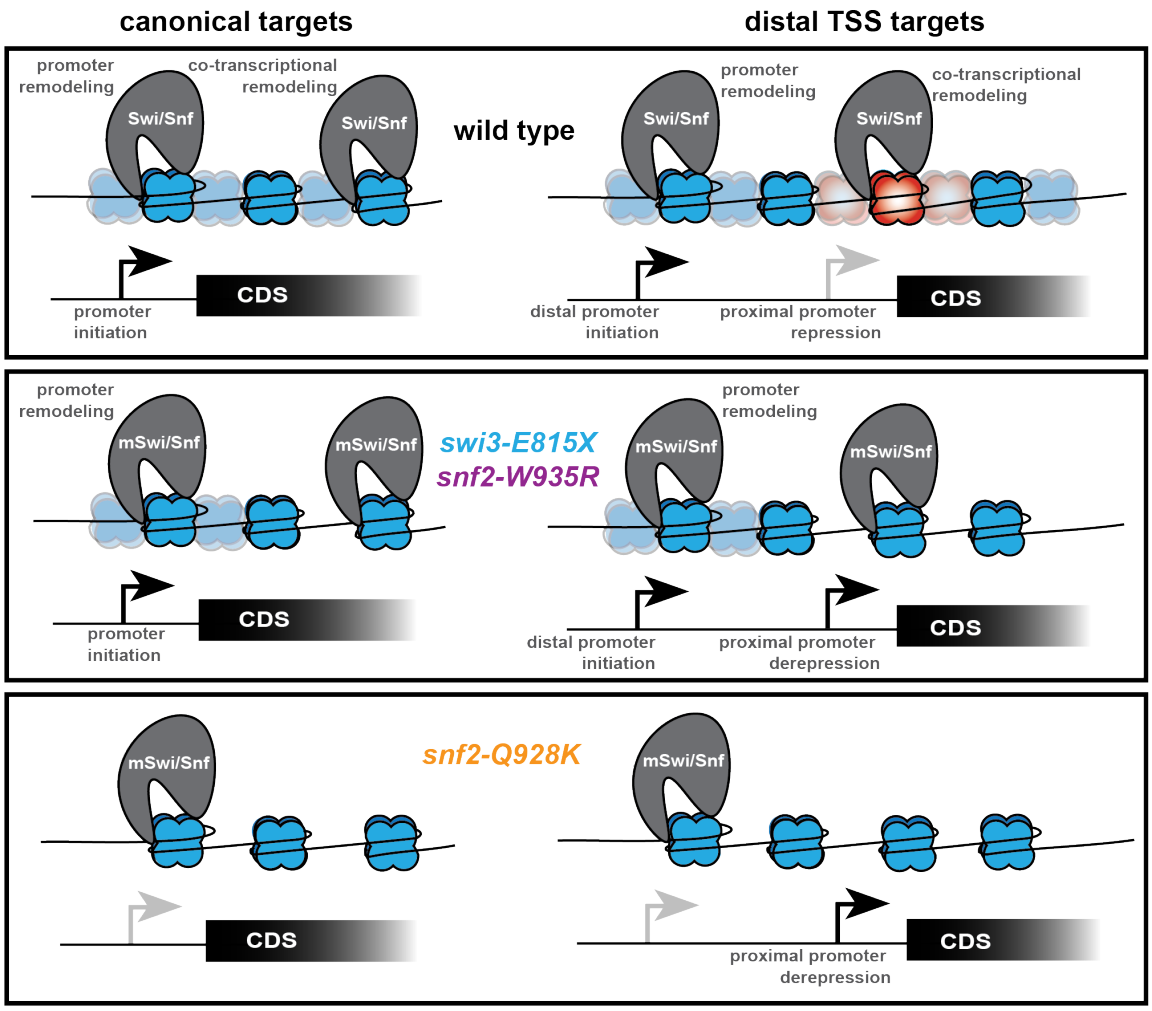

Figure 3.18: *Model for Swi/Snf regulation of TSS activation and repression*
In wild-type cells (top), the Swi/Snf complex is recruited to canonical promoters (left) or distal promoters (right) and performs nucleosome remodeling to aid in transcription initiation. Swi/Snf also performs a secondary function at its targets to remodel nucleosomes downstream of the active TSS, which represses TSS^{PROX} promoters for its TSS^{DIST} targets. Productive remodeling is indicated with translucent, "fuzzy" nucleosomes and transcriptionally interfering nucleosomes are indicated in red. Middle: in *swi3-E815X* and *snf2-W935R* mutants, transcription initiation function by the Swi/Snf complex remains intact but downstream remodeling is impaired. For canonical targets, these mutants compromise nucleosome remodeling within the gene body without compromising transcription levels. For TSS^{DIST} targets, reduced nucleosome remodeling downstream of the active TSS results in derepression of the TSS^{PROX}. Bottom: in *snf2Q928K* cells, nucleosome remodeling and transcription initiation at both canonical and TSS^{DIST} promoters is reduced. Reduced transcriptional readthrough results in derepression of the TSS^{PROX}.

Combined approaches to profile transcript isoforms revealed cases of Swi/Snf-mediated transcriptional interference

Original studies to identify LUTIs involved cross-referencing mRNA-seq, ribosome profiling, and mass spectrometry data to determine cases whereby poorly translated

mRNAs restrict protein levels (Brar et al., 2012; Cheng et al., 2018; Dalfsen et al., 2018). Given that uORF-based repression of translation is fairly robust (Cheng et al., 2018; Tresenrider et al., 2021), recent and ongoing work has focused on understanding the variable nature of LUTI-based transcriptional repression. This requires reliable, quantitative profiling of distinct transcript isoforms, for which mRNA-seq is not adequate. Though highly sensitive, mRNA-seq data do not capture overlapping, same-stranded transcripts in a reliable or quantitative manner.

In contrast, TL-seq combined with Nanopore direct mRNA-seq allow for quantitative measurement of multiple transcript isoforms corresponding to the same genomic locus and classification of readthrough transcripts (Tresenrider et al., 2021). Although these advantages permitted confident phenotyping of Swi/Snf mutants in this study, we failed to detect several previously-identified LUTIs with these techniques. This may be due to differences in gene networks and transcriptional responses in the W303 strain background used in this study compared to the SK1 background used previously in Van Dalfsen *et al* 2018. Additionally, our TL-seq analysis may not have been sensitive enough to detect low-abundant transcripts. Certain LUTIs have been shown to be susceptible to nonsense-mediated decay (Tresenrider et al., 2021). With higher turnover and lower expression from the LUTI promoter, detection becomes difficult. In future work, utilization of mutants defective for mRNA decay pathways can promote identification of new LUTIs. Despite missing some potential targets of interest, our reliance on differential gene expression analysis of TL-seq data yields high confidence in the findings presented.

One of several transcriptional interference mechanisms: disrupting promoter architecture

Eukaryotic promoters consist of a nucleosome free region (NFR) or nucleosome depleted region (NDR) flanked by two well-positioned nucleosomes with acetylated histones (Bai and Morozov, 2010; Venkatesh and Workman, 2015). While the TSS for most genes lies within 10-15 base pairs of the 5′ end of the +1 nucleosome, the NFR or NDR is thought to allow access for sequence-specific transcription factors and the pre-initiation complex to start transcription at the gene promoter (Gill et al., 2020; Jansen and Verstrepen, 2011; Rando and Winston, 2012). In the case of LUTIs and other transcripts with distal TSSs relative to the CDS-proximal TSS (TSS^{PROX}), transcription proceeds across the TSS^{PROX}, subjecting the proximal promoter to co-transcriptional chromatin changes that normally function to promote elongation and inhibit cryptic transcription initiation. Several transcriptional interference pathways have already been uncovered, many of which involving histone modification or nucleosome remodeling (Carrozza et al., 2005; Hartzog et al., 1998; Hennig et al., 2012; Pruneski et al., 2011; Smolle et al., 2012). For Swi/Snf-repressed TSS^{PROX} loci uncovered in this study, it seems that Swi/Snf remodeling of the -1 and +1 nucleosomes surrounding the proximal promoter contributes to TSS^{PROX} repression, possibly by creating increased nucleosome mobility into what was previously the NFR/NDR.

Based on this study along with previous findings, Swi/Snf remodeling of nucleosomes downstream of the TSS^{DIST} is one of several possible routes to achieve transcriptional interference of the TSS^{PROX}. There may, in fact, be other loci at which Swi/Snf acts in parallel with other described transcriptional interference pathways during UPR induction that evaded our detection due to compensation by other factors in the LUTI escape mutants. Based on our observations that the *snf2-Q928K* mutant impairs transcription of the distal isoform for many genes (Figure 3.2C) and that activation of $HNT1^{LUTI}$ is sufficient for Snf2 recruitment (Figure 3.12A), it seems that recruitment of the Swi/Snf complex to the distal promoter is a prerequisite for the downstream transcriptional interference activity by the complex. Recruitment of Swi/Snf may be mediated through interactions with acetylated histones or sequence-specific transcription factors at distal promoters. In support of this notion, Swi/Snf occupancy at several canonical UPR-induced promoters depends on the master UPR transcription factor Hac1 (Sahu et al., 2021). Swi/Snf interaction with Hac1 may also be the basis for its recruitment to $HNT1^{LUTI}$, a reported Hac1 target (Van Dalfsen et al., 2018).

What are the rules for Swi/Snf-mediated interference?

Although Swi/Snf interacts genetically with Hac1, Swi/Snf does not appear to regulate other previously identified Hac1 LUTI targets (Table 3.2), indicating transcriptional interference activity by Swi/Snf is regulated by additional factors or target gene features. One such feature may be the distance between the two TSSs, based on our observation that *swi3-E815X* and *snf2-W935R* do not strongly affect nucleosomes further downstream from the TSS (Figures 3.15A and 3.15C) and previous observations that Snf2 is most highly enriched at the -1, +1, +2, and +3 nucleosomes for its gene targets (Yen et al., 2012). In our attempt to test this hypothesis with the abnormally long $SOD1^{LUTI}$, we observed stronger Swi/Snf LUTI escape phenotypes with shorter synthetic versions of $SOD1^{LUTI}$ (Figure 3.16). However, these experiments also introduced sequence context and LUTI expression levels as variables that may control Swi/Snf activity at LUTI-regulated genes.

Higher LUTI expression being correlated with stronger repressive function by Swi/Snf is also intriguing, given that Swi/Snf is recruited to highly expressed constitutive and inducible genes to promote their activation (Rawal et al., 2018). Furthermore, high LUTI expression was found to be a strong predictor of LUTI-based transcriptional repression along with changes in nucleosome positioning (Tresenrider et al., 2021). Perhaps repressive activity by Swi/Snf occurs through nucleosome remodeling downstream from the active TSS^{DIST} to aid in Pol II promoter escape during the initiation-elongation transition. According to this notion, both shorter distance between TSSs and higher TSS^{DIST} expression would be expected to contribute to Swi/Snf repressive activity.

Concluding remarks

In this study, we used integrated genomic and single-locus assays to unveil a direct role for the Swi/Snf complex in transcriptional interference. In line with its characterized role in gene activation, the Swi/Snf complex activates transcription of non-canonical mRNAs initiating from CDS-distal promoters in response to protein folding stress, including three LUTI mRNAs. We found that the Swi/Snf complex also performs a secondary function at these loci to repress the TSS^{PROX} via nucleosome remodeling downstream of the TSS^{DIST}. For the LUTI-regulated gene *HNT1*, proper Snf2 occupancy, nucleosome remodeling, and $HNT1^{PROX}$ repression were dependent on $HNT1^{LUTI}$ transcriptional initiation and elongation, indicating repression of $HNT1^{PROX}$ is achieved via co-transcriptional nucleosome remodeling by Swi/Snf.

Our finding that the Swi/Snf complex can act as both a transcriptional activator and repressor simultaneously at the same genomic locus is relevant to ongoing investigations into the link between Swi/Snf mutations and cancer. The transcriptional landscape in human cells is complex, with a high prevalence of non-coding transcription and transcript isoform toggling (Hangauer et al., 2013; Wang et al., 2016). It is thought that Swi/Snf mutations lead to disease through both downregulation and upregulation of gene expression (Cenik and Shilatifard, 2021; Lu and Allis, 2017), however mechanisms for Swi/Snf-based gene repression have remained unclear. Our findings indicate one route through which Swi/Snf chromatin remodeling can lead to direct gene repression in yeast: transcriptional interference of coding transcripts. Thus, future work to investigate whether human Swi/Snf complexes also play a role in transcriptional interference for genes with tandem promoters, such as the LUTI-regulated proto-oncogene *MDM2* (Hollerer et al., 2019), will reveal whether transcriptional interference activity by the Swi/Snf complex is evolutionarily conserved.

Chapter 4 – Conclusions and Future Directions

4.1 Diversity and specificity among transcriptional interference pathways

Several *cis*-acting transcription interference pathways have been described. Transcriptional elongation through the gene promoter can interfere with expression of the coding mRNA through modifications to the chromatin or via displacement of TFs by elongation machinery (Hainer et al., 2011; Kim et al., 2016; Shuman, 2020), resulting in decreased expression for the affected gene. Among the pathways that involve chromatin dynamics, there are two main routes through which interference can be established: post translational modification of histones or nucleosome repositioning.

Histone methylation, in particular H3K36me3 and H3K4me2, induces a repressive chromatin state through the recruitment of transcriptional repressors, including histone deacetylases and chromatin remodelers (see Chapter 1). The histone methyltransferases involved, Set1 and Set2, travel with the elongation complex and deposit methylation marks across actively transcribed genes (Govind et al., 2010). Knockdown of these histone methylation/deacetylation pathways results in spurious transcription within gene bodies, which has defined their role in preventing cryptic transcription initiation (Carrozza et al., 2005; Kim et al., 2012). Additionally, these methylation pathways have also been shown to regulate promoters that are subject to upstream readthrough by an intergenic non-coding transcript (J. H. Kim et al., 2016; T. Kim et al., 2012).

Full repression of $NDC80^{PROX}$ by $NDC80^{LUTI}$ requires both the H3K36 methyltransferase Set2 and the HDAC Set3C which is recruited by Set1-dependent H3K4me2 (Chia et al., 2017). Knockdown of either pathway individually did not affect *NDC80* regulation, indicating both pathways act in parallel to repress $NDC80^{PROX}$ during $NDC80^{LUTI}$ transcription (Chia et al., 2017). Given that global characterization found that H3K36me3, but not H3K4me2, is associated with LUTI-based transcriptional interference (Tresenrider et al., 2021), *NDC80* may be a special case regarding the utilization of both pathways.

Nucleosome repositioning at the proximal promoter region is another strong predictor of LUTI-based interference, indicating nucleosome remodelers or histone chaperones are involved in the repression for certain LUTI regulated genes (Tresenrider et al., 2021). One study found that loss of the histone chaperone complex FACT results in derepression of 102 promoters that are subject to readthrough by an alternative transcript during meiosis, including LUTI-regulated promoters (Chia et al., 2021). Among these genes, roughly 2/3 (65) were also affected by knocking down H3K36me3 and H3K4me2 pathways (Chia et al., 2021). While there is overlap among these general transcription elongation pathways, there also appears to be pathway specialization for certain loci regulated by transcriptional interference.

In our approach to uncover novel regulators of LUTI-based interference, we uncovered a new route to achieve transcriptional interference: Swi/Snf co-transcriptional

nucleosome remodeling. This was surprising, given that Swi/Snf is primarily known to act at promoter regions to facilitate transcriptional activation. When we investigated this activity by Swi/Snf during cellular stress, we found that Swi/Snf regulates transcriptional interference for a subset of genes with alternative transcription. Thus, rather than playing a general role in LUTI-based interference, repression by Swi/Snf is specific to certain loci, as with the FACT and histone methylation pathways. The case of interference by Swi/Snf, however, differs from these other described pathways in that Swi/Snf performs two functions: activating the distal promoter and performing the downstream repression at the proximal promoter. These functions were only able to be separated through our isolation of specific mutants that differentially impact Swi/Snf's ability to activate transcription or perform co-transcriptional remodeling.

4.2 Broad functions by a conserved chromatin remodeler

Regulation of transcription and DNA repair by Swi/Snf: implications for disease

Swi/Snf has long been recognized as a gene activation complex that functions at promoters to aid in transcription initiation. Classic examples which served as the basis for the discovery of Swi/Snf in yeast include its activation of the sucrose invertase gene *SUC2* and the endonuclease gene required for mating type switching *HO* (Neigeborn and Carlson, 1984; Stern et al., 1984). Since these early single-locus studies, further work revealed that roughly 8-10% of yeast genes are regulated by Swi/Snf (Dutta et al., 2017). In particular, Swi/Snf specializes in activating inducible genes during various stress conditions, including the unfolded protein response, heat shock, nutrient stress, and osmotic stress (Dutta et al., 2014; Proft and Struhl, 2002; Sahu et al., 2021; Shivaswamy and Iyer, 2008). Similarly, mammalian Swi/Snf complexes are required for conditional gene expression that is crucial for development, including differentiation of neurons, adipocytes, hematopoietic cells, osteoblasts, and skeletal muscle (Romero and Sanchez-Cespedes, 2014). As such, mutations in Swi/Snf components have been linked to several developmental diseases and various forms of cancer (Kadoch and Crabtree, 2015; Romero and Sanchez-Cespedes, 2014).

Swi/Snf loss-of-function is thought to lead to developmental disease through disruption of gene regulation (Kadoch and Crabtree, 2015). However, the link between Swi/Snf and cancer is more complex with two prevailing models: disruption of gene regulation, namely through defective eviction of polycomb repressive complexes, and genome instability. The genome instability model arose from findings that Swi/Snf complexes have roles in DNA replication and repair (Chai et al., 2005; Cohen et al., 2010). Though an intriguing model given tumor heterogeneity among certain cancers with Swi/Snf mutations (Kadoch and Crabtree, 2015), it is difficult to test. Did the Swi/Snf mutation cause or arise from genome instability? Furthermore, certain Swi/Snf germline mutations that drive rhabdoid tumors and small-cell ovarian cancer do not exhibit high degrees of secondary mutations (Mathur and Roberts, 2018). Thus, additional work is needed to conclude whether roles for Swi/Snf in DNA replication/repair pathways is relevant to tumor formation or progression.

There is, however, functional evidence explaining how Swi/Snf mutations can lead to cancer through dysregulation of gene expression. For example, rhabdoid tumor cell lines exhibit loss of Swi/Snf occupancy at promoters and enhancers (Wang et al., 2017). Mouse models for invasive colon adenocarcinomas also revealed that loss of the Swi/Snf subunit BAF250 drives cancer and coincides with aberrant developmental gene regulation (Mathur et al., 2017). Dysregulation of polycomb repressive occupancy is thought to be a major contributor of Swi/Snf-related cancers, as Swi/Snf normally acts in opposition to polycomb to stimulate expression of proliferation repressor genes (Kadoch and Crabtree, 2015). Additionally, Swi/Snf mutant tumors are susceptible to polycomb inhibitors (Knutson et al., 2013). Thus, while genome instability may be an underlying mechanism for tumorigenesis in certain Swi/Snf-related cancers, numerous studies have provided concrete evidence implicating its function in transcriptional regulation.

Interestingly, loss of Swi/Snf function results in both up- and down-regulation of mRNA levels for different genes, suggesting Swi/Snf can repress as well as activate transcription (Dutta et al., 2017). Most mechanistic evidence, however, strictly supports roles for Swi/Snf remodeling in promoter activation. Namely, both yeast and human Swi/Snf have been shown to be required for creating accessible chromatin environments at actively transcribed genes (Chandy et al., 2006; Iurlaro et al., 2021; Rawal et al., 2018). The complex has also been known to associate with several gene-activating TFs (Neely et al., 2002; Prochasson et al., 2003). As such, Swi/Snf-repressed genes identified through conventional mRNA-seq may be instead repressed through a secondary Swi/Snf target, rather than by Swi/Snf itself. Additional mechanistic evidence, such as time course experiments integrating MNase, Snf2-ChIP, and transcriptional assays would aid in determining whether Swi/Snf repression of these genes is direct or indirect.

In this dissertation, we employed these combined approaches, with the additional use of specialized mRNA-sequencing techniques to profile transcript isoforms, to uncover a novel function by Swi/Snf in transcriptional interference. This revealed that certain promoters can be directly repressed by Swi/Snf within specialized transcriptional contexts. Our observations indicate Swi/Snf-dependent transcriptional interference is restricted to loci at which Swi/Snf is recruited to a gene-distal promoter and transcription of the gene-distal promoter reads through a downstream proximal promoter. Given these prerequisites, we expect this repressive function by Swi/Snf regulates a small proportion of yeast genes overall that were not previously identified due to limitations with conventional mRNA-seq approaches and the use of pleiotropic mutants.

Though transcriptional interference may not be a pervasive function by Swi/Snf, it represents an intriguing addition to its described functions in transcriptional activation and DNA replication/repair. Roles for Swi/Snf in promoting cellular homeostasis and proper development in humans may therefore rely in part on this previously hidden interference function. Intriguingly, inhibition of catalytic Swi/Snf activity in mouse embryonic stem cells revealed that although most affected genes exhibited decreased promoter/enhancer accessibility upon inhibition, certain loci exhibited increased accessibility within insulators or sites of transcription elongation (Iurlaro et al., 2021). This could indicate Swi/Snf co-

transcriptional remodeling function, which we revealed leads to promoter repression at loci with multiple tandem promoters in yeast, is conserved in mammals. We suggest our work can provide a blueprint for identifying loci affected by Swi/Snf interference in other stress conditions or species.

Dual roles for the Swi/Snf complex in transcription initiation and elongation

While most investigations into Swi/Snf cellular function have focused on its role as a co-activator at gene promoters, several studies have uncovered evidence indicating the Swi/Snf complex also functions in transcription elongation. For example, Snf2 binds with similar patterns and kinetics as Pol II along coding regions upon induction of transcription (Schwabish and Struhl, 2007). This same study uncovered a synthetic lethal relationship between *SNF2* and *DST1*, which encodes the elongation factor TFIIS (see Chapters 1 and 3), and *snf2Δ* cells were sensitive to elongation inhibiting drugs. ChIP data have also revealed that Snf2 occupies promoters and coding regions for heat-shock induced genes (Shivaswamy and Iyer, 2008) and transcription elongation of human *HSF1* is necessary for Swi/Snf recruitment at the *HSF1* locus (Corey et al., 2003). Finally, *snf2Δ* cells exhibit increased nucleosome occupancy at promoters and within gene bodies (Rawal et al., 2018).

The caveat with interpretation from these previous studies lies within the utilization of a *snf2Δ* null mutant, which reduces transcription levels at Swi/Snf target loci. In *snf2Δ* cells, it is difficult to distinguish whether differences in nucleosome occupancy within the gene body are due to reduced transcription versus loss of Swi/Snf activity on gene-body nucleosomes and what the biological significance of Swi/Snf-mediated co-transcriptional remodeling is. Here, we provide conclusive evidence that the Swi/Snf complex functions in co-transcriptional nucleosome remodeling by uncovering specific mutants and genomic contexts that impair nucleosome remodeling within gene bodies without reducing transcript levels from active TSSs.

Some of our evidence pointed towards the possibility that interference by Swi/Snf is limited to genes with shorter genomic distances between their two TSSs. Though our efforts to directly test this were inconclusive, previous work supports this hypothesis. Most compellingly, Snf2 was found to be most highly enriched at the -1, +1, +2, and +3 nucleosomes for canonical Swi/Snf targets (Yen et al., 2012). This is consistent with our Snf2 ChIP-seq data, which revealed its highest occupancy in wild type cells is localized to the 5′ regions of genes encompassing these nucleosomes (Chapter 3). Given this binding specificity, it's possible that rather than acting explicitly in elongation Swi/Snf mediates promoter escape at its target loci. This would be consistent with its known roles in promoter activation, as promoter escape is the transition phase between initiation and elongation (Chapter 1).

Swi/Snf remodeling and gene repression

Previous studies have uncovered a role for the Swi/Snf complex in gene repression in yeast as well as more complex organisms (Choi et al., 2015; Martens and Winston, 2002; Menon et al., 2019; Murphy et al., 1999; Zhu et al., 2013). Genome-wide studies in yeast have revealed that deletion of Swi/Snf genes results in both downregulation and upregulation of transcription for subsets of genes (Dutta et al. 2017, Sen et al. 2017). While upregulation of a gene in a *snf2Δ* mutant may indicate the Swi/Snf complex normally represses its transcription, it is difficult to conclude whether repression is achieved through Swi/Snf remodeling at that locus or indirect effects given the degree of pleiotropy in *snf2Δ* cells. By integrating transcriptome, genomic Snf2 occupancy, and genomic nucleosome data for wild-type cells compared to LUTI escape mutants in this study, we were able to infer with high confidence that the Swi/Snf complex induces bona fide TSS^{DIST} targets and represses transcription at downstream TSS^{PROX} promoters via co-transcriptional nucleosome remodeling.

In line with our findings, existing evidence for Swi/Snf-mediated gene repression involves noncoding transcription. In yeast, the Swi/Snf complex activates transcription of the non-coding transcript *SRG1* in serine replete conditions. *SRG1* transcription results in repression of the *SER3* promoter via co-transcriptional nucleosome deposition by the Paf1 complex, Spt6, Spt16, and Spt2 (Martens et al., 2005; Martens and Winston, 2002; Pruneski et al., 2011). In this case, Swi/Snf-based repression of *SER3* is indirect, whereas direct repression at the *SER3* promoter is achieved by other elongation factors.

In plants, Swi/Snf has also been shown to play a role in lncRNA-mediated transcriptional silencing. In contrast to our discovery that Swi/Snf acts in *cis*-mediated transcriptional interference, one study found that lncRNA-mediated silencing by Swi/Snf can occur through a *trans*-acting mechanism. According to the described mechanism, silencing factors assemble on the lncRNA which guides the silencing complex, including Swi/Snf components, to different genomic loci (Zhu et al., 2013). The role for Swi/Snf in this pathway was nonetheless surprising and distinct from its canonical functions in transcriptional activation. This study revealed that despite its unconventional mode of recruitment, the mechanism for Swi/Snf-mediated silencing may occur through Swi/Snf's remodeling function, as nucleosomes at silent loci were remodeled in a lncRNA-dependent manner. However, DNA methylation at silent loci was also found to be Swi/Snf dependent, which may suggest Swi/Snf establishes silencing through other mechanisms, such as recruitment of DNA methyltransferases.

Perhaps the most similar example to our findings is the Swi/Snf-dependent repression of the Blimp-1 gene. One study revealed loss of Swi/Snf function causes derepression of Blimp-1 in mouse immune cells (Choi et al., 2015). Evidence supporting direct repression of Blimp-1 includes observations that the catalytic subunit BRG1 (Snf2 homolog) was bound at the Blimp-1 promoter and that knockdown of *BRG1* resulted in increased Blimp-1 promoter accessibility and Pol II recruitment. However, Swi/Snf was also found to be required for Bcl6-dependent repression at this locus, and Bcl6 expression was lower in Swi/Snf knockdown lines, introducing the possibility that Swi/Snf repression of Blimp-1 is indirect. An intriguing element linking these findings to ours lies within the fact that Blimp-1 is a gene that exhibits alternative promoter usage (Morgan et al., 2009),

and Swi/Snf-dependent repression and chromatin changes were found to occur at the proximal promoter (Choi et al., 2015). It is unclear whether the distal promoter is active in the cell lines used for these experiments, though further investigation may reveal whether Swi/Snf repression of Blimp-1 involves transcriptional interference.

4.3 Future work

Investigating whether LUTI escape mutants affect transcription elongation

Although overall transcript levels are not impaired for most Swi/Snf targets in the *swi3-E815X* and *snf2-W935R* mutants, we cannot eliminate the possibility that these mutations affect transcription elongation rates or Pol II stalling frequency. As such, future work to specifically assay transcription elongation would aid in determining whether the phenotypes associated with LUTI escape mutants stem from altered transcription elongation rates. Reliable methods to profile transcription elongation *in vivo* involve immunoprecipitation of RNA polymerase or nascent RNA. Elongating Pol II can be differentiated from initiating Pol II by using specific antibodies that recognize Pol II CTD modifications. However, Pol II ChIP is fairly low resolution and exhibits a low signal/background ratio (Jonkers and Lis, 2015).

A more recently developed technique, native elongating transcript sequencing (NET-seq), captures global, single-nucleotide resolution views of elongating Pol II. NET-seq involves isolation of Pol II-associated transcripts through immunoprecipitation of Pol II followed by RNA purification (Churchman and Weissman, 2011). Using nascent RNA as the molecular readout provides two advantages over conventional Pol II ChIP: (1) It eliminates noise produced from pulldown of non-transcribing Pol II and (2) nascent RNA reads are sequenced from the 3′ end, yielding a smaller and more accurate footprint for elongating Pol II.

Importantly, the high resolution offered by NET-seq allows for quantitative measurement of Pol II pausing (Churchman and Weissman, 2011). We found that the *swi3-E815X* and *snf2-W935R* mutants exhibit synthetic growth phenotypes with deletion of *DST1*, a gene that encodes the TFIIS elongation factor required for alleviating Pol II stalling during elongation (Chapter 3). A compelling model to explain this synthetic phenotype is that the LUTI escape mutants cause higher rates of Pol II pausing at nucleosome barriers, though TFIIS relieves pausing and promotes normal transcription levels overall. Performing NET-seq in the LUTI escape mutants, with and without deletion of *DST1*, would test this hypothesis.

NET-seq experiments can inform whether the mutants result in higher degrees of Pol II pausing more generally at canonical Swi/Snf targets; however, there are limitations to using NET-seq for interpretation of interference phenotypes. For one, the presence of two promoters that are simultaneously active in the LUTI escape mutants for these loci makes it impossible to determine which nascent transcript is being measured at overlapping positions. Second, a hypothetical positive result revealing mutant-induced

Pol II pausing upstream of the proximal promoter would not fully address the mechanistic question at hand: does the proximal promoter become de-repressed in these mutants due to lower rates of Pol II elongation or due to increased nucleosome occupancy?

Although interpretation at these specific sites of interference would be difficult, interpretation of NET-seq data for the hundreds of Swi/Snf canonical targets would further inform our understanding of Swi/Snf's function in co-transcriptional remodeling. For instance, does Swi/Snf perform this function at all of its targets, or is this activity limited to specific contexts? Related to our hypothesis that Swi/Snf may be acting only at the 5′ end of transcribed regions, do the LUTI escape mutations impact elongation across the entire gene body or are affects limited to a certain window? NET-seq has been performed on several chromatin remodeling mutants (Couvillion et al., 2022), but never with a Swi/Snf mutant. Thus, these experiments would reveal new insights as to whether Swi/Snf impacts transcription elongation on a global scale.

Swi/Snf-based repression in metazoans: future work to test whether transcriptional interference is a conserved function

Alternative promoter usage is widespread in humans and Swi/Snf components are highly conserved from yeast to humans. Our novel finding that Swi/Snf establishes transcriptional interference at select genes in yeast and the crucial roles for Swi/Snf in human development motivate further investigation as to whether Swi/Snf also regulates transcriptional interference in human cells. Specific genes of interest include Blimp-1 based on its alternative promoter usage and previous evidence that Swi/Snf is required for its repression in mice (Choi et al., 2015; Morgan et al., 2009). Another locus of interest is *MDM2*, which has a distal promoter that drives expression of a LUTI. It is unknown whether $MDM2^{LUTI}$ expression induces nucleosome changes, and as such preliminary experiments might include MNase-qPCR assays in cells with and without LUTI expression. Previously CRISPRi was used to successfully knock down $MDM2^{LUTI}$ expression, resulting in higher levels of the MDM^{PROX} coding transcript. Additionally, factors required for $MDM2^{LUTI}$ activation, which is expressed naturally during endoderm differentiation, are unknown. Given our model that Swi/Snf is involved in both activation of the LUTI and repression of the proximal promoter, it would also be important to first characterize whether human Swi/Snf binds and regulates $MDM2^{LUTI}$ promoter.

Though these preliminary experiments could be performed by comparing wild type cells to full knockdown of Swi/Snf components, further exploration of Swi/Snf co-transcriptional remodeling may require more gentle genetic perturbations. Since the LUTI escape mutation *snf2-W935R* specifically impairs Swi/Snf transcriptional interference function (Chapters 2 and 3) and affects a conserved residue of the catalytic subunit, creating the analogous mutation in the human catalytic subunits may be a useful tool for functional analyses. However, this idea operates under the assumption that if co-transcriptional remodeling by Swi/Snf is conserved, so is the specific role for this particular residue, which may not be the case. In this regard, assays mimicking our $HNT1^{LUTI}$ *cis*-regulatory perturbations could prove informative (Chapter 3). If a proximal promoter is

repressed, exhibits nucleosome remodeling, and Snf2 binding upon expression of an alternative distal promoter, this would provide preliminary evidence that Swi/Snf is involved in its interference. But the outcome of inserting a terminator sequence would be even more telling. Based on our observations from *HNT1* experiments, Swi/Snf transcriptional interference function relies on transcription elongation of the interfering transcript. If this activity is conserved in humans, we predict terminator insertion would result in lower Swi/Snf occupancy at the proximal promoter, de-repression of the proximal promoter, and decreased nucleosome remodeling.

This repressive function by Swi/Snf can also be explored on a genome-wide scale using TL-seq and Nanopore sequencing to identify sites with alternative transcription that are regulated by Swi/Snf. Preliminary genes of interest could be gathered based on showing (1) alternative transcription (2) an inverse relationship between transcript isoforms, and (3) Swi/Snf occupancy coinciding with distal promoter expression. However, further functional characterization would require some perturbation to Swi/Snf activity. The challenge here again lies in finding mutant or cellular contexts that impair Swi/Snf transcriptional interference function without impairing its ability to activate canonical targets and distal promoters. If yeast LUTI escape alleles are not useful models for this in humans due to divergence, perhaps directed mutagenesis strategies, such as mutagenic PCR, could be useful to generate hypomorph alleles with similar phenotypes.

Swi/Snf biology is exponentially more complex in humans. There are numerous tissue-specific complexes comprised of different combinations from a pool of 29 subunits including two mutually exclusive catalytic subunits (Kadoch and Crabtree, 2015). While this introduces technical barriers to functional studies, it also introduces exciting possibilities regarding the specialization of Swi/Snf complexes within different genomic loci and cell types. Our methods to identify the specialized role for Swi/Snf in transcriptional interference at certain yeast genes can thus be employed to investigate this function in human cells.

Chapter 5 – Appendix A, Conditional Swi/Snf Phenotypes

5.1 Introduction

During our phenotypic characterization of LUTI escape mutants (Chapters 2 and 3), we uncovered several interesting Swi/Snf conditional phenotypes. First, we found that the Swi/Snf LUTI escape phenotype in the mutant *swi3-E815X* was not reproducible in the SK1 strain background as opposed to the W303 background initially used for selection of LUTI escape mutants. Furthermore, several viable Swi/Snf mutations in the W303 strain background were inviable in SK1, including null and LUTI escape mutants. Finally, we found that although the regulatory subunit Snf5 is required for vegetative growth, it is surprisingly dispensable in meiosis.

Hundreds of LUTIs are activated at distinct stages of budding yeast meiosis (Cheng et al., 2018). As such, we initially sought to characterize Swi/Snf LUTI escape mutants within the biological context of meiosis. Additionally, the 5′ leader sequence from *NDC80*^{LUTI}, which restricts synthesis of the limiting kinetochore subunit Ndc80 during meiotic prophase, was used to build LUTI reporter alleles used in LUTI escape mutant selection (Chapter 2) based on its strong repressive activity. Preliminary experiments to assay LUTI escape phenotypes involved measuring *NDC80* mRNA isoform levels and Ndc80 protein levels throughout meiosis in the SK1 background, which is far superior to W303 for performing synchronous meiosis experiments. In this chapter, I will present data revealing dramatic phenotypic differences among Swi/Snf mutants both between the SK1 and W303 strain backgrounds, and between vegetative and meiotic conditions. These findings point towards two interesting possibilities to be further investigated: (1) Additional factors, such as other chromatin remodelers, differentially modulate Swi/Snf function in SK1 compared to W303 and (2) yeast Swi/Snf subcomplexes can form in certain conditions, such as meiosis, that may regulate gene target specificity.

5.2 Swi/Snf mutations confer strain-dependent phenotypes

Loss of Swi3 function does not affect LUTI-based repression in meiosis

To address whether the *swi3-E815X* mutant affects *NDC80* regulation during meiosis, we built *swi3-E815X* mutant and *SWI3* control strains in the SK1 background, which undergoes efficient, synchronous meiotic divisions. We performed meiotic time course experiments in cells with a C-terminally tagged allele of Ndc80 at its endogenous locus and monitored Ndc80 protein levels by immunoblotting. In contrast to its impact on LUTI regulation in W303 cells undergoing vegetative growth, the SK1 *swi3-E815X* mutant did not upregulate Ndc80 protein levels during meiosis (Figures 5.1A and 5.1B). In fact, the *swi3-E815X* mutant exhibited prolonged low levels of Ndc80 during meiosis relative to the *SWI3* control cells. Because Ndc80 levels rise at onset of meiotic divisions in response to *NDC80*^{PROX} activation by the mid-meiotic transcription factor *NDT80* (J. Chen et al., 2017; Miller et al., 2012), we hypothesized the prolonged Ndc80 repression in *swi3-*

E815X cells could be due to a meiotic delay. Indeed, when we performed cellular staging by tubulin immunofluorescence, we found that *swi3-E815X* cells enter metaphase I about 30 minutes later than *SWI3* control cells before progressing through the meiotic divisions (Figure 5.1B). This delay was surprising, given that previous characterization of the *swi3-E815X* mutant in W303 revealed very few gene expression defects and no growth defects (Chapters 2 and 3). Unlike W303, the deletion of *SWI3* is not viable in SK1 (Figure 5.1C), indicating there are broad genetic-background dependencies for Swi/Snf phenotypes.

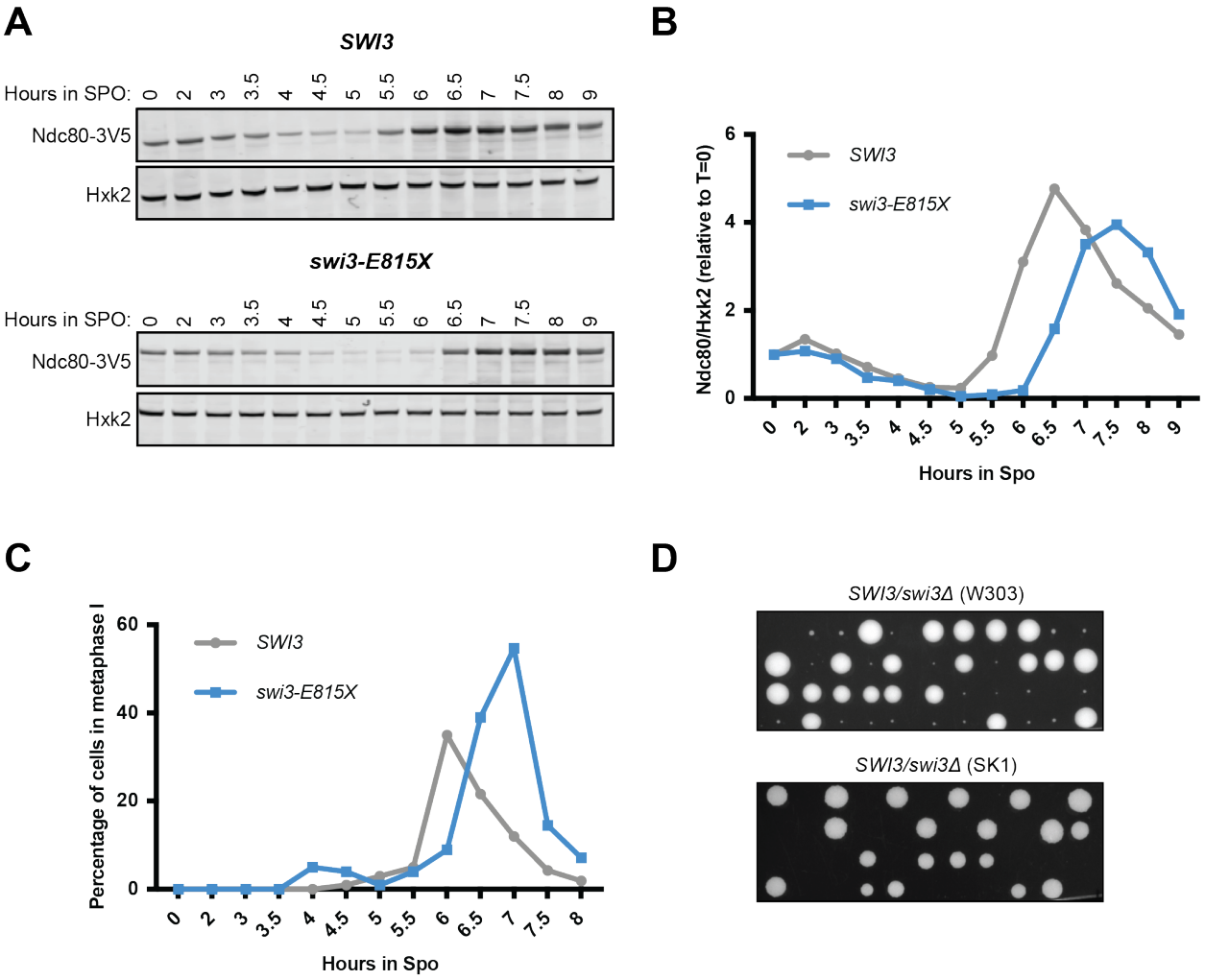

Figure 5.1: *The swi3-E815X mutation does not affect NDC80^{LUTI} regulation in meiosis*
(A) Immunoblot specific to the V5 epitope. Hexokinase is used as a loading control. Wild-type control cells (UB20320) or *swi3-E815X* mutants (UB20322) harboring an *NDC80-3V5* allele were collected at timepoints throughout meiosis. To induce synchronous entry to meiosis, strains also harbored *pCUP1-IME1* and *pCUP1-IME4* alleles (Chia and Werven, 2016). $CuSO_4$ (final [50 μM]) was added at 2 h to induce meiotic entry **(B)** Quantification of immunoblot in (A). **(C)** Quantification of cells in metaphase I based on tubulin immunofluorescence. 100 cells were scored from each sample for each time point. **(D)** Growth, on YPD, from haploid spores dissected from hemizygous *swi3Δ* W303 (top, UB18635) or SK1 (bottom, UB19590) strains. Small colonies from the W303 dissection all harbored the *swi3Δ* allele. No *swi3Δ* haploids survived in SK1.

We wondered whether the *swi3-E815X* mutation conferred less of an effect on Swi/Snf function in SK1 or during meiosis compared to vegetative W303 cells. If this were true, we predicted Swi/Snf may regulate LUTI-based repression during meiosis but that its impact on LUTI regulation cannot be tested using this particular allele. As such, we tested whether complete removal of the Swi3 protein through its conditional depletion during meiosis would affect *NDC80* regulation. We used the auxin-inducible degradation system with a copper-inducible *TIR1* allele to deplete Swi3 early in meiosis and monitored both Swi3-3V5-AID and Ndc80-3V5 protein levels by immunoblotting and *NDC80* mRNA isoform levels by RNA blotting. Depletion of Swi3 was efficient and resulted in moderate upregulation of Ndc80 during early meiosis (Figures 5.2A-C). We also observed slightly higher levels of the $NDC80^{PROX}$ isoform during early meiosis with Swi3 depletion. However, Swi3 depletion resulted in severe meiotic defects (Figure 5.2D). A high proportion (~50%) of Swi3-depleted cells had not entered meiosis during the timepoints with observed higher Ndc80 protein and $NDC80^{PROX}$ levels (Figures 5.2A and 5.2D), making these results inconclusive based on population heterogeneity.

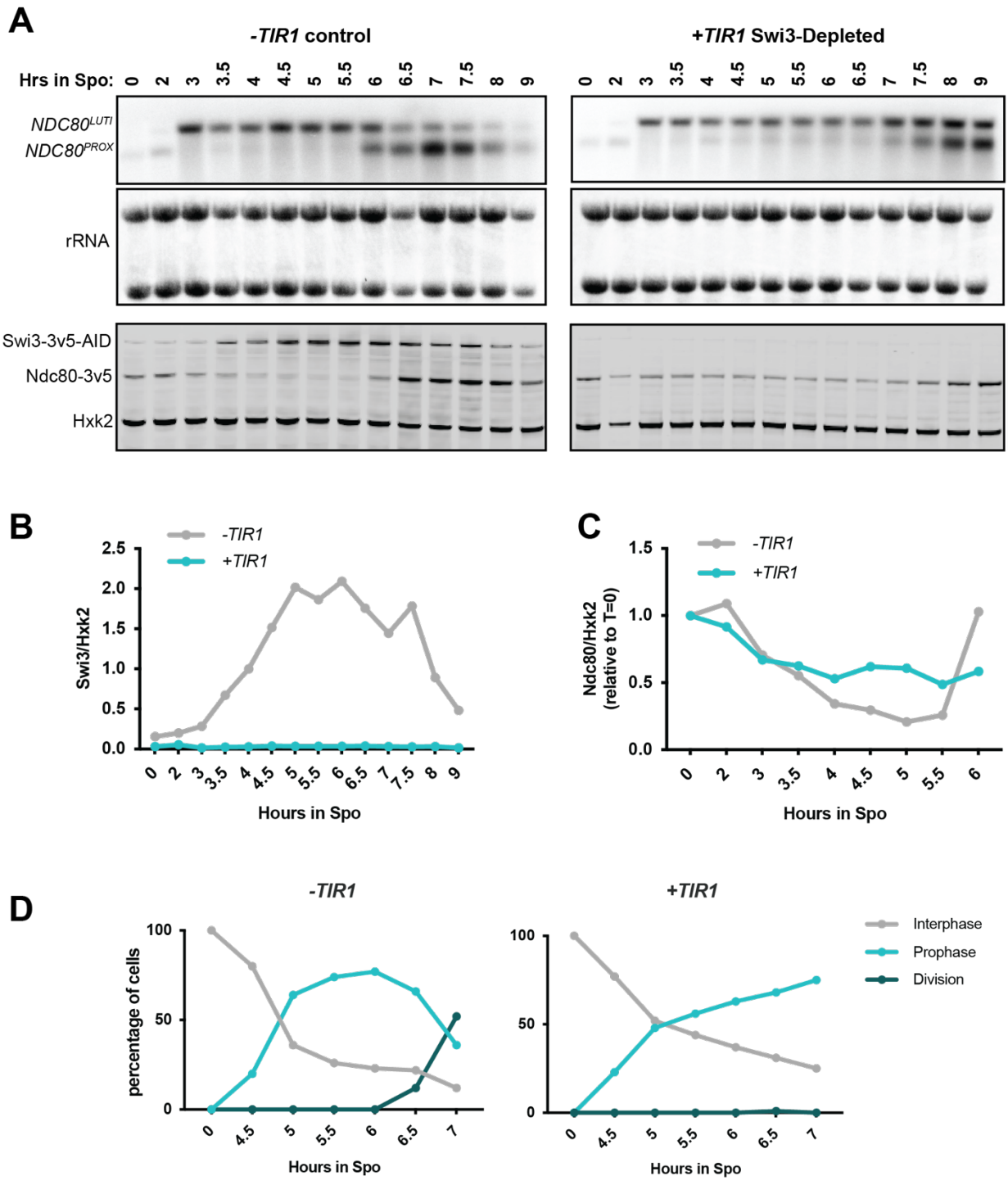

Figure 5.2: *Meiotic Swi3 depletion severely impacts meiotic progression*
(A) RNA blot probed for the *NDC80* CDS (top) and immunoblot specific to the V5 epitope. For the RNA blot, rRNA bands are detected by methylene blue staining. For the immunoblot, Hexokinase is used as a loading control. Cells harboring a *SWI3-3V5-AID* allele and *NDC80-3V5* allele, with (UB21552) or without *pCUP1-TIR1* (UB21551), were collected at timepoints throughout meiosis. To induce synchronous entry to meiosis, strains also harbored *pCUP1-IME1* and *pCUP1-IME4* alleles (Chia and Werven, 2016). $CuSO_4$ (final [50 µM]) was added at 2 h to induce *TIR1* expression and meiotic entry. Auxin (final [500 µM]) was

also added to both flasks at 2 h. **(B)** Quantification of Swi3 immunoblot in (A). **(C)** Quantification of Ndc80 immunoblot in (A). To measure protein turnover as a result of LUTI-based regulation, protein is normalized to the starting point at t = 0. **(D)** Progression through meiosis as measured by DAPI staining and fluorescent microscopy. N = 100 cells were counted at each timepoint.

Identification of a LUTI escape modifier allele

Based on the strain background differences controlling the viability of *swi3Δ* mutants (Figure 5.1C), we wondered whether the lack of LUTI escape phenotypes during meiosis for the *swi3-E815X* mutant was also due to genetic differences between the W303 and SK1 strain backgrounds. We tested this by measuring $HNT1^{LUTI}$ levels in W303 and SK1 cells during vegetative growth with and without UPR induction with the drug DTT. As expected (see Chapter 3), W303 *swi3-E815X* cells showed upregulation of the $HNT1^{PROX}$ mRNA during $HNT1^{LUTI}$ expression (Figure 5.3A). However, the *swi3-E815X* mutant did not impact *HNT1* regulation in the SK1 background (Figure 5.3A).

We reasoned that we could identify genetic determinants, or modifiers, of the *swi3-E815X* LUTI escape phenotype through a serial backcrossing and sequencing strategy. We crossed W303 *swi3-E815X* with SK1 *swi3-E815X* cells, each harboring the *lexO-*$HIS3^{LUTI}$ reporter allele and LexA-ER-B112 transcription factor used for LUTI escape mutant selection (Figure 5.3B, Chapter 2). When we phenotyped hybrids from this cross on selective -his media with β-estradiol to induce $HIS3^{LUTI}$, we observed 2:2 segregation among isolates taken from the same tetrad (Figure 5.3C). This Mendelian pattern of inheritance indicates the LUTI escape modifier phenotype is controlled by a single gene.

We performed two more rounds of backcrossing to SK1, each time selecting a hybrid that confers the LUTI escape phenotype (Figure 5.3B). After the third round, we saved 20 isolates that exhibited the LUTI escape phenotype and 20 control isolates that did not. We pooled cells within each group and performed whole genome sequencing on these pools along with W303 and SK1 cells as a control. Variant calling identified a recombination block, consisting of eight genes, that matched with 100% identity to the W303 genome for the pooled group with the phenotype and 100% identity to the SK1 genome for the pooled group with no phenotype (Figure 5.3D).

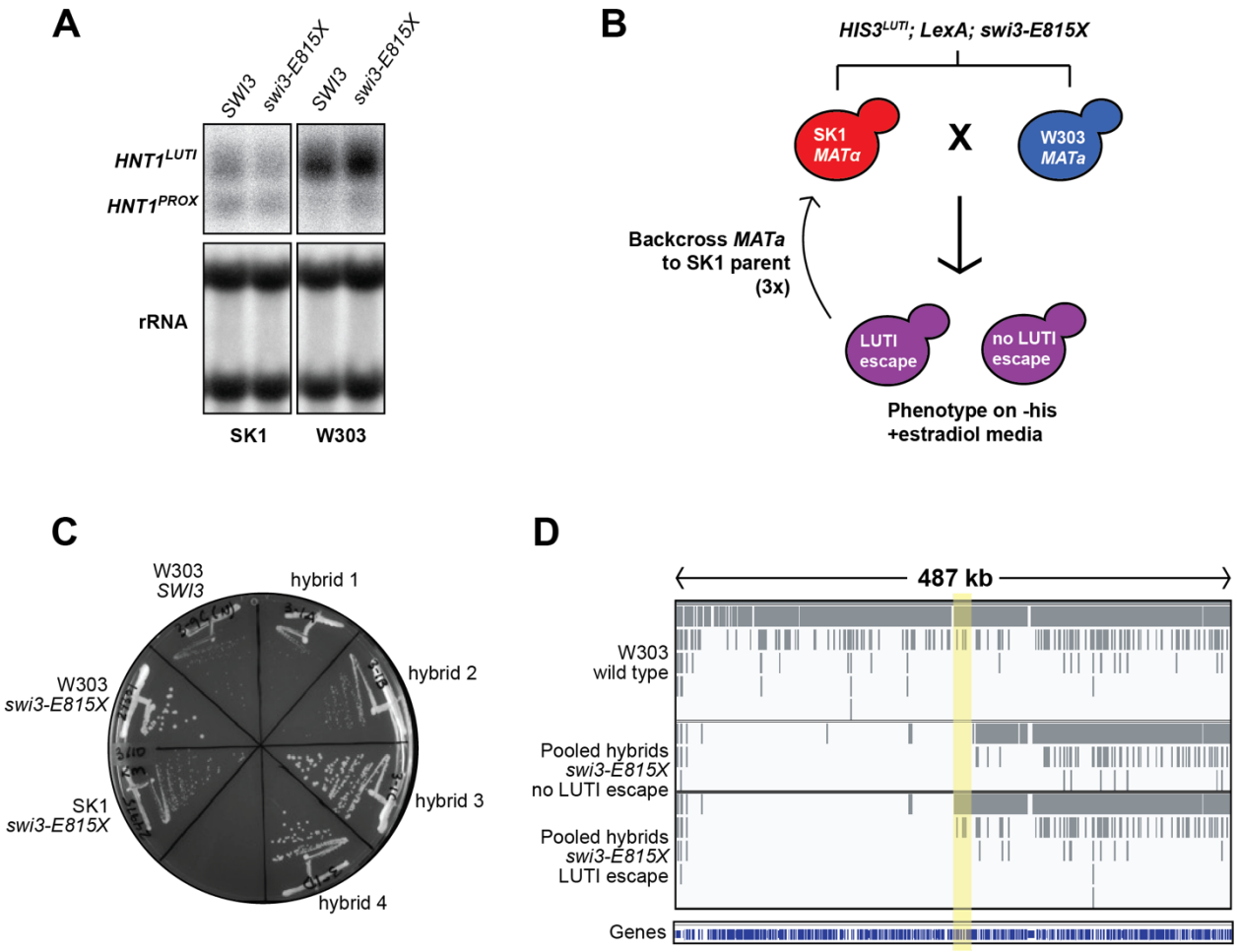

Figure 5.3: *Selecting for the LUTI escape phenotype in hybrid W303/SK1 swi3-E815X cells*
(A) RNA blot probed for the *HNT1* CDS in SK1 and W303 *SWI3* cells (UB19793 [SK1] or UB19205 [W303]) or *swi3-E815X* cells (UB19889 [SK1], UB19209 [W303]). Cells were untreated or treated with 5 mM DTT for 1 h and collected for RNA extraction. rRNA bands were detected by methylene blue staining. **(B)** Strategy for SK1/W303 backcrossing and segregant analysis strategy. MATa *swi3-E815X* cells harboring the *lexO-HIS3*^{LUTI} reporter (UB24301) and the LexA-ER-B112 heterologous TF were mated to SK1 MATα cells (UB24976) with the same genotype. Individual colonies arising from tetrads were scored on -his media with 25 nM β-estradiol and hybrid strains with stronger LUTI escape phenotypes were carried forward for another round of mating to SK1 and phenotyping. After 3 rounds, hybrid strains with and without LUTI escape phenotypes were saved and pooled for genomic DNA extraction and sequencing. **(C)** Example of LUTI escape phenotyping among SK1/W303 hybrids. Control strains depict strong LUTI escape in the W303 *swi3-E815X* mutant (UB24301) compared to the W303 *SWI3* cells (UB29791) or SK1 *swi3-E815X* cells (UB24976). The four hybrid strains plated all arose from the same tetrad, revealing 2:2 mendelian segregation of the W303 LUTI escape modifier allele. **(D)** Variants detected from whole genome sequencing of control W303 cells (top), pooled hybrids with no LUTI escape phenotypes (middle), and pooled hybrids with LUTI escape phenotypes (bottom) aligned to the SK1 reference genome. Analysis revealed a single recombination block (highlighted in yellow) matching only the W303 genotype among *swi3-E815X* hybrids with LUTI escape phenotypes and only the SK1 genotype in *swi3-E815X* hybrids with no LUTI escape phenotype. This region harbors eight protein-coding genes (See table 5.1).

Gene	Function	No. of variants within ORF	No. of coding changes (nonsynonymous)
AAT1	mito aspartate aminotransferase	1	0
SEG2	eisosome component, may be important for stability and/or assembly of eisosomes	12	6
GFA1	glutamine fructose-6-phosphate amidotransferase	10	2
LAP4	vacuolar aminopeptidase	4	0
HSL1	kinase, regulates morphogenesis and septin checkpoint	21	3
YPF1	protein of perinuclear ER membrane, protein degradation	6	3
UTP11	production of 18S rRNA and assembly of small ribosomal subunit	0	0
MTC2	unknown function, synthetic sick w/ cdc13, named for maintenance of telomere capping	3	1

Table 5.1: *List of gene candidates that modify LUTI escape*
The W303 recombination block associated with stronger LUTI escape phenotypes in *swi3-E815X* hybrid cells harbors eight protein coding sequences. All genes except for *UTP11* have sequence differences within the ORF between the two strain backgrounds. Among the remaining seven genes, only five contained nonsynonymous changes.

Although this region contained eight genes, only five of the genes have coding differences between the two strain backgrounds (Table 5.1). As such, we assayed these five candidates for their role in regulating LUTI escape phenotypes. First, we tested whether the modifier phenotype was dominant or recessive by assaying $HIS3^{LUTI}$ escape in diploid cells and found that a diploid generated by mating a hybrid to SK1 did confer the LUTI escape phenotype, indicating the modifier phenotype is dominant (Figure 5.4A). Next, we integrated the W303 allele for each of the five genes at the *LEU2* transgenic locus in *swi3-E815X* SK1 cells. $GFA1^{W303}$ was the only allele that led to stronger LUTI escape in SK1 cells (Figure 5.4B). *GFA1* encodes a glutamine-fructose-6-phosphate amidotransferase involved in catalyzing the first step of UDP-N-acetyl glucosamine (UDP-GlcNAc) biosynthesis (Lagorce et al., 2002). This protein does not have known roles in transcription but may have roles in protein stability based on its role in protein glycosylation. In W303, positions 298 (within the glutamine amidotransferase domain) and 643 (within the phosphosugar binding domain) of Gfa1 are valine residues, whereas in SK1 these positions are alanine residues.

Because phenotyping the $GFA1^{W303}$ modifier had so far been limited to growth assays, we next investigated whether $GFA1^{W303}$ regulates the LUTI escape phenotype in *swi3-E815X* cells at the level of transcription. We performed RNA blotting to measure

HIS3^{LUTI} and *HIS3*^{PROX} levels in SK1 *swi3-E815X* cells with and without the *GFA1*^{W303} transgenic allele. While the *swi3-E815X* mutant displayed modest upregulation of *HIS3*^{PROX} on its own relative to *SWI3* control cells, the *GFA1*^{W303} modifier allele did not additionally increase *HIS3*^{PROX} levels. We conclude that *GFA1*^{W303} exerts its effects on the LUTI escape phenotype through regulating growth or Ndc80 protein stability, but not at the level of transcription. Additionally, SK1 *swi3-E815X* cells do exhibit subtle LUTI escape phenotypes that are normally masked by growth-based assays to measure survival on -his selective media without the *GFA1*^{W303} allele.

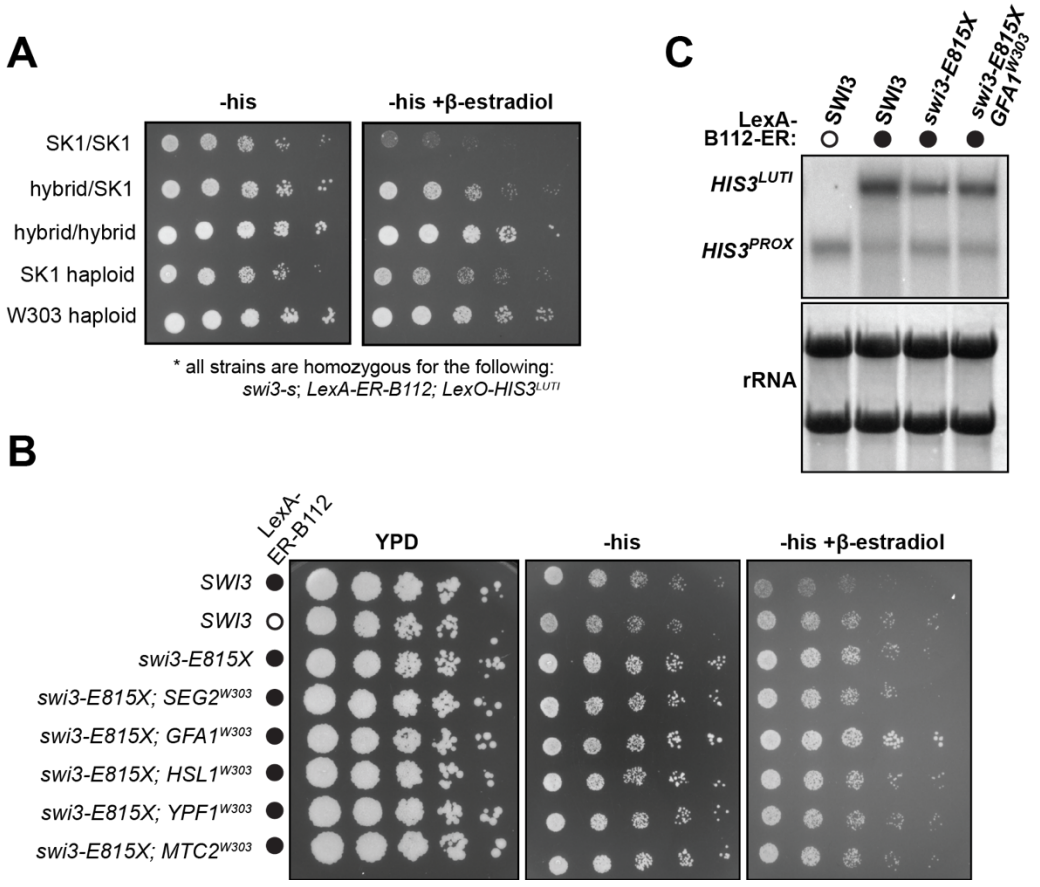

Figure 5.4: *GFA1*^{W303} *modulates LUTI escape growth-based phenotypes without impacting LUTI-based transcriptional interference*
(A) Serial dilution and plating assay to test dominance/recessive phenotype for the W303 LUTI escape modifier allele. Diploid cells or haploid controls were plated on media lacking histidine with 25 nM β-estradiol. **(B)** Serial dilution and plating assay to score LUTI escape phenotypes among SK1 cells harboring the *lexO-HIS3*^{LUTI} reporter. W303 alleles of each candidate gene were integrated at the *LEU2* locus. Strains, top to bottom: UB24820, UB24822, UB24975, UB26207, UB26208, UB26211, UB26212, UB26215. **(C)** RNA blot probed for the *HIS3* CDS in SK1 control cells with (UB24820) or without (UB24822) *HIS3*^{LUTI} induction and SK1 *swi3-E815X* cells with (UB24975) or without (UB26208) the *GFA1*^{W303} modifier allele.

5.3 Conditional requirements for a key regulatory subunit: Snf5 is essential in SK1 during mitosis but dispensable in meiosis

In addition to *SWI3* experiments, we also tested whether the regulatory subunit Snf5 was required for LUTI escape phenotypes in meiosis. We found that the LUTI escape mutant *snf5-Q225X* collected in W303 (Chapter 2) was not viable in SK1, and thus used a conditional depletion strategy to measure the effects of this mutation on LUTI-based gene regulation for the gene *NDC80*. We tagged *SNF5* at its endogenous locus with a 3V5-AID epitope-degron tag and integrated the *snf5-Q225X* LUTI escape allele at the *LEU2* transgenic locus under the native *SNF5* promote. This strategy enabled conditional depletion of non-mutant Snf5 protein while leaving expression of the mutant protein intact.

Surprisingly, depletion of the non-mutant protein did not result in any changes in Ndc80 protein levels or evidence of meiotic progression defects (Figures 5A-C). Even with full depletion of Snf5 and no transgenic rescue allele, cells regulated Ndc80 normally and sporulated well (Figures 5A-C). We verified that our depletion strategy was effective at eliminating Snf5 function by performing depletion in vegetative cells, using Swi3 depletion as a positive control. In these conditions, Snf5-depleted cells were not viable (Figure 5.5D). Together, these results reveal striking differences in the dependency for Snf5, a key regulatory subunit, in mitotically growing cells compared to meiotic cells.

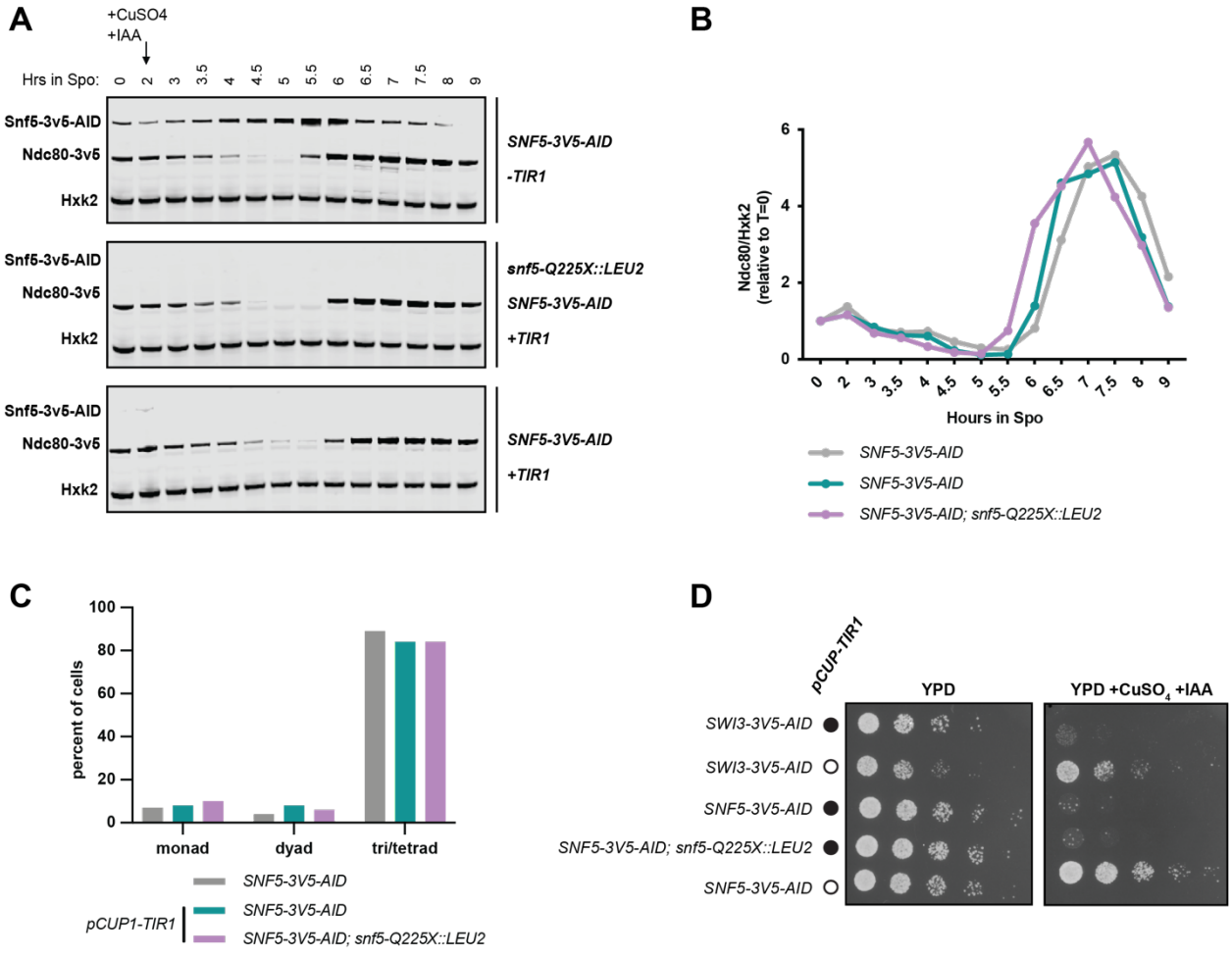

Figure 5.5: *Snf5 is dispensable for meiosis but essential for vegetative growth*
(A) Immunoblot specific to the V5 epitope. Hexokinase is used as a loading control. Cells harboring *pCUP1-TIR1, SNF5-3V5-AID,* and *NDC80-3V5*, with (UB23505) or without (UB23503) a transgenic copy of the LUTI escape allele *snf5-Q225X*, were collected at timepoints throughout meiosis. Control cells (UB23506) with the *SNF5-3V5-AID* allele lacking *pCUP-TIR1* were used to monitor normal Ndc80-3V5 levels and meiotic progression. To induce synchronous entry to meiosis, strains also harbored *pCUP1-IME1* and *pCUP1-IME4* alleles (Chia and Werven, 2016). $CuSO_4$ (final [50 μM]) was added at 2 h to induce *TIR1* expression and meiotic entry. Auxin (final [500 μM]) was also added to both flasks at 2 h. **(B)** Quantification of Ndc80 immunoblot in (A). To measure protein turnover as a result of LUTI-based regulation, protein is normalized to the starting point at t = 0. **(C)** Sporulation measured at 24 h by light microscopy. N = 100 cells were counted from each flask. **(D)** Serial dilution and plating assay to test the effect of depleting Swi3 (UB21552 [+*TIR1*] or UB21551 [-*TIR1*]) or Snf5 (UB23503 [+*TIR1*] or UB23506 [-*TIR1*]) during vegetative growth. Growth with Snf5 depletion in the *snf5-Q225X::LEU2* strain background (UB23505) was also measured.

5.4 Conclusions and Future directions

Gene network control of Swi/Snf phenotypes

Our work to investigate the role of Swi/Snf in LUTI-based transcriptional interference during meiosis led to the finding that the LUTI escape phenotype in *swi3-E815X* SK1 cells is less potent compared to *swi3-E815X* W303 cells. Furthermore, the Swi/Snf subunits Snf5 and Swi3 were found to be required for viability in SK1 despite being viable, albeit severely sick, in W303. W303 is a derivative of the lab domesticated strain S288C, and only differs from S288C at ~8,000 positions (Schacherer et al., 2007). SK1, which is a "wilder" strain of yeast, differs from S288C at over 37,000 genomic positions. Therefore, it is perhaps unsurprising that strain background-dependencies would surface for Swi/Snf phenotypes. At least 95 physical interactions and 336 genetic interactions with the Swi3 subunit alone have been described (Cherry et al., 1997). Of note, Swi/Snf participates in genetic pathways with several broad regulators of transcription, including SAGA, RSC, and Cyc8 (Chandy et al., 2006; Proft and Struhl, 2002; Rawal et al., 2018; Sahu et al., 2021).

Future work to investigate strain-background regulation of Swi/Snf phenotypes, including the differential requirement for *SWI3* in SK1 versus W303, might involve first identifying sequence changes among these key transcriptional regulators that act in pathways with Swi/Snf. Candidates with coding changes could then be further investigated by replacing the W303 allele for the SK1 allele and testing whether any of these alleles to rescue viability for *swi3Δ* SK1 cells. An unbiased strategy similar to the one used to identify the $GFA1^{W303}$ modifier allele could be used to uncover modifiers of *swi3Δ* viability. For this, *swi3Δ* W303 cells could be crossed to wild type SK1 cells, then viable haploid progeny harboring the deletion could be selected and backcrossed again to SK1, repeating over several rounds. Although there would be no negative control group due to its inherent inviability, sequencing of viable *swi3Δ* hybrid cells would reveal loci

that consistently match the W303 genotype and thus allow for survival of *swi3Δ* mutants in W303.

In our attempt to identify genetic determinants of the LUTI escape phenotype within *swi3-E815X* cells, we inadvertently selected for an allele that regulates growth and/or protein levels rather than transcriptional control of LUTI regulated genes. Our investigation into the effects of *swi3-E815X* and $GFA1^{W303}$ on LUTI regulation are consistent with a model in which Swi/Snf does regulate LUTI-based repression in SK1, although LUTI escape is weaker in SK1 mutants compared to W303. This weak phenotype for the $HIS3^{LUTI}$ reporter is further masked by decreased growth rate and/or reduced His3 protein stability conferred by the $GFA1^{SK1}$ allele. Though we were able to rescue the stronger LUTI escape phenotype in SK1 for growth-based assays through integration of the $GFA1^{W303}$ allele, we ultimately did not uncover new insights related to the weaker transcriptional LUTI escape phenotype in SK1 *swi3-E815X* cells.

Given that Swi/Snf and the related chromatin remodeler RSC have been shown to cooperate at certain loci (Rawal et al., 2018), future work to investigate Swi/Snf LUTI escape phenotypes might involve assaying compensation by RSC during meiosis. For example, LUTI escape phenotypes with depletion of a common subunit shared by these two remodelers, such as a component of the actin-related module, would provide evidence in support of their cooperation in meiosis at LUTI regulated genes. These experiments may be technically challenging, as RSC is an essential remodeler responsible for transcription of both Pol II and Pol III transcribed genes (Rando and Winston, 2012). Another strategy may involve combining known hypomorphic RSC alleles with the *swi3-E815X* allele, which exhibits a slight meiotic delay but ultimately undergoes meiotic divisions with high sporulation (Figure 5.1). In either case, proper staging of meiotic progression would be essential for interpreting the described experiments.

Potential subcomplex formation in meiosis

Snf5 is a regulatory subunit of Swi/Snf that primarily acts in targeting the complex to genomic loci through interactions with transcription factors (TFs) (Neely et al., 2002; Prochasson et al., 2003). Additionally, Snf5 is thought to aid in nucleosome remodeling by serving as an anchor against the nucleosome during DNA translocation by Snf2 (Han et al., 2020; Sen et al., 2017). Given its important role in Swi/Snf function and the fact that Snf5 depletion is lethal in SK1 cells undergoing vegetative growth, the finding that Snf5 is dispensable for meiotic progression is striking. One potential explanation for this finding would be that instead of forming the canonical 12-subunit complex, Swi/Snf forms one or more subcomplex during meiosis. In support of this possibility, we found that the structural subunit Swi3 is required for proper meiotic progression (Figure 5.2), thus Swi/Snf function is not altogether dispensable during meiosis.

Swi/Snf subcomplexes have previously been shown to form in budding yeast upon deletion of *SNF5* (Sen et al., 2017) as well as deletion of other subunits (Dutta et al., 2017). In humans, loss of function for the *SNF5* homolog *SMARCB1* is associated with

malignant rhabdoid tumors and results in formation of an aberrant Swi/Snf complex that is essential for proliferation of SMARCB1-deficient cancer cell lines (Wang et al., 2019). Additionally, in response to oxidative stress Snf5 and several other Swi/Snf subunits relocalize from the nucleus to the cytosol, while the catalytic subunit Snf2 remains nuclear (Dastidar et al., 2012). Thus, while Swi/Snf subcomplex formation is generally associated with mutant or disease states, subunit partition can also occur in natural cellular contexts. Swi/Snf is targeted to genomic loci through both regulatory subunit interactions with other TFs and through interactions with acetylated histone through the Snf2 bromodomain (Dutta et al., 2014). Relocalization of regulatory subunits, such as Snf5, to the cytosol would likely shift the balance from TF-based targeting to favor increased occupancy at genes with acetylated histones through the Snf2 bromodomain (Dutta et al., 2017).

We found that the Snf5 protein is expressed during meiosis and peaks in expression during meiotic divisions. However, we do not know whether Snf5 interacts with Snf2 during meiosis or whether it is constitutively nuclear. Future experiments to investigate the meiotic subcomplex hypothesis would include first tracking localization of Snf5 and Snf2 throughout meiosis by fluorescent microscopy. If Snf5 localization is indeed cytosolic any phase of meiosis, follow-up work would include tracking localization of the remaining 10 subunits to generate a list of possible subcomplexes that form. Subcomplex function could then be further characterized through mRNA-seq and ChIP-seq experiments with conditional depletion of various nuclear subunits.

If Snf5 is constitutively nuclear during meiosis, next steps would involve investigating the possibly that Snf5 complexes with other chromatin remodeling ATPases outside of Swi/Snf. This possibility could be tested performing ChIP-seq experiments pulling down on Snf5 and Snf2 to first gauge whether they bind disparate targets in meiosis. Next, Snf5 immunoprecipitation from meiotic samples followed by mass spectrometry could identify novel Snf5 binding partners.

Finally, if no evidence supports the subcomplex model, this would indicate Snf5-based targeting of Swi/Snf is simply unimportant during meiosis despite canonical complex formation. This would nonetheless be an intriguing path to explore, as it would indicate dramatic rewiring of Swi/Snf-dependent gene expression during meiosis. In unstressed, vegetative cells, Swi/Snf activates expression of many highly expressed “housekeeping” genes, including ribosomal protein (RP) genes (Rawal et al., 2018; Shivaswamy and Iyer, 2008). RP gene expression is dynamically regulated during meiosis, with corresponding mRNA levels being high during meiotic entry and in spores, but low during meiotic divisions (Eisenberg et al., 2018). Perhaps regulation of Swi/Snf occupancy is rewired in meiosis, either through subcomplex formation or posttranslational modification of certain subunits, to favor decreased transcription of RP genes. General characterization of meiotic Swi/Snf targets through mRNA-seq and ChIP-seq experiments would aid in forming a baseline understanding of differential Swi/Snf regulation between vegetative growth and meiosis.

Chapter 6 – Appendix B, Methods

6.1 Strain and plasmid construction

All yeast strains described in Chapters 2 and 3 were derived from the W303 background. Yeast strains in Chapter 5 (Appendix A) were derived from the W303 or SK1 backgrounds. Genotypes are listed in Table 6.1. All gene deletions were made via Pringle-based insertion of a drug resistance cassette replacing the endogenous CDS, except for the case of the *hnt1Δ* in which the CDS and 275 bases upstream of the CDS was replaced with a drug resistance cassette. The *pLexO-HIS3*^{LUTI} reporter construct was generated by cloning the *NDC80*^{LUTI} 5′ leader sequence and the *HIS3* CDS into a *LEU2* single integration vector harboring a 3X *lexO* array upstream of a *CYC1* minimal promoter via three-piece Gibson Assembly (Gibson et al., 2009). The *pTEF1-ADE2*^{LUTI} reporter construct was derived from the *pLexO-HIS3*^{LUTI} in a two-step process: First the *HIS3* CDS was replaced with the *ADE2* CDS by two-piece Gibson Assembly to create a *pLexO-ADE2*^{LUTI} plasmid, then the Lex-inducible promoter was replaced with the *TEF1* promoter amplified from gDNA by two-piece Gibson Assembly. Transgenic *SNF2, SNF5,* and *SWI3* wild-type or LUTI escape alleles with their endogenous gene promoter and terminator sequences were amplified from genomic DNA and cloned into a *LEU2* single integration plasmid via two-piece Gibson Assembly.

For strains used in Snf2 ChIP experiments, Pringle-based insertion was used to insert a 3V5 epitope tag at the C-terminal end of the endogenous *SNF2* CDS (for UB29161, UB30070, and UB30071), or the *LEU2* transgenic copy of *SNF2, snf2-W935R,* and *snf2-Q928K* (for UB30387, UB30391, and UB30389). Wild type and *pDISTΔ* transgenic constructs for *HNT1*, *ADI1*, *ODC2*, and *ERG27* were generated by cloning the CDS for each gene with upstream sequence including the distal TSS and 300 bases upstream (WT) or the sequence immediately downstream of the the distal TSS (*pDISTΔ*) into a *TRP1* single integration vector harboring a C-terminal 3V5 epitope sequence. The *HNT1*$^{LUTI\text{-}CYC1t}$ construct was generated by cloning the *CYC1* terminator into the *HNT1*^{LUTI}*-3V5 TRP1* single integration vector 40 bp downstream of the *HNT1*^{LUTI} TSS via two-piece Gibson Assembly. To generate conditional depletion alleles using the AID system, Pringle-based insertion was used to insert a 3V5-AID tag at the C-terminal end of either *SWI3* or *SNF5*.

The *LexO-SOD1*^{LUTI} strains were constructed by Pringle-based insertion of an 8X LexO array upstream of the *CYC1* minimal promoter at positions 1700 bp, 860 bp, or 330 bp upstream of the *SOD1*^{PROX} TSS. To make the *SOD1*$^{LUTI\text{-}560}$ strain, the *SOD1*$^{LUTI\text{-}860}$ strain was edited using CRISPR/Cas9 with a gRNA directed to the region shared between the *SOD1*$^{LUTI\text{-}860}$ and *SOD1*$^{LUTI\text{-}330}$ strain and a repair template to delete this sequence. For all Gibson Assembly reactions, the NEBuilder HiFi Master Mix was used according to kit instructions (E5520S, *New England Biolabs*). All single integration plasmids were digested with PmeI before transformations and integrations were verified by PCR. All strains and plasmids used in this study are available upon request.

Table 6.1: Strains

Strain	Genotype
UB7, *W303* wild type	*MATa, ade2-1, leu2-3, ura3, trp1-1, his3-11,15, can1-100, GAL, psi+*
UB4784, ADE+ *W303* wild type	*MATa, ADE2, leu2-3, ura3, trp1-1, his3-11,15, can1-100, GAL, phi+*
UB13670	*MATa, ADE2, leu2-3, ura3, trp1-1, his3-11,15, can1-100, GAL, psi+* *his3::3xLexO-NDC80leader::HIS3*
UB17314	*MATa, ADE2, leu2-3, ura3, trp1-1, his3-11,15, can1-100, GAL, psi+* *trp1::pGPD1-LexA-ER-HA-B112::TRP1* *his3::3xLexO-NDC80leader::HIS3*
UB18635	*MATa, ADE2, leu2-3, ura3, trp1-1, his3-11,15, can1-100, GAL, phi+* *MATalpha, ADE2, leu2-3, ura3, trp1-1, his3-11,15, can1-100, GAL, phi+* *swi3::KANMX (swi3 hemizygote)*
UB19205	*MATa, ADE2, leu2-3, ura3, trp1-1, his3-11,15, can1-100, GAL, phi+* *swi3::KANMX* *leu2::SWI3::LEU2*
UB19209	*MATa, ADE2, leu2-3, ura3, trp1-1, his3-11,15, can1-100, GAL, phi+* *swi3::KANMX* *leu2::swi3-E815X::LEU2*
UB19590	*MATa, ho::LYS2, lys2, ura3, leu2::hisG, his3::hisG, trp1::hisG* *MATalpha, ho::LYS2, lys2, ura3, leu2::hisG, his3::hisG, trp1::hisG* *swi3::KANMX (swi3 hemizygote)*
UB19793	*MATa, ho::LYS2, lys2, ura3, leu2::hisG, his3::hisG, trp1::hisG* *swi3::KANMX* *leu2::SWI3::LEU2*
UB19889	*MATa, ho::LYS2, lys2, ura3, leu2::hisG, his3::hisG, trp1::hisG* *swi3::KANMX* *leu2::swi3-E815X::LEU2*
UB20060	*MATa, ADE2, leu2-3, ura3, trp1-1, his3-11,15, can1-100, GAL, phi+* *snf2::KANMX*
UB20320	*MATa, ho::LYS2, lys2, ura3, leu2::hisG, his3::hisG, trp1,* *irt1:cup1::Hphmx* *ime4::cup1::NAT* *swi3::KANMX* *leu2::SWI3::LEU2* *Ndc80-3V5:KanMX* *MATalpha, ho::LYS2, lys2, ura3, leu2::hisG, his3::hisG, trp1,* *irt1:cup1::Hphmx* *ime4::cup1::NAT* *swi3::KANMX* *leu2::SWI3::LEU2* *Ndc80-3V5:KanMX*
UB20322	*MATa, ho::LYS2, lys2, ura3, leu2::hisG, his3::hisG, trp1,* *irt1:cup1::Hphmx* *ime4::cup1::NAT* *swi3::KANMX* *leu2::swi3-E815X::LEU2* *Ndc80-3V5:KanMX* *MATalpha, ho::LYS2, lys2, ura3, leu2::hisG, his3::hisG, trp1,*

	irt1:cup1::Hphmx *ime4::cup1::NAT* *swi3::KANMX* *leu2::swi3-E815X::LEU2* *Ndc80-3V5:KanMX*
UB21551	*MATa, ho::LYS2, lys2, ura3, leu2::hisG, his3::hisG, trp1* *MATalpha, ho::LYS2, lys2, ura3, leu2::hisG, his3::hisG, trp1* *Ndc80-3V5:KanMX* *Ndc80-3V5:KanMX* *irt1:cup1::Hphmx* *irt1:cup1::Hphmx* *ime4::cup1::NAT* *ime4::cup1::NAT* *SWI3-3V5-AID::KanMX* *SWI3-3V5-AID::KanMX*
UB21552	*MATa, ho::LYS2, lys2, ura3, leu2::hisG, his3::hisG, trp1* *MATalpha, ho::LYS2, lys2, ura3, leu2::hisG, his3::hisG, trp1* *Ndc80-3V5:KanMX* *Ndc80-3V5:KanMX* *irt1:cup1::Hphmx* *irt1:cup1::Hphmx* *ime4::cup1::NAT* *ime4::cup1::NAT* *SWI3-3V5-AID::KanMX* *SWI3-3V5-AID::KanMX* *his3::pCup1-OsTIR1(codon optimized)::HIS3* *his3::pCup1-OsTIR1(codon optimized)::HIS3*
UB21565	*MATa, ade2-1, leu2-3, ura3, trp1-1, his3-11,15, can1-100, GAL, psi+* *ura3::pTEF1-ADE2luti::URA3*
UB22912	*MATa, ade2-1, leu2-3, ura3, trp1-1, his3-11,15, can1-100, GAL, psi+* *trp1::pGPD1-LexA-ER-HA-B112::TRP1* *ura3::pTEF1-ADE2luti::URA3* *his3::3xLexO-NDC80leader::HIS3*
UB23503	*MATa, ho::LYS2, lys2, ura3, leu2::hisG, his3::hisG, trp1::hisG* *MATalpha, ho::LYS2, lys2, ura3, leu2::hisG, his3::hisG, trp1::hisG* *Ndc80-3V5:KanMX* *Ndc80-3V5:KanMX* *irt1:cup1::Hphmx* *irt1:cup1::Hphmx* *ime4::cup1::NAT* *ime4::cup1::NAT* *SNF5-3V5-AID::KANMX* *SNF5-3V5-AID::KANMX* *his3::pCup1-OsTIR1(codon optimized)::HIS3* *his3::pCup1-OsTIR1(codon optimized)::HIS3*
UB23505	*MATa, ho::LYS2, lys2, ura3, leu2::hisG, his3::hisG, trp1::hisG* *MATalpha, ho::LYS2, lys2, ura3, leu2::hisG, his3::hisG, trp1::hisG* *Ndc80-3V5:KanMX* *Ndc80-3V5:KanMX* *irt1:cup1::Hphmx* *irt1:cup1::Hphmx* *ime4::cup1::NAT* *ime4::cup1::NAT* *SNF5-3V5-AID::KANMX*

	SNF5-3V5-AID::KANMX *leu2::snf5-Q225X::LEU2* *leu2::snf5-Q225X::LEU2* *his3::pCup1-OsTIR1(codon optimized)::HIS3* *his3::pCup1-OsTIR1(codon optimized)::HIS3*
UB23506	*MATa, ho::LYS2, lys2, ura3, leu2::hisG, his3::hisG, trp1::hisG* *MATalpha, ho::LYS2, lys2, ura3, leu2::hisG, his3::hisG, trp1::hisG* *Ndc80-3V5:KanMX* *Ndc80-3V5:KanMX* *irt1:cup1::Hphmx* *irt1:cup1::Hphmx* *ime4::cup1::NAT* *ime4::cup1::NAT* *SNF5-3V5-AID::KANMX* *SNF5-3V5-AID::KANMX*
UB23545	*MATa, ade2-1, leu2-3, ura3, trp1-1, his3-11,15, can1-100, GAL, psi+* *swi3::KANMX* *leu2::swi3-E815X::LEU2* *ura3::pTEF1-ADE2luti::URA3*
UB23996	*MATa, ade2-1, leu2-3, ura3, trp1-1, his3-11,15, can1-100, GAL, psi+* *trp1::pGPD1-LexA-ER-HA-B112::TRP1* *ura3::pTEF1-ADE2luti::URA3* *his3::3xLexO-NDC80leader::HIS3* *isw2::HygB*
UB23999	*MATa, ade2-1, leu2-3, ura3, trp1-1, his3-11,15, can1-100, GAL, psi+* *trp1::pGPD1-LexA-ER-HA-B112::TRP1* *ura3::pTEF1-ADE2luti::URA3* *his3::3xLexO-NDC80leader::HIS3* *chd1::HygB* *isw2::HygB*
UB24000	*MATa, ade2-1, leu2-3, ura3, trp1-1, his3-11,15, can1-100, GAL, psi+* *trp1::pGPD1-LexA-ER-HA-B112::TRP1* *ura3::pTEF1-ADE2luti::URA3* *his3::3xLexO-NDC80leader::HIS3* *chd1::HygB*
UB24051	*MATa, ade2-1, leu2-3, ura3, trp1-1, his3-11,15, can1-100, GAL, psi+* *ura3::pTEF1-ADE2luti::URA3* *his3::3xLexO-NDC80leader::HIS3*
UB24057	*MATa, ade2-1, leu2-3, ura3, trp1-1, his3-11,15, can1-100, GAL, psi+* *trp1::pGPD1-LexA-ER-HA-B112::TRP1* *ura3::pTEF1-ADE2luti::URA3* *his3::3xLexO-NDC80leader::HIS3* *isw1::HygB*
UB24251	*MATa, ADE2, leu2-3, ura3, trp1-1, his3-11,15, can1-100, GAL, phi+* *hnt1::HNT1-3V5::KANMX* *swi3::KANMX* *leu2::SWI3::LEU2*
UB24253	*MATa, ADE2, leu2-3, ura3, trp1-1, his3-11,15, can1-100, GAL, phi+* *hnt1::HNT1-3V5::KANMX*

	swi3::KANMX *leu2::swi3-E815X::LEU2*
UB24301	*MATa, ADE2, leu2-3, ura3, trp1-1, his3-11,15, can1-100, GAL, phi+* *his3::3xLexO-NDC80leader::HIS3* *trp1::pGPD1-LexA-ER-HA-B112::TRP1* *swi3::KANMX* *leu2::swi3-E815X::LEU2*
UB24820	*MATa, ho::LYS2, lys2, ura3, leu2::hisG, his3::hisG, trp1::hisG* *his3::3xLexO-NDC80leader::HIS3* *trp1::pGPD1-LexA-ER-HA-B112::TRP1*
UB24822	*MATa, ho::LYS2, lys2, ura3, leu2::hisG, his3::hisG, trp1::hisG* *his3::3xLexO-NDC80leader::HIS3*
UB24975	*MATa, ho::LYS2, lys2, ura3, leu2::hisG, his3::hisG, trp1::hisG* *swi3::KANMX* *leu2::swi3-E815X::LEU2* *his3::3xLexO-NDC80leader::HIS3* *trp1::pGPD1-LexA-ER-HA-B112::TRP1*
UB24976	*MATalpha, ho::LYS2, lys2, ura3, leu2::hisG, his3::hisG, trp1::hisG* *swi3::KANMX* *leu2::swi3-E815X::LEU2* *his3::3xLexO-NDC80leader::HIS3* *trp1::pGPD1-LexA-ER-HA-B112::TRP1*
UB26207	*MATa, ho::LYS2, lys2, ura3, leu2::hisG, his3::hisG, trp1::hisG* *swi3::KANMX* *leu2::swi3-E815X::LEU2* *his3::3xLexO-NDC80leader::HIS3* *trp1::pGPD1-LexA-ER-HA-B112::TRP1* *ura3::W303SEG2::URA3*
UB26208	*MATa, ho::LYS2, lys2, ura3, leu2::hisG, his3::hisG, trp1::hisG* *swi3::KANMX* *leu2::swi3-E815X::LEU2* *his3::3xLexO-NDC80leader::HIS3* *trp1::pGPD1-LexA-ER-HA-B112::TRP1* *ura3::W303GFA1::URA3*
UB26211	*MATa, ho::LYS2, lys2, ura3, leu2::hisG, his3::hisG, trp1::hisG* *swi3::KANMX* *leu2::swi3-E815X::LEU2* *his3::3xLexO-NDC80leader::HIS3* *trp1::pGPD1-LexA-ER-HA-B112::TRP1* *ura3::W303HSL1::URA3*
UB26212	*MATa, ho::LYS2, lys2, ura3, leu2::hisG, his3::hisG, trp1::hisG* *swi3::KANMX* *leu2::swi3-E815X::LEU2* *his3::3xLexO-NDC80leader::HIS3* *trp1::pGPD1-LexA-ER-HA-B112::TRP1* *ura3::W303YPF1::URA3*
UB26215	*MATa, ho::LYS2, lys2, ura3, leu2::hisG, his3::hisG, trp1::hisG* *swi3::KANMX* *leu2::swi3-E815X::LEU2* *his3::3xLexO-NDC80leader::HIS3* *trp1::pGPD1-LexA-ER-HA-B112::TRP1* *ura3::W303MTC2::URA3*
UB27669	*MATa, ade2-1, leu2-3, ura3, trp1-1, his3-11,15, can1-100, GAL, psi+* *ura3::pTEF1-ADE2luti::URA3*

	snf2::KanMX
UB27673	*MATa, ade2-1, leu2-3, ura3, trp1-1, his3-11,15, can1-100, GAL, psi+* *ura3::pTEF1-ADE2luti::URA3* *swi3::KanMX*
UB27896	*MATa, ADE2, LEU2, ura3, trp1-1, his3-11,15, can1-100, GAL, phi+* *swi3::KANMX*
UB28096	*MATa, ADE2, leu2-3, ura3, trp1-1, his3-11,15, can1-100, GAL, phi+* *swi3::KANMX* *leu2::swi3-E815X::LEU2* *dst1::HygB*
UB28907	*MATa, ADE2, leu2-3, ura3, trp1-1, his3-11,15, can1-100, GAL, phi+* *SNF2::LEU2* *trp1::pGPD1-LexA-ER-HA-B112::TRP1* *his3::3xLexO-NDC80leader::HIS3*
UB28911	*MATa, ADE2, leu2-3, ura3, trp1-1, his3-11,15, can1-100, GAL, phi+* *snf2::KANMX* *SNF2::LEU2* *trp1::pGPD1-LexA-ER-HA-B112::TRP1* *his3::3xLexO-NDC80leader::HIS3*
UB28914	*MATa, ADE2, leu2-3, ura3, trp1-1, his3-11,15, can1-100, GAL, phi+* *snf2::KANMX* *SNF2::LEU2*
UB28915	*MATa, ADE2, leu2-3, ura3, trp1-1, his3-11,15, can1-100, GAL, phi+* *snf2::KANMX* *snf2-Q928K::LEU2*
UB28919	*MATa, ADE2, leu2-3, ura3, trp1-1, his3-11,15, can1-100, GAL, phi+* *snf2::KANMX* *snf2-Q928K::LEU2* *trp1::pGPD1-LexA-ER-HA-B112::TRP1* *his3::3xLexO-NDC80leader::HIS3*
UB28922	*MATa, ADE2, leu2-3, ura3, trp1-1, his3-11,15, can1-100, GAL, phi+* *snf2::KANMX* *snf2-W935R::LEU2*
UB28923	*MATa, ade2-1, leu2-3, ura3, trp1-1, his3-11,15, can1-100, GAL, phi+* *snf2::KANMX* *snf2-W935R::LEU2* *ura3::pTEF1-ADE2luti::URA3*
UB28925	*MATa, ADE2, leu2-3, ura3, trp1-1, his3-11,15, can1-100, GAL, phi+* *snf2::KANMX* *snf2-W935R::LEU2* *trp1::pGPD1-LexA-ER-HA-B112::TRP1* *his3::3xLexO-NDC80leader::HIS3*
UB29161	*MATa, ADE2, leu2-3, ura3, trp1-1, his3-11,15, can1-100, GAL, phi+* *SNF2-VL-3V5::HISMX*
UB29166	*MATa, ADE2, leu2-3, ura3, trp1-1, his3-11,15, can1-100, GAL, phi+* *snf2-W935R::LEU2* *trp1::pGPD1-LexA-ER-HA-B112::TRP1* *his3::3xLexO-NDC80leader::HIS3*
UB29170	*MATa, ADE2, leu2-3, ura3, trp1-1, his3-11,15, can1-100, GAL, phi+* *snf2-Q928K::LEU2*

	trp1::pGPD1-LexA-ER-HA-B112::TRP1 *his3::3xLexO-NDC80leader::HIS3*
UB29188	*MATa, ADE2, LEU2, ura3, trp1-1, his3-11,15, can1-100, GAL, phi+* *trp1::pGPD1-LexA-ER-HA-B112::TRP1* *his3::3xLexO-NDC80leader::HIS3*
UB29385	*MATa, ADE2, LEU2, ura3, TRP1, his3-11,15, can1-100, GAL, phi+* *his3::3xLexO-NDC80leader::HIS3*
UB29694	*MATa, ADE2, leu2-3, ura3, trp1-1, his3-11,15, can1-100, GAL, phi+* *his3::3xLexO-NDC80leader::HIS3* *trp1::pGPD1-LexA-ER-HA-B112::TRP1* *leu2::swi3-E815X::LEU2*
UB29781	*MATa, ADE2, LEU2, ura3, trp1-1, his3-11,15, can1-100, GAL, phi+* *snf2::KANMX*
UB29782	*MATa, ade2-1, leu2-3, ura3, trp1-1, his3-11,15, can1-100, GAL, psi+* *trp1::pGPD1-LexA-ER-HA-B112::TRP1* *ura3::pTEF1-ADE2luti::URA3* *his3::3xLexO-NDC80leader::HIS3* *isw1::HygB* *isw2::HygB*
UB29784	*MATa, ade2-1, leu2-3, ura3, trp1-1, his3-11,15, can1-100, GAL, psi+* *trp1::pGPD1-LexA-ER-HA-B112::TRP1* *ura3::pTEF1-ADE2luti::URA3* *his3::3xLexO-NDC80leader::HIS3* *isw1::HygB* *chd1::HygB*
UB29791	*MATa, ADE2, leu2-3, ura3, trp1-1, his3-11,15, can1-100, GAL, phi+* *swi3::KANMX* *leu2::SWI3::LEU2* *his3::3xLexO-NDC80leader::HIS3* *trp1::pGPD1-LexA-ER-HA-B112::TRP1*
UB29792	*MATa, ADE2, leu2-3, ura3, trp1-1, his3-11,15, can1-100, GAL, phi+* *leu2::SWI3::LEU2* *his3::3xLexO-NDC80leader::HIS3* *trp1::pGPD1-LexA-ER-HA-B112::TRP1*
UB30034	*MATa, ade2-1, leu2-3, ura3, trp1-1, his3-11,15, can1-100, GAL, phi+* *ura3::pTEF1-ADE2luti::URA3* *snf2::KANMX* *SNF2::LEU2*
UB30070	*MATa, ADE2, leu2-3, ura3, trp1-1, his3-11,15, can1-100, GAL, phi+* *SNF2-VL-3V5::HISMX* *swi3::KANMX* *leu2::SWI3::LEU2*
UB30071	*MATa, ADE2, leu2-3, ura3, trp1-1, his3-11,15, can1-100, GAL, phi+* *SNF2-VL-3V5::HISMX* *swi3::KANMX* *leu2::swi3-E815X::LEU2*
UB30085	*MATa, ade2-1, leu2-3, ura3, trp1-1, his3-11,15, can1-100, GAL, psi+* *trp1::pGPD1-LexA-ER-HA-B112::TRP1* *ura3::pTEF1-ADE2luti::URA3* *his3::3xLexO-NDC80leader::HIS3*

	isw1::HygB *chd1::HygB* *isw2::HygB*
UB30152	*MATa, ADE2, leu2-3, ura3, trp1-1, his3-11,15, can1-100, GAL, psi+* *snf2::KANMX* *SNF2::LEU2* *hnt1::HNT1-3V5::KANMX*
UB30154	*MATa, ADE2, leu2-3, ura3, trp1-1, his3-11,15, can1-100, GAL, psi+* *snf2::KANMX* *snf2-Q928K::LEU2* *hnt1::HNT1-3V5::KANMX*
UB30156	*MATa, ADE2, leu2-3, ura3, trp1-1, his3-11,15, can1-100, GAL, phi+* *snf2::KANMX* *snf2-W935R::LEU2* *hnt1::HNT1-3V5::KANMX*
UB30185	*MATa, ade2-1, leu2-3, ura3, trp1-1, his3-11,15, can1-100, GAL, phi+* *snf2::KANMX* *snf2-Q928K::LEU2* *ura3::pTEF1-ADE2luti::URA3*
UB30190	*MATa, ade2-1, leu2-3, ura3, trp1-1, his3-11,15, can1-100, GAL, psi+* *swi3::KANMX* *leu2::SWI3::LEU2* *ura3::pTEF1-ADE2luti::URA3*
UB30387	*MATa, ADE2, leu2-3, ura3, trp1-1, his3-11,15, can1-100, GAL, phi+* *snf2::KANMX* *leu2::LEU2::SNF2-3V5::HISMX*
UB30389	*MATa, ADE2, leu2-3, ura3, trp1-1, his3-11,15, can1-100, GAL, phi+* *snf2::KANMX* *leu2::LEU2::snf2-Q928K-3V5::HISMX*
UB30391	*MATa, ADE2, leu2-3, ura3, trp1-1, his3-11,15, can1-100, GAL, phi+* *snf2::KANMX* *leu2::LEU2::snf2-W935R-3V5::HISMX*
UB30456	*MATa, ade2-1, leu2-3, ura3, trp1-1, his3-11,15, can1-100, GAL, psi+* *trp1::pGPD1-LexA-ER-HA-B112::TRP1* *ura3::pTEF1-ADE2luti::URA3* *his3::3xLexO-NDC80leader::HIS3* *swp82::KanMX*
UB30507	*MATa, ade2-1, leu2-3, ura3, trp1-1, his3-11,15, can1-100, GAL, psi+* *trp1::pGPD1-LexA-ER-HA-B112::TRP1* *ura3::pTEF1-ADE2luti::URA3* *his3::3xLexO-NDC80leader::HIS3* *snf11::KanMX*
UB31746	*MATalpha, ADE2, leu2-3, ura3, trp1-1, his3-11,15, can1-100, GAL, psi+* *swp82::KanMX*
UB31748	*MATa, ho::LYS2 lys2 ura3 leu2::hisG his3::hisG trp1::hisG* *Snf2-3V5::HISMX* SK1

UB31807	*MATa, ADE2, leu2-3, ura3, trp1-1, his3-11,15, can1-100, GAL, phi+* *snf11::KanMX*
UB32339	*MATa, ADE2, leu2-3, ura3, trp1-1, his3-11,15, can1-100, GAL, phi+* *trp1:: HNT1-3V5::TRP1* *HNT1::KANMX* transgene contains HNT1luti TSS and UPRE sites Endogenous locus lacks HNT1 5' regulatory region and CDS
UB32342	*MATa, ADE2, leu2-3, ura3, trp1-1, his3-11,15, can1-100, GAL, phi+* *trp1:: HNT1(lutiΔ)-3V5::TRP1* *HNT1::KANMX* transgene lacks HNT1luti TSS and UPRE sites Endogenous locus lacks HNT1 5' regulatory region and CDS
UB33424	*MATa, ADE2, leu2-3, ura3, trp1-1, his3-11,15, can1-100, GAL, psi+* *trp1::pGPD1-LexA-ER-HA-B112::TRP1* *his3::3xLexO-NDC80leader::HIS3* *snf11:KANMX*
UB33427	*MATa, ADE2, leu2-3, ura3, trp1-1, his3-11,15, can1-100, GAL, psi+* *trp1::pGPD1-LexA-ER-HA-B112::TRP1* *his3::3xLexO-NDC80leader::HIS3* *swp82::KANMX*
UB33482	*MATa, ADE2, leu2-3, ura3, trp1-1, his3-11,15, can1-100, GAL, psi+* *trp1::pGPD1-LexA-ER-HA-B112::TRP1* *his3::3xLexO-NDC80leader::HIS3* *swi3::KANMX*
UB34040	*MATa, ADE2, leu2-3, ura3, trp1-1, his3-11,15, can1-100, GAL, psi+* *trp1::pGPD1-LexA-ER-HA-B112::TRP1* *his3::3xLexO-NDC80leader::HIS3* *snf2::KANMX*
UB36048	*MATa, ADE2, leu2-3, ura3, trp1-1, his3-11,15, can1-100, GAL, phi+* *trp1::HNT1(pLUTI-CYC1t)-3V5::TRP1* *HNT1::KANMX* CYC1 terminator inserted between luti and prox TSS Endogenous locus lacks HNT1 5' regulatory region and CDS
UB36182	*MATa, ADE2, leu2-3, ura3, trp1-1, his3-11,15, can1-100, GAL, phi+* *dst1::HygB* *swi3::KANMX* *leu2::SWI3::LEU2*
UB36185	*MATa, ADE2, leu2-3, ura3, trp1-1, his3-11,15, can1-100, GAL, phi+* *dst1::HygB* *snf2::KANMX* *SNF2::LEU2*
UB36186	*MATa, ADE2, leu2-3, ura3, trp1-1, his3-11,15, can1-100, GAL, phi+* *dst1::HygB* *snf2::KANMX* *snf2-W935R::LEU2*
UB36188	*MATa, ADE2, leu2-3, ura3, trp1-1, his3-11,15, can1-100, GAL, phi+* *dst1::HygB* *snf2::KANMX* *snf2-Q928K::LEU2*
UB36454	*MATalpha, ADE2, leu2-3, ura3, trp1-1, his3-11,15, can1-100, GAL, phi+* *swi3::KANMX* *leu2::SWI3::LEU2* *trp1::pGPD1-LexA-ER-HA-B112::TRP1* *8xLexO-SOD1luti::KANMX*

UB36456	*MATalpha, ADE2, leu2-3, ura3, trp1-1, his3-11,15, can1-100, GAL, phi+* *swi3::KANMX* *leu2::SWI3::LEU2* *trp1::pGPD1-LexA-ER-HA-B112::TRP1* *8xLexO-SOD1luti-860::KANMX*
UB36457	*MATalpha, ADE2, leu2-3, ura3, trp1-1, his3-11,15, can1-100, GAL, phi+* *swi3::KANMX* *leu2::SWI3::LEU2* *trp1::pGPD1-LexA-ER-HA-B112::TRP1* *8xLexO-SOD1luti-330::KANMX*
UB36458	*MATalpha, ADE2, leu2-3, ura3, trp1-1, his3-11,15, can1-100, GAL, phi+* *swi3::KANMX* *leu2::swi3-E815X::LEU2* *trp1::pGPD1-LexA-ER-HA-B112::TRP1* *8xLexO-SOD1luti::KANMX*
UB36460	*MATalpha, ADE2, leu2-3, ura3, trp1-1, his3-11,15, can1-100, GAL, phi+* *swi3::KANMX* *leu2::swi3-E815X::LEU2* *trp1::pGPD1-LexA-ER-HA-B112::TRP1* *8xLexO-SOD1luti-860::KANMX*
UB36462	*MATalpha, ADE2, leu2-3, ura3, trp1-1, his3-11,15, can1-100, GAL, phi+* *swi3::KANMX* *leu2::swi3-E815X::LEU2* *trp1::pGPD1-LexA-ER-HA-B112::TRP1* *8xLexO-SOD1luti-330::KANMX*
UB36511	*MATa, ADE2, leu2-3, ura3, trp1-1, his3-11,15, can1-100, GAL, phi+* *trp1::ADI1-3V5::TRP1*
UB36513	*MATa, ADE2, leu2-3, ura3, trp1-1, his3-11,15, can1-100, GAL, phi+* *trp1::ADI1(pDISTΔ)-3V5::TRP1*
UB36515	*MATa, ADE2, leu2-3, ura3, trp1-1, his3-11,15, can1-100, GAL, phi+* *trp1::ODC2-3V5::TRP1*
UB36521	*MATa, ADE2, leu2-3, ura3, trp1-1, his3-11,15, can1-100, GAL, phi+* *trp1::ODC2(pDISTΔ)-3V5::TRP1*
UB36594	*MATa, ADE2, leu2-3, ura3, trp1-1, his3-11,15, can1-100, GAL, phi+* *trp1::ERG27-3V5::TRP1*
UB36596	*MATa, ADE2, leu2-3, ura3, trp1-1, his3-11,15, can1-100, GAL, phi+* *trp1::ERG27(pDISTΔ)-3V5::TRP1*
UB36633	*MATalpha, ADE2, leu2-3, ura3, trp1-1, his3-11,15, can1-100, GAL, phi+* *snf2::KANMX* *snf2-W935R::LEU2* *trp1::pGPD1-LexA-ER-HA-B112::TRP1* *8xLexO-SOD1luti::KANMX*
UB36635	*MATalpha, ADE2, leu2-3, ura3, trp1-1, his3-11,15, can1-100, GAL, phi+* *snf2::KANMX* *snf2-W935R::LEU2* *trp1::pGPD1-LexA-ER-HA-B112::TRP1* *8xLexO-SOD1luti-860::KANMX*
UB36637	*MATalpha, ADE2, leu2-3, ura3, trp1-1, his3-11,15, can1-100, GAL, phi+* *snf2::KANMX* *snf2-W935R::LEU2* *trp1::pGPD1-LexA-ER-HA-B112::TRP1* *8xLexO-SOD1luti-330::KANMX*
UB36684	*MATa, ADE2, leu2-3, ura3, trp1-1, his3-11,15, can1-100, GAL, phi+* *trp1::pGPD1-LexA-ER-HA-B112::TRP1* *8xLexO-SOD1luti::KANMX*

	snf2::KANMX *SNF2::LEU2*
UB36686	*MATa, ADE2, leu2-3, ura3, trp1-1, his3-11,15, can1-100, GAL, phi+* *trp1::pGPD1-LexA-ER-HA-B112::TRP1* *8xLexO-SOD1luti-860::KANMX* *snf2::KANMX* *SNF2::LEU2*
UB36688	*MATa, ADE2, leu2-3, ura3, trp1-1, his3-11,15, can1-100, GAL, phi+* *trp1::pGPD1-LexA-ER-HA-B112::TRP1* *8xLexO-SOD1luti-330::KANMX* *snf2::KANMX* *SNF2::LEU2*
UB36973	*MATa, ADE2, leu2-3, ura3, trp1-1, his3-11,15, can1-100, GAL, phi+* *snf2::KANMX* *SNF2::LEU2* *trp1::pGPD1-LexA-ER-HA-B112::TRP1* *8xLexO-SOD1luti-550::KANMX*
UB36974	*MATalpha, ADE2, leu2-3, ura3, trp1-1, his3-11,15, can1-100, GAL, phi+* *snf2::KANMX* *snf2-W935R::LEU2* *trp1::pGPD1-LexA-ER-HA-B112::TRP1* *8xLexO-SOD1luti-550::KANMX*
UB36976	*MATalpha, ADE2, leu2-3, ura3, trp1-1, his3-11,15, can1-100, GAL, phi+* *swi3::KANMX* *leu2::swi3-E815X::LEU2* *trp1::pGPD1-LexA-ER-HA-B112::TRP1* *8xLexO-SOD1luti-550::KANMX*
UB36989	*MATalpha, ADE2, leu2-3, ura3, trp1-1, his3-11,15, can1-100, GAL, phi+* *trp1::pGPD1-LexA-ER-HA-B112::TRP1* *8xLexO-SOD1luti-550::KANMX* *swii3::KANMX* *leu2::SWI3::LEU2*

Table 6.1: *Strains used in this study.*

Table 6.2: oligonucleotides

Primer Name	**Sequence from 5′ to 3′**
SRG1_RTqPCR_F	GGTTTTCTGAGCGGGATGAA
SRG1_RTqPCR_R	CCTTATCCTCTGCTCCCTCC
SER3_RTqPCR_F	ATCTGCCCCACAATTTGCTG
SER3_RTqPCR_R	GCTTTCACGGCTTGGATCAA
ACT1_RTqPCR_F	GTACCACCATGTTCCCAGGTATT
ACT1_RTqPCR_R	AGATGGACCACTTTCGTCGT
5oligocap (TL-seq 5' adapter)	dCdAdCdTdCdTrGrArGrCrArArUrArCrC
Second strand biotinylated oligo (TL-seq)	GCAC/iBiodT/GCACTCTGAGCAATACC
V5_probe_F	CTAGTGGATCCAGGTAAACCTAT
V5_probe_R	taatacgactcactataggCCAGTCCTAATAGAGGATTAGG

HNT1_probe_F	CATGGTGCGAAGTTGCATG
HNT1_probe_R	taatacgactcactataggCCACCCTACAATCAAACCAC
HNT1_RTqPCR_F (also used in ChIP and MNase qPCR assays, anneals between LUTI and PROX TSS)	TGGTGCGAATCGTTACAGAA
HNT1_RTqPCR_R (also used in ChIP and MNase qPCR assays, anneals between LUTI and PROX TSS)	AATGCTTCAGTAGGGCGGTA
HNT1_LUTIpromoter1_F	GCAAGGACCCAAATAGGAG
HNT1_LUTIpromoter1_R	GATTTACCGGTGTTTCCTTTG
HNT1_LUTIpromoter2_F	CAAAGGAAACACCGGTAAATC
HNT1_LUTIpromoter2_R	CTGTAGACAAGTGTCAATTCAACC
HNT1_LUTI_TSS_F	GGTTGAATTGACACTTGTCTACAG
HNT1_LUTI_TSS_R	TTCTGTAACGATTCGCACCA
HNT1_PROX_TSS_F	TACCGCCCTACTGAAGCATT
HNT1_PROX_TSS_R	CGTGCTGATTGTCCTTTTACTTC
HNT1_ORF1_F	GAAGTAAAAGGACAATCAGCACG
HNT1_ORF1_R	CAAGCGTAGCAGGAGCAGAC
HNT1_ORF2_F	GTCTGCTCCTGCTACGCTTG
HNT1_ORF2_R	CATCATTGGTGTGAGTGTAAGC
HNT1_ORF3_F	GCTTACACTCACACCAATGATG
HNT1_ORF3_R	ATGGAATTTCGCCTGTTGCATAG
HMR_F	ACGATCCCCGTCCAAGTTATG
HMR_R	CTTCAAAGGAGTCTTAATTTCCCTG
PHO5_F	CCATTTGGGATAAGGGTAAACATC
PHO5_R	AGAGATGAAGCCATACTAACCTCG
HAC1_probe_F	GCAGTCAGGTTTGAATTCATTTGAATTGAATGATTTC
HAC1_probe_R	taatacgactcactataggGCCTCTTCTTCTTCGGTTGAAGTAGCACACAC
SOD1_probe_F	CAACCACTGTCTCTTACGAGATCGC
SOD1_probe_R	taatacgactcactataggCACCATTTTCGTCCGTCTTTACG
NDC80_probe_F	GAGAGGTAGAATCGTCCCTG
NDC80_probe_R	TCCTCTTGAATAGCGCTTTGG
HIS3_probe_F	gcacactggagttgggtttt
HIS3_probe_R	taatacgactcactataggCTATGCGTTCTCGCTTCAG

Table 6.2: *Oligonucleotides used in this study.*

6.2 Growth conditions

Selecting LUTI escape mutants

For selecting LUTI escape mutants, cells were grown overnight at 30°C in liquid YPD (1% yeast extract, 2% peptone, 2% dextrose, tryptophan (96 mg/L), uracil (24 mg/L), adenine (12 mg/L) to saturation. A final concentration of 25 nM β-estradiol was added to overnight YPD flasks to deplete intracellular His3 protein. The day of plating, cells were back-diluted to an OD_{600} = 0.1, then grown at 30°C until they reached OD_{600} ~0.6. After quantifying cell density using a hemacytometer, cells were pelleted by microcentrifugation (2 min at 2000 g), washed with sterile water, and plated on synthetic complete media (SC; 6.7 g/L yeast nitrogen base without amino acids, 2% dextrose, 20 mg/L adenine, 20 mg/L arginine, 60 mg/mL leucine, 20 mg/mL tryptophan, 20 mg/L methionine, 30 mg/L lysine, 30 mg/L tyrosine, 50 mg/L phenylalanine, and 200 mg/L threonine) lacking histidine with 25 nM β-estradiol and 200 μM 3-amino-1,2,4-triazole (3-AT) to completely silence His3 activity in control cells. Cells were plated at a density of 3 million cells/25 ml plate and grown for four days at 30°C. Viable colonies were selected after three and four days post-plating.

Spotting assays, *ADE2^{LUTI}* phenotyping, and growth curves

For serial dilution and plating assays, cells were collected from an overnight YPD plate grown at 30°C and resuspended in water to a concentration of OD_{600} = 0.2. Next, four 1:5 serial dilutions were performed and 2.5 ul of each dilution was plated. For *HIS3^{LUTI}* phenotyping, cells were plated on a control plate (SC -his with 200 μM 3-AT) and a selective plate (SC -his with 200 μM 3-AT and 25 nM β-estradiol) then allowed to grow for three days at 30°C prior to imaging. For *dst1Δ* phenotyping, cell dilutions were plated on YPD then allowed to grow for two days at 30°C prior to imaging. *ADE2^{LUTI}* phenotyping was performed by streaking cells grown overnight at 30°C on a YPD plate to a YPD plate lacking supplemental adenine. Cells were then grown overnight at 30°C and imaged. Cells for growth curve experiments were grown overnight at 30°C in liquid YPD then back-diluted to an OD_{600} = 0.1 in liquid YPD or YPS (YPD recipe with 2% sucrose instead of 2% dextrose) in a 96-well plate. Cells were transferred to a 96-well plate in triplicate, sealed with a Breathe Easy Cover (*Sigma-Aldrich*), and grown at 30°C for 24 hours in a plate reader. Absorbance readings were collected every 15 minutes at absorbance = 600 nm with agitation before each reading.

Cell collections

For all vegetative cell collections, yeast cells were grown in liquid YPD. Cells were grown at 30°C overnight prior to collection, back-diluted to OD_{600} = 0.1 the day of collection and grown to mid-log phase at 30°C (OD_{600} ~0.6 for RNA and protein collections) or late-log phase (OD_{600} ~0.8 for ChIP and MNase collections). For UPR-induction, dithiothreitol (DTT) was added to liquid cultures to a final concentration of 5 mM when cells reached mid- or late-log phase. For all DTT sequencing experiments, cells were split at mid-log (TL-seq) or late-log (ChIP-seq and MNase-seq) phase into a 5 mM DTT-treated flask or untreated control flask and harvested 1 hour post-induction. For DTT

time course experiments, cells were collected at 0 min once they had reached mid- or late-log phase, UPR stress was induced with 5 mM DTT, and cells were collected at indicated time points following induction. For *HNT1*$^{LUTI\text{-}CYC1t}$ and *HNT1*^{lutiΔ} experiments, cells were split at late-log phase into a 5 mM DTT-treated flask or untreated control flask and harvested 30 min post-induction.

For meiotic time courses described in Chapter 5 (Appendix A), diploid cells harboring the *pCUP1-IME1* and *pCUP1-IME4* alleles were grown in YPD for 20-24 hours at room temperature. Subsequently, cells were transferred to BYTA (1% yeast extract, 2% bacto tryptone, 1% potassium acetate, 50 mM potassium phthalate) and grown for ~18 hours at 30°C. The cells were pelleted, washed with sterile milliQ water, and resuspended at 1.85 OD_{600} in sporulation (SPO) media (2% potassium acetate, 0.02% raffinose, pH 7). To initiate synchronous sporulation, expression of *IME1* and *IME4* was induced at 2 h after transfer to SPO by adding $CuSO_4$ to a final concentration of 50 μM. For conditional depletion of Snf5-3V5-AID or Swi3-3V5-AID, *pCUP1-TIR1* was also induced along with *IME1* and *IME4* by $CuSO_4$ addition and auxin was added to a final concentration of 500 μM.

6.3 Nucleic acid extractions

DNA extractions for sequencing

Cells were grown in 2 ml liquid YPD cultures overnight at 30°C. 1.5 ml of culture was pelleted by microcentrifugation, supernatant was removed and cells were lysed with ~300 mg 500 micron acid-washed glass beads, 500 µl lysis buffer (2% Triton X-100, 1% SDS, 100 mM NaCl, 10 mM Tris-HCl pH 8, 1 mM EDTA), and 500 µl 25:24:1 phenol:chloroform:isoamyl alcohol. Cells were vortexed in the lysis mixture for 5 min at room temperature and the aqueous phase was separated by microcentrifugation (5 min at 20,000 g). A second extraction was performed in 25:24:1 phenol:chloroform:isoamyl alcohol and DNA was precipitated in 1 ml 100% ethanol at room temperature. The pellet was resuspended in 400 µl TE buffer (10 mM Tris-HCl, 1 mM EDTA, pH 8) and treated with 30 µg RNase A for 30 min at 37°C. The RNase-treated DNA was precipitated in 1 ml 100% ethanol with 10 µl 4 M ammonium acetate and pelleted by microcentrifugation (2 min at 20,000 g). After decanting the pellets were air-dried and resuspended in 50 µl TE. DNA concentration was measured using the Qubit DNA BR Assay Kit (Q32853, *ThermoFisher Scientific*).

RNA extraction for RT-qPCR and RNA blotting

2 ml of cells were collected by centrifugation and snap frozen in liquid nitrogen. Cells were thawed on ice and resuspended in 400 µl TES buffer (10 mM Tris pH 7.5, 10 mM EDTA, 0.5% SDS). An equal volume of citrate-buffered acid phenol (pH 4.3, P4682, *Sigma-Aldrich*) was added to cells, and they were incubated at 65°C for 30 min in a Thermomixer (*Eppendorf*) shaking at 1400 RPM. After microcentrifugation (20,000 g for 10 min at 4°C) the aqueous phase was transferred to a second tube with 350 µl chloroform. The aqueous phase was again separated by microcentrifugation (20,000 g for 5 min at room temperature) and RNA was precipitated in 100% isopropanol with 350

mM sodium acetate (pH 5.2) overnight at –20°C. Pellets were washed with 80% ethanol and resuspended in DEPC water. Total RNA was quantified by Nanodrop.

RNA extraction for mRNA-seq, TL-seq, and direct mRNA-seq

Cells were collected by vacuum filtration and snap frozen in liquid nitrogen. For mRNA-seq, ~15 OD_{600} units of cells were collected. For TL-seq and direct mRNA-seq, ~100 OD_{600} units of cells were collected. Cells were thawed on ice and resuspended in 400 µl TES buffer (10 mM Tris pH 7.5, 10 mM EDTA, 0.5% SDS) per 15 OD_{600} units. An equal volume of citrate-buffered acid phenol (pH 4.3, P4682, *Sigma-Aldrich*) was added to cells, and they were incubated at 65°C for 30 minutes in a Thermomixer C (*Eppendorf*) shaking at 1400 RPM. After microcentrifugation (20,000 g for 10 min) the aqueous phase was transferred to a second tube with 350 µl chloroform. The aqueous phase was separated by microcentrifugation (20,000 g for 5 min) and RNA was precipitated in 100% isopropanol with 350 mM sodium acetate (pH 5.2) overnight at –20°C. Pellets were washed with 80% ethanol and resuspended in DEPC water for 10 min at 37°C. Total RNA was quantified using the Qubit RNA BR Assay Kit (Q10211, *ThermoFisher Scientific*).

6.4 Chromatin extractions and processing

Chromatin Immunoprecipitation (ChIP)

Roughly 50 OD_{600} units of cells were collected in 50 ml conical tubes and fixed with 1% formaldehyde with periodic inversion for 15 min at room temperature. The crosslinking reaction was quenched with 125 mM glycine and tubes were gently agitated on a rocker platform (*Bellco Biotechnology*) at room temperature for 5 min. Cells were pelleted, washed with cold 1X PBS, then resuspended in 1 ml cold FA lysis buffer (50 mM Hepes pH 7.5, 150 mM NaCl, 1 mM EDTA, 1% Triton, 0.1% sodium deoxycholate) with 0.1% SDS and protease inhibitors (11836153001, *Roche*). In all cases, SDS was freshly added to buffers from a 20% stock solution. For ChIP-seq experiments, SK1 spike-in cells harboring a Snf2-3V5 allele (UB31748) that had been crosslinked in the same manner were added at a ratio of 1:5 prior to lysis. Roughly 500 µl Zirconia beads were added to cell suspension and cells were lysed by Beadbeater (Mini-Beadbeater-96, *Biospec Products)*. Lysates were collected by centrifuging at 500 g for 1 minute at 4°C. Unbroken cells and debris were removed by microcentrifugation for 3 min at 2000 g. Supernatant was collected and centrifuged again for 20,000 g for 15 min resulting with pelleted chromatin. Pellets were resuspended in 1 ml FA lysis buffer with 0.1% SDS and protease inhibitors into falcon tubes containing 300 µl sonication beads. Samples were sonicated in a Bioruptor Pico (*Diagenode*) for 30 seconds on / 30 seconds off for 6 cycles to average fragment size of 150-400 bp. Samples were centrifuged once more at 20,000 g for 1 minute and the supernatant was carried forward to the immunoprecipitation (IP). From the isolated chromatin, 30 µl were set aside as input prior to IP.

For Snf2 immunoprecipitation, 25 µl of mouse anti-V5 agarose slurry (A7345, *MilliporeSigma*) were washed twice with 1 ml FA lysis buffer with 0.1% SDS. For each wash, the beads nutated at 4°C for 5 min and were subsequently pelleted by microcentrifugation (1000 g for 30 seconds). Sheared chromatin was added to the washed beads and the IP was incubated overnight with nutation at 4°C. IPs were washed

at 4°C twice with FA lysis buffer and 0.1% SDS, twice with high salt buffer (FA lysis buffer with 0.1% SDS, and 250 mM NaCl) and twice with high detergent buffer (10 mM Tris pH 8, 250 mM LiCl, 0.5% NP-40, 0.5% sodium deoxycholate, and 1 mM EDTA). To IP and input samples, 130 µl TE (10 mM Tris pH 8, 1 mM EDTA) with 1% SDS was added. The precipitate was eluted from the beads by shaking at 450 RPM at 65°C in a thermomixer (*Eppendorf*) overnight.

Samples were cleaned up using QIAQuick PCR Purification Kit (28106, *QIAGEN*), diluted 1:10, and analyzed by qPCR with Absolute Blue qPCR Mix (AB4162B, *ThermoFisher Scientific*) using primer pairs directed against the *HNT1* locus or the *HMR* control locus. C_T mean values were first corrected for primer efficiency as calculated from standard curves performed on input samples for each primer pair, then corrected values corresponding to each *HNT1* primer pair were normalized over the corrected *HMR* signal. All ChIP experiments were performed on two biological replicates.

Micrococcal nuclease digestion (MNase)

Roughly 50 OD_{600} units of cells were fixed in 1% formaldehyde with light shaking at RT for 15 minutes. Crosslinking was quenched by 125 mM of glycine for 5 minutes at RT. Cells were pelleted and washed with cold 1X PBS. For MNase-seq experiments, SK1 spike-in cells (UB31748) that had been crosslinked in the same manner were added at a ratio of 1:5 prior to spheroplasting. Cells were spheroplasted in 20 ml of Spheroplast Solution (1 M Sorbitol, 50 mM Tris pH 7.5, 10 mM β-mercaptoethanol) with 100 µL of 10 mg/ml zymolase until they appeared non-refractive and shadow-like after ~12-15 minutes. Spheroplasted cells were resuspended in 2 ml MNase Digestion Buffer (1 M Sorbitol, 50 mM NaCl, 10 mM Tris pH 7.5, 5 mM $MgCl_2$, 1 mM $CaCl_2$, 0.075% NP-40, 0.5 mM spermidine, 1 mM β-mercaptoethanol). Digestions were performed with 600 µl of spheroplasts, 30 units of Exonuclease III (M0206S, *New England Biolabs*), and either 10, 20, or 40 units of MNase (LS004797, *Worthington*). 10 units of proteinase K (P8107S, *New England Biolabs*) were added to each digestion and undigested control. Crosslinks were then reversed by incubating samples at 65°C overnight and DNA was purified by 25:24:1 phenol:chloroform:isoamyl alcohol DNA extraction, followed by ethanol precipitation. Precipitated DNA was washed with 70% ethanol and resuspended in 1X NEBuffer #2 (B7002S, *New England Biolabs*) with 2 µl RNase A (20 mg/ml, 12091021, *Invitrogen*). Samples were incubated for 30 min and run on a 2% agarose gel to examine digestion efficiency. Of the samples digested with 10, 20, and 40 units of MNase, only the samples with a ratio of mononucleosomes to dinucleosomes closest to 80/20 were carried forward. Samples were once again purified by phenol/chloroform/isoamyl alcohol DNA extraction and ethanol precipitation, digests were eluted in 1X NEBuffer #3 (B7003S, *New England Biolabs*) and undigested gDNA was eluted in TE. Digests were then treated with 10 units alkaline phosphatase (CIP, P4978, *Sigma Aldrich*), incubated for 1 hour at 37°C, and size selected by running samples on a 1.8% LMT agarose gel at 120 V for 25 minutes at 4°C and gel extracting the mononucleosome band with a Monarch Gel Extraction Kit (T1020S, *New England Biolabs*). Purified samples were carried forward for qPCR or library preparation. All experiments were performed on two biological replicates.

6.5 Preparation of sequencing libraries and whole genome sequencing

mRNA sequencing (mRNA-seq)

RNA-seq libraries for three biological replicates were generated with the NEXTflex™ Rapid Directional mRNA-Seq Bundle with poly(A) beads (NOVA-5138, *Bioo Scientific*) according to manufacturer's instructions. 10 µg of total RNA was used as input for all libraries. AMPure XP beads (A63881, Beckman Coulter) were used to select fragments between 200-500 bp. Libraries were quantified using the Agilent 4200 TapeStation (*Agilent Technologies, Inc*). Samples were submitted for 100 bp SE sequencing by the Vincent J. Coates Genomics Sequencing Laboratory with a NovaSeq SP.

Poly(A) selection for TL-Seq and direct mRNA-seq

Poly(A) selection was performed on 600 µg of RNA using the Poly(A)Purist™ MAG kit (AM1922, *Ambion*) following manufacturer's instructions. Poly(A) RNA was precipitated at -20°C for 18 hours in 1.1 ml 100% ethanol with 40 µl 3 M sodium acetate and 1 µl glycogen (5 mg/ml), washed with 1 ml 80% ethanol, dissolved in 21 µl nuclease-free water, and quantified with a Qubit using the RNA BR assay kit (Q10211, *ThermoFisher Scientific*).

Transcript Leader Sequencing (TL-Seq)

TL-seq was performed on two biological replicates for each sample as described in (Tresenrider et al., 2022) with minor modifications. 5-15 µg poly(A)-selected mRNA was fragmented for 3 minutes at 70°C using alkaline hydrolysis fragmentation reagent (AM8740, *Ambion*). Fragmented mRNAs were purified by performing a 1.8X bead cleanup with RNAClean XP beads (A63987, *Beckman Coulter*). Fragments were dephosphorylated with 20 units Shrimp Alkaline Phosphatase (rSAP, M0371, *New England Biolabs*) for 1 hour at 37°C with 1 µl RNaseOUT (10777019, *Invitrogen*), then purified by acid phenol extraction at 65°C for 45 min in a thermomixer with shaking at 1400 RPM. Dephosphorylated mRNA fragments were precipitated in 100% ethanol with 40 µl 3 M sodium acetate and 1 µl linear acrylamide (AM9520, *Ambion*) at -20°C for >16 hours, washed with 80% ethanol, and resuspended in nuclease-free water. Samples were then treated with 5 units Cap-Clip acid pyrophosphatase (C-CC15011H, *Tebu-Bio*) with 1 µl RNaseOUT. To control for inefficient phosphatase activity in the previous step, a sample from wild-type cells in each condition (untreated or 5 mM DTT) that was not subject to decapping was carried forward along with the Cap-Clip treated samples. Samples were once again purified by acid phenol extraction and ethanol precipitation, then ligated to a custom 5′ adapter (10 µM oligocap) by T4 RNA Ligase I (M0437, *New England Biolabs*) with 1 µl RNaseOUT for 16 hours at 16°C. The ligation reaction was purified by performing a 1.8X bead cleanup with RNAClean XP beads and eluted in 12 µl nuclease-free water. Purified 5′ ligated RNAs were mixed with 1 µl random hexamers (50 µM, N8080127, *ThermoFisher Scientific*), 1 µl dNTP mix (10 mM, 18427013, *Invitrogen*), and 1 µl RNaseOUT then denatured at 65°C for 5 min and cooled on ice. Reverse transcription reactions were performed using SuperScript IV reverse transcriptase (18090010, *Invitrogen*). RNA templates were then degraded by incubating reactions with 5 units of RNase H (M0297, *New England Biolabs*) and 1 µl RNase cocktail enzyme mix

(AM2296, *Ambion*). cDNA products were purified by performing a 1.8X bead cleanup with AMPure XP beads (A63881, *Beckman Coulter*), eluted in 23.5 µl nuclease-free water, then subject to second-strand synthesis using 1.5 µl biotinylated oligo (10 µM) and 25 µl KAPA Hi-Fi hot start ready mix 2x (KK2601, *Roche*). Second strand reactions were incubated at 95°C for 3 minutes, 98°C for 15 s, 50°C for 2 minutes, 65°C for 15 minutes and held at 4°C. Double stranded DNA (dsDNA) was purified by performing a 1.8X AMPure XP bead cleanup and quantified using the Qubit dsDNA HS assay kit (Q32851, *Invitrogen*).

All dsDNA (ranging from 2-12 ng per sample) was carried forward into end repair, adenylation, and adapter ligation using the NEXTflex™ Rapid DNA-Seq Kit 2.0 Bundle (NOVA-5188-12, *Bioo Scientific*) according to manufacturer's instructions. Following post-ligation cleanup and prior to PCR amplification, samples were bound to MyOne Streptavidin C1 Dynabeads™ (65001, *ThermoFisher Scientific*) to capture biotinylated dsDNA. Library amplification over 14-15 PCR cycles, depending on input amount, was done on the biotinylated dsDNA fraction bound to the beads using NEXTflex™ kit amplification reagents. Amplified libraries were quantified by the Qubit dsDNA HS assay kit. Adaptor-dimers were removed by electrophoresis of the libraries on Novex 6% TBE gels (EC62655BOX, *Invitrogen*) at 120 V for 1 hour, and excising the smear above ~150 bp. Gel slices containing libraries were shredded by centrifugation at 13,000 *g* for 3 minutes. Gel shreds were re-suspended in 500 µl crush and soak buffer (500 mM NaCl, 1.0 mM EDTA and 0.05% SDS) and incubated at 65°C for 2 hours on a thermomixer (1400 RPM for 15 s, rest for 45 s). Subsequently, the buffer was transferred into a Costar SpinX column (8161, *Corning Incorporated*) with two 1 cm glass pre-filters (1823010, *Whatman*). Columns were centrifuged at 13000 *g* for 1 min. DNA libraries in the flowthrough were precipitated at −20°C for 18 hours in ethanol with 0.3 M sodium acetate and 1 µl linear acrylamide (AM9520, *Ambion*). Purified libraries were further quantified and inspected on an Agilent 4200 TapeStation (*Agilent Technologies, Inc*). The libraries were sent for 100 bp SE sequencing by the Vincent J. Coates Genomics Sequencing Laboratory with a NovaSeq SP 100SR.

Direct mRNA-seq

500 ng of poly(A)-selected mRNA was used as input for the Direct RNA Sequencing Kit (SQK-RNA002, *Oxford Nanopore Technologies*), used as directed with a modified reverse transcription (RT) step. Marathon reverse transcriptase (kindly gifted from Dr. Kathleen Collins) was used for the RT instead of Superscript III. The RT reaction was performed in 1X first strand buffer (20 mM Tris-HCl pH 7.5, 75 mM KCl, and 5 mM $MgCl_2$), with 0.8 mM dNTPs, 8 mM DTT, and 20 µM Marathon reverse transcriptase. The RT reaction was incubated at 37°C for 50 min then 70°C for 10 min. Downstream steps were followed according to kit instructions. The library was loaded onto an R9.4.1 flow cell (FLO-MIN106, *Oxford Nanopore Technologies*) and sequenced on a minION (MIN-101B, *Oxford Nanopore Technologies*). MinKNOW (v22.05.5, *Oxford Nanopore Technologies*) was run without live base calling for 72 hours. Bases were called from fast5 files using Guppy (v6.0.1, *Oxford Nanopore Technologies*). Reads were aligned to the S288C reference genome (SacCer3) using the EPI2ME Desktop Agent (v3.5.6, *Oxford*

Nanopore Technologies). Bam files were visualized directly in Integrated Genomics Viewer (IGV, *Broad Institute*).

Sequencing libraries for DNA-, ChIP-, and MNase-Seq

DNA-seq, ChIP-seq, and MNase-seq libraries were generated with the NEXTflex™ Rapid DNA-Seq Kit 2.0 Bundle (NOVA-5188-12, *Bioo Scientific*) according to manufacturer's instructions. AMPure XP beads (A63881, *Beckman Coulter*) were used to select fragments between 200-800 bp (DNA-seq), 200-500 bp (ChIP-seq), or 150-250 bp (MNase-Seq). Libraries were quantified using the Agilent 4200 TapeStation (Agilent Technologies, Inc). Samples were submitted for 150 bp PE sequencing (DNA-seq) 100 bp SE sequencing (ChIP-seq), or 100 bp PE sequencing (MNase-seq) on a NovaSeq 6000 by the Vincent J. Coates Genomics Sequencing Laboratory.

6.6 Single-locus measurements of RNA and protein levels

RNA blotting

10 µg of total RNA was denatured in a glyoxal/DMSO mix (1 M deionized glyoxal, 50% DMSO, 10 mM sodium phosphate (NaPi) buffer pH 6.5–6.8) at 70°C for 10 minutes. Denatured samples were mixed with loading buffer (10% glycerol, 2 mM NaPi buffer pH 6.5, 0.4% bromophenol blue) and separated on an agarose gel (1.1% agarose, 0.01 M NaPi buffer) for 3 hours at 100 V. RNA was transferred to a nitrocellulose membrane by capillary action using 10X SSC (1.5 M NaCl, 150 mM $Na_3Citrat\text{-}2H_2O$) overnight and crosslinked using a UV Crosslinker (*Stratagene*). rRNA bands were visualized using methylene blue staining. The membranes were blocked in ULTRAhyb Ultrasensitive Hybridization Buffer (AM8669, *ThermoFisher Scientific)* for 1 hour before overnight hybridization. Radioactive probes were synthesized using a MAXIScript T7 Transcription Kit (AM1314, *Invitrogen*). After synthesis, 1 µl of TURBO DNAse (2238G2, *Invitrogen*) was added and probes were incubated at 37°C for 10 min. Before spinning the probe mix through a hydrated NucAway column (AM10070, Invitrogen), 1 µl of EDTA (0.5M, pH 8) was added. Probes were eluted through the columns by spinning at 3,000 RPM for 3 min at room temperature, then added to hybridization tubes and incubated overnight. Membranes were washed twice in Low Stringency Buffer (2X SSC, 0.1% SDS) and three times in High Stringency Buffer (0.1X SSC, 0.1% SDS). All hybridization and wash steps were done at 68°C.

Reverse transcription and qPCR

For each sample, 2.5 µg of RNA was treated with 1 unit of Turbo DNase using the TURBO DNA-free Kit (AM1907, *Invitrogen*) and incubated for 30 min at 37°C. 2.5 µl DNase inactivation reagent was added to stop the reaction and incubated for 5 min at room temperature. Samples were centrifuged for 2 minutes at 20,000 g and DNase-treated RNA was collected from the top layer.

2 µl of the treated RNA was then added to a 4.5 µl master mix containing 1 µl dNTPs (10 mM), 1 µl random hexamers (50 ng/µl), and nuclease-free water. Samples were incubated for 5 minutes at 65°C then cooled on ice for 1 minute.

cDNA was synthesized via reverse transcription using the SuperScript™ III (18080044, *Invitrogen*) according to manufacturer's instructions. Quantification was performed using 5.2 µl Absolute Blue qPCR Mix (AB4162B, *ThermoFisher Scientific*) and 4.8 µl of cDNA diluted 1:20 in nuclease-free water. Samples were run on a StepOnePlus (*Applied Biosystems*) qPCR machine in triplicate. The C_T mean from each primer pair directed against the experimental target was normalized using the ΔC_T method.

Immunoblotting

To prepare lysates for SDS-PAGE, 2 OD_{600} units were pelleted at 2,000 g for 2 min at 4°C, resuspended in 1 ml of 5% trichloroacetic acid (SA433, *Thermo Fisher Scientific*) and incubated at 4°C for a minimum of 10 min. Samples were then spun at 2,000 g for 2 min at room temperature and cell pellets were washed by vortexing with 1 ml of 100% acetone. Samples were spun at maximum speed at room temperature for 5 min, acetone was pipetted off, and pellets were dried in a fume hood overnight. Once dried, pellets were resuspended in 100 µl of lysis buffer (50 mM Tris, pH 7.5, 1 mM EDTA, 3 mM DTT, and 1X cOmplete protease inhibitor cocktail [11836145001, *Roche*]) and lysed on a beadbeater for 5 min at room temperature with 100 µl of acid-washed glass beads. Next, 50 µl of 3X SDS buffer (18.75 mM Tris, pH 6.8, 6% β-mercaptoethanol, 30% glycerol, 9% SDS, 0.05% bromophenol blue) was added, and samples were boiled at 95°C for 5 min.

4–8 µl of samples and 3 µl of Precision Plus Protein Dual Color Standard (1610374, *Bio-Rad*) were loaded into 4–12% Bis-Tris Bolt gels (*Thermo Fisher Scientific*) and run at 150 V for 45 min. Protein was then transferred to 0.45 µm nitrocellulose membranes (*Bio-Rad*) with cold 1X Trans-Blot Turbo buffer in a semi-dry transfer apparatus (Trans-Blot Turbo Transfer System, *Bio-Rad*). Membranes were incubated at room temperature for 1 hour in PBS Odyssey Blocking Buffer (927-4000, *LI-COR*) and incubated in primary antibody solutions at 4°C overnight. Membranes were then washed three times in 1X PBS with 0.1% Tween-20 (PBS-T, 5 min per wash) at room temperature before incubating in secondary antibody solutions at room temperature for 2.5 hours. Membranes were washed three times in PBS-T at room temperature prior to imaging with the Odyssey system (*LI-COR Biosciences*).

All primary and secondary antibodies were diluted in PBS Odyssey Buffer with 0.1% Tween-20. Primary antibodies: mouse α-V5 antibody (R960-25, *Thermo Fisher Scientific*) used at a concentration of 1:2,000; rat α-tubulin (MCA78G, *Bio-Rad*) used at a concentration of 1:10,000. Secondary antibodies: goat α-mouse or α-rabbit secondary antibody conjugated to IRDye 800CW used at a concentration of 1:15,000 (926-32213, *LI-COR*); α-rabbit secondary conjugated to IRDye 680RD at a concentration of 1:15,000 (926-68071, *LI-COR*).

Immunoblot quantification was performed by quantifying signals from bands in Image Studio (*LI-COR*). For all blots quantified in this study, raw V5 signal was normalized to raw alpha-tubulin signal. For Hnt1 time course experiments, all normalized Hnt1-3V5 values from timepoints after t = 0 were then normalized to the levels at t = 0 to measure protein turnover.

6.7 Quantification and statistical analysis

Plotting and statistics for all bar charts, column plots, and scatterplots were performed using Prism Graphpad (v9.5.1).

Identification of LUTI escape mutants

Fastq files were aligned to the SacCer3 reference genome with BWA-MEM (H. Li, 2013) and SAMBLASTER (v0.1.24, Faust and Hall, 2014) was used to remove discordant reads. SAMtools (v1.7, Danecek et al., 2021) was used to sort and index BAM files, then GATK (Auwera & O'Connor, 2020) HaplotypeCaller was run on sorted BAM files with '-ERC GVCF' to call variants. Genotyping was performed with GATK GenotypeGVCFs. Output VCF files were split into SNPs and indels with GATK SelectVariants. SNPs were filtered with GATK VariantFiltration "QD < 2.0" --filter-name "QD2" -filter "QUAL < 1000.0" --filter-name "QUAL1000" -filter "SOR > 3.0" --filter-name "SOR3" -filter "FS > 60.0" --filter-name "FS60" -filter "MQ < 40.0" --filter-name "MQ40" -filter "MQRankSum < -12.5" --filter-name "MQRankSum-12.5" -filter "ReadPosRankSum < -8.0" --filter-name "ReadPosRankSum-8" -filter "DP < 10" --filter-name "DP10", while indels were filtered with GATK VariantFiltration "QD < 2.0" --filter-name "QD2" -filter "QUAL < 1000.0" --filter-name "QUAL1000" -filter "FS > 200.0" --filter-name "FS200" -filter "ReadPosRankSum < -20.0" --filter-name "ReadPosRankSum-20" -filter "DP < 10" --filter-name "DP10". Next, a custom Python script was used to filter out reads in which the variant allele represents < 95% of total reads and output the filtered variants in BED format. Finally, variants that were also present in the parental control strain were filtered out using BEDtools subtract (v2.25.0, Quinlan and Hall, 2010). Mutations of interest were confirmed experimentally and tested for dominant/recessive phenotypes by backcrossing mutant strains to the parental control strain, phenotyping diploids and progeny, and performing Sanger-based sequencing to associate genotypes with phenotypes.

mRNA-seq

Hisat2 (v2.1.0, Kim et al., 2019) was used to align reads to the sacCer3 reference genome (v64). Quantification of RNA as transcripts per million (TPM) was done with StringTie (v2.1.6, Pertea et al., 2015). Differential expression analysis was performed using DESeq2 (v1.36.0, Love et al., 2014) using default options. Hierarchical clustering was performed using Cluster3 (de Hoon et al., 2004) and visualized in Treeview (v1.2.0, Saldanha, 2004). TPM values for three biological replicates of each sample were log-adjusted and arrays were normalized in Cluster3 prior to clustering. Hierarchical clustering was performed on (1) genes based on Euclidian distance and (2) arrays using correlation-based similarity metrics. Average linkage was used as the hierarchical clustering method. Spearman heatmaps were produced in Jupyter Notebook (Kluyver et al., 2016) using seaborn (Waskom, 2021) and Matplotlib (Hunter, 2007). Average scores

for Spearman's rank sum correlation coefficient for each pairwise comparison are reported in the text.

TL-seq and identification of TSS^{DIST}/TSS^{PROX} targets

From the sequencing reads, the 3′ Illumina adaptor (AGATCGGAAGAGC) was trimmed using cutadapt with the–*minimum-length* option set to 20 bp (v2.3, Martin, 2011). From the 3′ trimmed output, the 5′ Illumina adaptor (CACTCTGAGCAATACC) was trimmed from reads with cutadapt. To select for reads representing the 5′ end of a transcript, only reads in which the 5′ adaptor was recognized and then trimmed were carried forward. Hisat2 was used to align reads to the sacCer3 reference genome. BAM files were loaded into CAGEr (v2.2.0, Haberle et al., 2015) and the CAGEexp object was created via getCTSS with correctSystematicG = FALSE and removeFirstG = FALSE. Next, reads were normalized by the normalizeTagCount function with method = c("simpleTPM"). TSSs were then clustered with clusterCTSS with the following parameters: threshold = 1, thresholdIsTpm = TRUE, nrPassThreshold = 4, method = "distclu", maxDist = 20, removeSingletons = TRUE, keepSingletonsAbove = 5. Consensus clusters were generated in a three-step process: (1) cumulativeCTSSdistribution was run on tagClusters with useMulticore = T, (2) quantilePositions was run on tagClusters with qLow = 0.1 and qUp = 0.9, and (3) aggregateTagClusters was run with tpmThreshold = 5, qLow = 0.1, qUp = 0.9, maxDist = 50. Consensus clusters were annotated using annotateConsensusClusters with an imported sacCer3 GFF file.

TPM tables from CAGEr-identified CTSS consensus clusters were exported as CSV files. Bed files used for metagene analysis centered on TSS positions were exported with rtracklayer and bedGraph files were exported with rtracklayer for visualization in IGV. Finally, Differential expression analysis was performed on consensus clusters using DESeq2 and results were exported for further analysis. For comparing wild-type samples in the untreated condition with DTT treatment, *SNF2* (n = 2) and *SWI3* (n = 2) wild-type control samples were combined for a total of n = 4 biological replicates per condition. This combination was determined based on genotypic and technical similarity between the wild-type samples ($\rho \geq 0.96$ [untreated] and ≥ 0.98 [DTT]) to improve statistical power and simplify plotting. Lists of TSSs with significant upregulation (adjusted p-value < 0.05) in one or more LUTI escape mutant were curated in Excel and further manual curation was performed to identify sites with transcriptional readthrough. These sites were required to meet two criteria: (1) an upstream initiating transcript that extends through the TSS^{PROX} was visible in direct mRNA-seq reads and (2) the distal TSS was also called as a consensus cluster from CAGEr. Finally, sites that did not exhibit Snf2 binding as indicated by MACS2 peak calling in wild-type cells treated with DTT (see below) were eliminated from further analysis.

ChIP-seq

Spike-in normalization was performed following the SNP-ChIP pipeline (Vale-Silva et al., 2019). First, reads from ChIP and input samples were aligned to a hybrid S288C-SK1 reference genome using Bowtie (v1.2.0, Langmead et al., 2009) with options -q -m 1 -v 0 -p 8 -S. Then, read counts mapping to each chromosome of the SK1 or S288C

sequence were generated with SAMtools idxstats. Tables of read counts were used as input for spike-in normalization factor calculation using the R script published in (Vale-Silva et al., 2019). Supporting code and the S288C-SK1 hybrid reference genome is availble on Github (https://github.com/hochwagenlab/ChIPseq_functions).

Original fastq files were then re-aligned to the sacCer3 reference genome using Bowtie with options -q -p 8 -S. MACS2 (v2.1.1, Zhang et al., 2008) was used to call peaks with SPMR and normalize ChIP signals over input with bdgcmp. The output bedGraph files were then normalized by multiplying all coverage values with the spike-in normalization factor calculated as descibed above. Enrichment of Snf2 at DTT-induced alternative TSSs plotted in Figures 3B and S3A was calculated by averaging values from the normalized bedGraph files in the region between the TSS^{DIST} and TSS^{PROX} for each gene. For plotting enrichment, wild-type control strains *SNF2* and *SWI3* were combined as biological replicates on the bases of genotypic and technical similarity ($\rho \geq 0.98$ [untreated] and ≥ 0.98 [DTT]). Normalized bedGraph files were converted to BigWig format for visualization in IGV and metagene analysis with deeptools (v3.5.1, Ramírez et al., 2016) bedGraphToBigWig. Metagene analysis was performed with deeptools computeMatrix reference-point using bed files corresponding to TSS regions generated from TL-seq analysis (see above) and visualized with plotProfile with --plotType heatmap.

MNase-seq

Alignment and spike-in normalization of MNase reads were performed as described above for ChIP-seq normalization, using undigested gDNA from each sample as "input." Aligned reads were filtered using deeptools alignmentSieve with options --minFragmentLength 130 --maxFragmentLength 170. deeptools bamCoverage was used to generate bedGraph files, which were then multiplied by the spike-in normalization factor for each sample. Normalized bedGraph files were used to calculate nucleosome occupancy for plots in Figures S3D and S6C-D. Again, wild-type *SNF2* and *SWI3* samples were combined as wild-type biological replicates for plotting of nucleosome occupancy based on genotypic and technical similarity ($\rho \geq 0.96$ [untreated] and $\rho \geq 0.93$ [DTT]). Nucleosome fuzziness scores were calculated with DANPOS3 (K. Chen et al., 2013), which also outputs position coordinates. Determination of -1, +1, +2, and +5 nucleosome regions used for analysis in Figures 3I-J and S6D was performed as follows: BEDtools closest was run using a file containing TSS coordinates from TL-seq analysis (see above) and a file containing nucleosome coordinates from wild-type, unstressed cells output from DANPOS3. For the -1 nucleosome, options "-id -t first" were used. For the +1 nucleosome, options "-iu -t last" were used. For nucleosomes downstream of the +1, the previous nucleosome position was used as the reference coordinate file instead of the TSS coordinates (e.g. bedtools closest -a plus1.bed -b all_pos.bed -iu -t last > plus2.bed).

Plotting nucleosome occupancy in the NDR/NFR regions for Figures S3D and S6C was performed by analyzing sum occupancy, as calculated from spike-in normalized bedGraph files, in the region between the -1 and +1 nucleosomes. Averaged fuzziness and occupancy values are plotted for biological replicates (n = 4 for wild type and n = 2 for mutants). For nucleosome occupancy plotting, a cutoff score of 5 for normalized read depth in wild-type was applied. Individual fuzziness scores for the UPR TSS^{DIST}/TSS^{PROX}

targets are reported in Table S2. Normalized bedGraph files were converted to BigWig format for visualization in IGV and metagene analysis with deeptools bedGraphToBigWig. Metagene analyses were performed on BigWig files with deeptools computeMatrix reference-point using BED files corresponding to TSS regions generated from TL-seq analysis (see above) and visualized with plotProfile.

Resource availability

All reagents used in this study are available upon request from the corresponding author. Sequencing data generated in this study are available at NCBI GEO under the accession: GSE229952. The custom code used in filtering of DNA-seq data for LUTI escape mutants is available at: https://github.com/katemorse/LUTI_escape_filtering.git.

References

Arribere, J. A., & Gilbert, W. V. (2013). Roles for transcript leaders in translation and mRNA decay revealed by transcript leader sequencing. *Genome Research*, *23*(6), 977–987. https://doi.org/10.1101/gr.150342.112

Auwera, G. van der, & O'Connor, B. D. (2020). *Genomics in the cloud: Using Docker, GATK, and WDL in Terra* (First edition). O'Reilly Media.

Bai, L., & Morozov, A. V. (2010). Gene regulation by nucleosome positioning. *Trends in Genetics*, *26*(11), 476–483. https://doi.org/10.1016/j.tig.2010.08.003

Batista, P. J., & Chang, H. Y. (2013). Long Noncoding RNAs: Cellular Address Codes in Development and Disease. *Cell*, *152*(6), 1298–1307. https://doi.org/10.1016/j.cell.2013.02.012

Bird, A. J., Gordon, M., Eide, D. J., & Winge, D. R. (2006). Repression of ADH1 and ADH3 during zinc deficiency by Zap1-induced intergenic RNA transcripts. *The EMBO Journal*, *25*(24), 5726–5734. https://doi.org/10.1038/sj.emboj.7601453

Bowman, G. D. (2010). Mechanisms of ATP-dependent nucleosome sliding. *Current Opinion in Structural Biology*, *20*(1), 73–81. https://doi.org/10.1016/j.sbi.2009.12.002

Brar, G. A., Yassour, M., Friedman, N., Regev, A., Ingolia, N. T., & Weissman, J. S. (2012). High-Resolution View of the Yeast Meiotic Program Revealed by Ribosome Profiling. *Science*, *335*(6068), 552–557. https://doi.org/10.1126/science.1215110

Buratowski, S. (2009). Progression through the RNA Polymerase II CTD Cycle. *Molecular Cell*, *36*(4), 541–546. https://doi.org/10.1016/j.molcel.2009.10.019

Carrozza, M. J., Li, B., Florens, L., Suganuma, T., Swanson, S. K., Lee, K. K., Shia, W.-J., Anderson, S., Yates, J., Washburn, M. P., & Workman, J. L. (2005). Histone H3 Methylation by Set2 Directs Deacetylation of Coding Regions by Rpd3S to Suppress Spurious Intragenic Transcription. *Cell*, *123*(4), 581–592. https://doi.org/10.1016/j.cell.2005.10.023

Cenik, B. K., & Shilatifard, A. (2021). COMPASS and SWI/SNF complexes in development and disease. *Nature Reviews. Genetics*, *22*(1), 38–58. https://doi.org/10.1038/s41576-020-0278-0

Chai, B., Huang, J., Cairns, B. R., & Laurent, B. C. (2005). Distinct roles for the RSC and Swi/Snf ATP-dependent chromatin remodelers in DNA double-strand break repair. *Genes & Development*, *19*(14), 1656–1661. https://doi.org/10.1101/gad.1273105

Chandy, M., Gutiérrez, J. L., Prochasson, P., & Workman, J. L. (2006). SWI/SNF Displaces SAGA-Acetylated Nucleosomes. *Eukaryotic Cell*, *5*(10), 1738–1747. https://doi.org/10.1128/EC.00165-06

Chen, J., Tresenrider, A., Chia, M., McSwiggen, D. T., Spedale, G., Jorgensen, V., Liao, H., Werven, F. J. van, & Ünal, E. (2017). Kinetochore inactivation by expression of a repressive mRNA. *ELife*, *6*. https://doi.org/10.7554/eLife.27417

Chen, K., Xi, Y., Pan, X., Li, Z., Kaestner, K., Tyler, J., Dent, S., He, X., & Li, W. (2013). DANPOS: Dynamic analysis of nucleosome position and occupancy by sequencing. *Genome Research*, *23*(2), 341–351. https://doi.org/10.1101/gr.142067.112

Chen, K., Yuan, J., Sia, Y., & Chen, Z. (2023). Mechanism of action of the SWI/SNF family complexes. *Nucleus*, *14*(1), 2165604. https://doi.org/10.1080/19491034.2023.2165604

Cheng, Z., Otto, G. M., Powers, E. N., Keskin, A., Mertins, P., Carr, S. A., Jovanovic, M., & Brar, G. A. (2018). Pervasive, Coordinated Protein-Level Changes Driven by Transcript Isoform Switching during Meiosis. *Cell*, *172*(5), 910-923.e16. https://doi.org/10.1016/j.cell.2018.01.035

Cherry, J. M., Ball, C., Weng, S., Juvik, G., Schmidt, R., Adler, C., Dunn, B., Dwight, S., Riles, L., Mortimer, R. K., & Botstein, D. (1997). Genetic and physical maps of Saccharomyces cerevisiae. *Nature*, *387*(6632 Suppl), 67–73.

Chia, M., Li, C., Marques, S., Pelechano, V., Luscombe, N. M., & van Werven, F. J. (2021). High-resolution analysis of cell-state transitions in yeast suggests widespread transcriptional tuning by alternative starts. *Genome Biology*, *22*(1), 34. https://doi.org/10.1186/s13059-020-02245-3

Chia, M., Tresenrider, A., Chen, J., Spedale, G., Jorgensen, V., Ünal, E., & Werven, F. J. van. (2017). Transcription of a 5' extended mRNA isoform directs dynamic chromatin changes and interference of a downstream promoter. *ELife*, *6*. https://doi.org/10.7554/eLife.27420

Chia, M., & Werven, F. J. van. (2016). Temporal Expression of a Master Regulator Drives Synchronous Sporulation in Budding Yeast. *G3 (Bethesda, Md.)*, *6*(11), 3553–3560. https://doi.org/10.1534/g3.116.034983

Choi, J., Jeon, S., Choi, S., Park, K., & Seong, R. H. (2015). The SWI/SNF chromatin remodeling complex regulates germinal center formation by repressing Blimp-1 expression. *Proceedings of the National Academy of Sciences of the United States of America*, *112*(7), E718-727. https://doi.org/10.1073/pnas.1418592112

Churchman, L. S., & Weissman, J. S. (2011). Nascent transcript sequencing visualizes transcription at nucleotide resolution. *Nature*, *469*(7330), 368–373. https://doi.org/10.1038/nature09652

Cohen, S. M., Chastain, P. D., Rosson, G. B., Groh, B. S., Weissman, B. E., Kaufman, D. G., & Bultman, S. J. (2010). BRG1 co-localizes with DNA replication factors and is required for efficient replication fork progression. *Nucleic Acids Research*, *38*(20), 6906–6919. https://doi.org/10.1093/nar/gkq559

Core, L., & Adelman, K. (2019). Promoter-proximal pausing of RNA polymerase II: A nexus of gene regulation. *Genes & Development*, *33*(15–16), 960–982. https://doi.org/10.1101/gad.325142.119

Corey, L. L., Weirich, C. S., Benjamin, I. J., & Kingston, R. E. (2003). Localized recruitment of a chromatin-remodeling activity by an activator in vivo drives transcriptional elongation. *Genes & Development*, *17*(11), 1392–1401. https://doi.org/10.1101/gad.1071803

Costa, P. J., & Arndt, K. M. (2000). Synthetic lethal interactions suggest a role for the Saccharomyces cerevisiae Rtf1 protein in transcription elongation. *Genetics*, *156*(2), 535–547. https://doi.org/10.1093/genetics/156.2.535

Couvillion, M., Harlen, K. M., Lachance, K. C., Trotta, K. L., Smith, E., Brion, C., Smalec, B. M., & Churchman, L. S. (2022). Transcription elongation is finely tuned by dozens of regulatory factors. *ELife*, *11*, e78944. https://doi.org/10.7554/eLife.78944

Cox, J. S., & Walter, P. (1996). A novel mechanism for regulating activity of a transcription factor that controls the unfolded protein response. *Cell*, *87*(3), 391–404. https://doi.org/10.1016/s0092-8674(00)81360-4

Cruz, C., Della Rosa, M., Krueger, C., Gao, Q., Horkai, D., King, M., Field, L., & Houseley, J. (2018). Tri-methylation of histone H3 lysine 4 facilitates gene expression in ageing cells. *ELife*, *7*, e34081. https://doi.org/10.7554/eLife.34081

Danecek, P., Bonfield, J. K., Liddle, J., Marshall, J., Ohan, V., Pollard, M. O., Whitwham, A., Keane, T., McCarthy, S. A., Davies, R. M., & Li, H. (2021). Twelve years of SAMtools and BCFtools. *GigaScience*, *10*(2), giab008. https://doi.org/10.1093/gigascience/giab008

Dastidar, R. G., Hooda, J., Shah, A., Cao, T. M., Henke, R. M., & Zhang, L. (2012). The nuclear localization of SWI/SNF proteins is subjected to oxygen regulation. *Cell & Bioscience*, *2*(1), 30. https://doi.org/10.1186/2045-3701-2-30

Davie, J. K., & Kane, C. M. (2000). Genetic interactions between TFIIS and the Swi-Snf chromatin-remodeling complex. *Molecular and Cellular Biology*, *20*(16), 5960–5973. https://doi.org/10.1128/MCB.20.16.5960-5973.2000

de Hoon, M. J. L., Imoto, S., Nolan, J., & Miyano, S. (2004). Open source clustering software. *Bioinformatics*, *20*(9), 1453–1454. https://doi.org/10.1093/bioinformatics/bth078

Dechassa, M. L., Sabri, A., Pondugula, S., Kassabov, S. R., Chatterjee, N., Kladde, M. P., & Bartholomew, B. (2010). SWI/SNF Has Intrinsic Nucleosome Disassembly Activity that Is Dependent on Adjacent Nucleosomes. *Molecular Cell*, *38*(4), 590–602. https://doi.org/10.1016/j.molcel.2010.02.040

Dutta, A., Gogol, M., Kim, J.-H., Smolle, M., Venkatesh, S., Gilmore, J., Florens, L., Washburn, M. P., & Workman, J. L. (2014). Swi/Snf dynamics on stress-responsive genes is governed by competitive bromodomain interactions. *Genes & Development*, *28*(20), 2314–2330. https://doi.org/10.1101/gad.243584.114

Dutta, A., Sardiu, M., Gogol, M., Gilmore, J., Zhang, D., Florens, L., Abmayr, S. M., Washburn, M. P., & Workman, J. L. (2017). Composition and Function of Mutant Swi/Snf Complexes. *Cell Reports*, *18*(9), 2124–2134. https://doi.org/10.1016/j.celrep.2017.01.058

Eisenberg, A. R., Higdon, A., Keskin, A., Hodapp, S., Jovanovic, M., & Brar, G. A. (2018). Precise Post-translational Tuning Occurs for Most Protein Complex Components during Meiosis. *Cell Reports*, *25*(13), 3603-3617.e2. https://doi.org/10.1016/j.celrep.2018.12.008

Eisenberg, A. R., Higdon, A. L., Hollerer, I., Fields, A. P., Jungreis, I., Diamond, P. D., Kellis, M., Jovanovic, M., & Brar, G. A. (2020). Translation Initiation Site Profiling Reveals Widespread Synthesis of Non-AUG-Initiated Protein Isoforms in Yeast. *Cell Systems*, *11*(2), 145-160.e5. https://doi.org/10.1016/j.cels.2020.06.011

Faust, G. G., & Hall, I. M. (2014). *SAMBLASTER*: Fast duplicate marking and structural variant read extraction. *Bioinformatics*, *30*(17), 2503–2505. https://doi.org/10.1093/bioinformatics/btu314

Garg, A., Sanchez, A. M., Shuman, S., & Schwer, B. (2018). A long noncoding (lnc)RNA governs expression of the phosphate transporter Pho84 in fission yeast and has cascading effects on the flanking prt lncRNA and pho1 genes. *The Journal of*

Biological Chemistry, *293*(12), 4456–4467. https://doi.org/10.1074/jbc.RA117.001352

Gibson, D. G., Young, L., Chuang, R.-Y., Venter, J. C., Hutchison, C. A., & Smith, H. O. (2009). Enzymatic assembly of DNA molecules up to several hundred kilobases. *Nature Methods*, *6*(5), 343–345. https://doi.org/10.1038/nmeth.1318

Gill, J. K., Maffioletti, A., García-Molinero, V., Stutz, F., & Soudet, J. (2020). Fine Chromatin-Driven Mechanism of Transcription Interference by Antisense Noncoding Transcription. *Cell Reports*, *31*(5), 107612. https://doi.org/10.1016/j.celrep.2020.107612

Gopalakrishnan, R., Marr, S. K., Kingston, R. E., & Winston, F. (2019). A conserved genetic interaction between Spt6 and Set2 regulates H3K36 methylation. *Nucleic Acids Research*, *47*(8), 3888–3903. https://doi.org/10.1093/nar/gkz119

Govind, C. K., Qiu, H., Ginsburg, D. S., Ruan, C., Hofmeyer, K., Hu, C., Swaminathan, V., Workman, J. L., Li, B., & Hinnebusch, A. G. (2010). Phosphorylated Pol II CTD Recruits Multiple HDACs, Including Rpd3C(S), for Methylation-Dependent Deacetylation of ORF Nucleosomes. *Molecular Cell*, *39*(2), 234–246. https://doi.org/10.1016/j.molcel.2010.07.003

Haberle, V., Forrest, A. R. R., Hayashizaki, Y., Carninci, P., & Lenhard, B. (2015). CAGEr: Precise TSS data retrieval and high-resolution promoterome mining for integrative analyses. *Nucleic Acids Research*, *43*(8), e51–e51. https://doi.org/10.1093/nar/gkv054

Hainer, S. J., Pruneski, J. A., Mitchell, R. D., Monteverde, R. M., & Martens, J. A. (2011). Intergenic transcription causes repression by directing nucleosome assembly. *Genes & Development*, *25*(1), 29–40. https://doi.org/10.1101/gad.1975011

Han, Y., Reyes, A. A., Malik, S., & He, Y. (2020). Cryo-EM structure of SWI/SNF complex bound to a nucleosome. *Nature (London)*, *579*(7799), 452–455. https://doi.org/10.1038/s41586-020-2087-1

Hangauer, M. J., Vaughn, I. W., & McManus, M. T. (2013). Pervasive transcription of the human genome produces thousands of previously unidentified long intergenic noncoding RNAs. *PLoS Genetics*, *9*(6), e1003569. https://doi.org/10.1371/journal.pgen.1003569

Hartzog, G. A., Wada, T., Handa, H., & Winston, F. (1998). Evidence that Spt4, Spt5, and Spt6 control transcription elongation by RNA polymerase II in Saccharomyces cerevisiae. *Genes & Development*, *12*(3), 357–369. https://doi.org/10.1101/gad.12.3.357

Hassan, A. H., Awad, S., & Prochasson, P. (2006). The Swi2/Snf2 Bromodomain Is Required for the Displacement of SAGA and the Octamer Transfer of SAGA-acetylated Nucleosomes. *Journal of Biological Chemistry*, *281*(26), 18126–18134. https://doi.org/10.1074/jbc.M602851200

Hennig, B. P., Bendrin, K., Zhou, Y., & Fischer, T. (2012). Chd1 chromatin remodelers maintain nucleosome organization and repress cryptic transcription. *EMBO Reports*, *13*(11), 997–1003. https://doi.org/10.1038/embor.2012.146

Hollerer, I., Barker, J. C., Jorgensen, V., Tresenrider, A., Dugast-Darzacq, C., Chan, L. Y., Darzacq, X., Tjian, R., Ünal, E., & Brar, G. A. (2019). Evidence for an Integrated Gene Repression Mechanism Based on mRNA Isoform Toggling in Human Cells. *G3 (Bethesda, Md.)*, *9*(4), 1045–1053. https://doi.org/10.1534/g3.118.200802

Hunter, J. D. (2007). Matplotlib: A 2D Graphics Environment. *Computing in Science & Engineering*, *9*(3), 90–95. https://doi.org/10.1109/MCSE.2007.55

Hyun, K., Jeon, J., Park, K., & Kim, J. (2017). Writing, erasing and reading histone lysine methylations. *Experimental & Molecular Medicine*, *49*(4), e324–e324. https://doi.org/10.1038/emm.2017.11

Iurlaro, M., Stadler, M. B., Masoni, F., Jagani, Z., Galli, G. G., & Schübeler, D. (2021). Mammalian SWI/SNF continuously restores local accessibility to chromatin. *Nature Genetics*, *53*(3), 279–287. https://doi.org/10.1038/s41588-020-00768-w

Jackson, R. J., Hellen, C. U. T., & Pestova, T. V. (2010). The mechanism of eukaryotic translation initiation and principles of its regulation. *Nature Reviews Molecular Cell Biology*, *11*(2), 113–127. https://doi.org/10.1038/nrm2838

Jansen, A., & Verstrepen, K. J. (2011). Nucleosome Positioning in Saccharomyces cerevisiae. *Microbiology and Molecular Biology Reviews*, *75*(2), 301–320. https://doi.org/10.1128/MMBR.00046-10

Jonkers, I., & Lis, J. T. (2015). Getting up to speed with transcription elongation by RNA polymerase II. *Nature Reviews Molecular Cell Biology*, *16*(3), 167–177. https://doi.org/10.1038/nrm3953

Jorgensen, V., Chen, J., Vander Wende, H., Harris, D. E., McCarthy, A., Breznak, S., Wong-Deyrup, S. W., Chen, Y., Rangan, P., Brar, G. A., Sawyer, E. M., Chan, L. Y., & Ünal, E. (2020). Tunable Transcriptional Interference at the Endogenous Alcohol Dehydrogenase Gene Locus in Drosophila melanogaster. *G3 (Bethesda, Md.)*, *10*(5), 1575–1583. https://doi.org/10.1534/g3.119.400937

Kadoch, C., & Crabtree, G. R. (2015). Mammalian SWI/SNF chromatin remodeling complexes and cancer: Mechanistic insights gained from human genomics. *Science Advances*, *1*(5), e1500447. https://doi.org/10.1126/sciadv.1500447

Kassabov, S. R., Zhang, B., Persinger, J., & Bartholomew, B. (2003). SWI/SNF Unwraps, Slides, and Rewraps the Nucleosome. *Molecular Cell*, *11*(2), 391–403. https://doi.org/10.1016/S1097-2765(03)00039-X

Kim, D., Paggi, J. M., Park, C., Bennett, C., & Salzberg, S. L. (2019). Graph-based genome alignment and genotyping with HISAT2 and HISAT-genotype. *Nature Biotechnology*, *37*(8), 907–915. https://doi.org/10.1038/s41587-019-0201-4

Kim, J. H., Lee, B. B., Oh, Y. M., Zhu, C., Steinmetz, L. M., Lee, Y., Kim, W. K., Lee, S. B., Buratowski, S., & Kim, T. (2016). Modulation of mRNA and lncRNA expression dynamics by the Set2-Rpd3S pathway. *Nature Communications*, *7*, 13534. https://doi.org/10.1038/ncomms13534.

Kim, M., Krogan, N. J., Vasiljeva, L., Rando, O. J., Nedea, E., Greenblatt, J. F., & Buratowski, S. (2004). The yeast Rat1 exonuclease promotes transcription termination by RNA polymerase II. *Nature*, *432*(7016), 517–522. https://doi.org/10.1038/nature03041

Kim, T., Xu, Z., Clauder-Münster, S., Steinmetz, L. M., & Buratowski, S. (2012). Set3 HDAC Mediates Effects of Overlapping Noncoding Transcription on Gene Induction Kinetics. *Cell*, *150*(6), 1158–1169. https://doi.org/10.1016/j.cell.2012.08.016

Kireeva, M. L., Walter, W., Tchernajenko, V., Bondarenko, V., Kashlev, M., & Studitsky, V. M. (2002). Nucleosome Remodeling Induced by RNA Polymerase II. *Molecular Cell*, *9*(3), 541–552. https://doi.org/10.1016/S1097-2765(02)00472-0

Kluyver, T., Ragan-Kelley, B., Pérez, F., Bussonnier, M., Frederic, J., Hamrick, J., Grout, J., Corlay, S., Ivanov, P., Abdalla, S., & Willing, C. (n.d.). *Jupyter Notebooks—A publishing format for reproducible computational workflows*.

Knutson, S. K., Warholic, N. M., Wigle, T. J., Klaus, C. R., Allain, C. J., Raimondi, A., Porter Scott, M., Chesworth, R., Moyer, M. P., Copeland, R. A., Richon, V. M., Pollock, R. M., Kuntz, K. W., & Keilhack, H. (2013). Durable tumor regression in genetically altered malignant rhabdoid tumors by inhibition of methyltransferase EZH2. *Proceedings of the National Academy of Sciences*, *110*(19), 7922–7927. https://doi.org/10.1073/pnas.1303800110

Kornberg, R. D. (2007). The molecular basis of eukaryotic transcription. *Proceedings of the National Academy of Sciences*, *104*(32), 12955–12961. https://doi.org/10.1073/pnas.0704138104

Kubik, S., Bruzzone, M. J., Challal, D., Dreos, R., Mattarocci, S., Bucher, P., Libri, D., & Shore, D. (2019). Opposing chromatin remodelers control transcription initiation frequency and start site selection. *Nature Structural & Molecular Biology*, *26*(8), 744–754. https://doi.org/10.1038/s41594-019-0273-3

Kubik, S., O'Duibhir, E., Jonge, W. J. de, Mattarocci, S., Albert, B., Falcone, J.-L., Bruzzone, M. J., Holstege, F. C. P., & Shore, D. (2018). Sequence-Directed Action of RSC Remodeler and General Regulatory Factors Modulates +1 Nucleosome Position to Facilitate Transcription. *Molecular Cell*, *71*(1), 89-102.e5. https://doi.org/10.1016/j.molcel.2018.05.030

Lagorce, A., Le Berre-Anton, V., Aguilar-Uscanga, B., Martin-Yken, H., Dagkessamanskaia, A., & François, J. (2002). Involvement of GFA1, which encodes glutamine-fructose-6-phosphate amidotransferase, in the activation of the chitin synthesis pathway in response to cell-wall defects in Saccharomyces cerevisiae. *European Journal of Biochemistry*, *269*(6), 1697–1707. https://doi.org/10.1046/j.1432-1327.2002.02814.x

Langmead, B., Trapnell, C., Pop, M., & Salzberg, S. L. (2009). Ultrafast and memory-efficient alignment of short DNA sequences to the human genome. *Genome Biology*, *10*(3), R25. https://doi.org/10.1186/gb-2009-10-3-r25

Laprade, L., Winston, F., & Martens, J. A. (2004). Intergenic transcription is required to repress the Saccharomyces cerevisiae SER3 gene. *Nature*, *429*(6991), 571–574. https://doi.org/10.1038/nature02538

Larschan, E., & Winston, F. (2001). The *S. cerevisiae* SAGA complex functions in vivo as a coactivator for transcriptional activation by Gal4. *Genes & Development*, *15*(15), 1946–1956. https://doi.org/10.1101/gad.911501

Li, H. (n.d.). *Aligning sequence reads, clone sequences and assembly contigs with BWA-MEM*.

Li, M., Xia, X., Tian, Y., Jia, Q., Liu, X., Lu, Y., Li, M., Li, X., & Chen, Z. (2019). Mechanism of DNA translocation underlying chromatin remodelling by Snf2. *Nature*, *567*(7748), 409–413. https://doi.org/10.1038/s41586-019-1029-2

Lindquist, S. (1986). THE HEAT-SHOCK RESPONSE. *Annual Review of Biochemistry*, *55*(1), 1151–1191. https://doi.org/10.1146/annurev.bi.55.070186.005443

Love, M. I., Huber, W., & Anders, S. (2014). Moderated estimation of fold change and dispersion for RNA-seq data with DESeq2. *Genome Biology*, *15*(12), 550. https://doi.org/10.1186/s13059-014-0550-8

Lu, C., & Allis, C. D. (2017). SWI/SNF complex in cancer. *Nature Genetics*, *49*(2), 178–179. https://doi.org/10.1038/ng.3779

Malagon, F., Tong, A. H., Shafer, B. K., & Strathern, J. N. (2004). Genetic interactions of DST1 in Saccharomyces cerevisiae suggest a role of TFIIS in the initiation-elongation transition. *Genetics*, *166*(3), 1215–1227. https://doi.org/10.1534/genetics.166.3.1215

Mallo, M., & Alonso, C. R. (2013). The regulation of Hox gene expression during animal development. *Development*, *140*(19), 3951–3963. https://doi.org/10.1242/dev.068346

Marasco, L. E., & Kornblihtt, A. R. (2023). The physiology of alternative splicing. *Nature Reviews Molecular Cell Biology*, *24*(4), 242–254. https://doi.org/10.1038/s41580-022-00545-z

Martens, J. A., & Winston, F. (2002). Evidence that Swi/Snf directly represses transcription in S. cerevisiae. *Genes & Development*, *16*(17), 2231–2236. https://doi.org/10.1101/gad.1009902

Martens, J. A., Wu, P.-Y. J., & Winston, F. (2005). Regulation of an intergenic transcript controls adjacent gene transcription in Saccharomyces cerevisiae. *Genes & Development*, *19*(22), 2695–2704. https://doi.org/10.1101/gad.1367605

Martin, M. (2011). Cutadapt removes adapter sequences from high-throughput sequencing reads. *EMBnet.Journal*, *17*(1), 10. https://doi.org/10.14806/ej.17.1.200

Mathur, R., Alver, B. H., San Roman, A. K., Wilson, B. G., Wang, X., Agoston, A. T., Park, P. J., Shivdasani, R. A., & Roberts, C. W. M. (2017). ARID1A loss impairs enhancer-mediated gene regulation and drives colon cancer in mice. *Nature Genetics*, *49*(2), 296–302. https://doi.org/10.1038/ng.3744

Mathur, R., & Roberts, C. W. M. (2018). SWI SNF (BAF) Complexes: Guardians of the Epigenome. *Annual Review of Cancer Biology*, *2*(1), 413–427. https://doi.org/10.1146/annurev-cancerbio-030617-050151

Menon, D. U., Shibata, Y., Mu, W., & Magnuson, T. (2019). Mammalian SWI/SNF collaborates with a polycomb-associated protein to regulate male germline transcription in the mouse. *Development (Cambridge, England)*, *146*(19), dev174094. https://doi.org/10.1242/dev.174094

Miller, M. P., Unal, E., Brar, G. A., & Amon, A. (2012). Meiosis I chromosome segregation is established through regulation of microtubule–kinetochore interactions. *ELife*, *1*, e00117. https://doi.org/10.7554/eLife.00117

Moretto, F., Wood, N. E., Kelly, G., Doncic, A., & Werven, F. J. van. (2018). A regulatory circuit of two lncRNAs and a master regulator directs cell fate in yeast. *Nature Communications*, *9*(1), 780–12. https://doi.org/10.1038/s41467-018-03213-z

Morgan, M. A. J., Magnusdottir, E., Kuo, T. C., Tunyaplin, C., Harper, J., Arnold, S. J., Calame, K., Robertson, E. J., & Bikoff, E. K. (2009). Blimp-1/Prdm1 Alternative Promoter Usage during Mouse Development and Plasma Cell Differentiation. *Molecular and Cellular Biology*, *29*(21), 5813–5827. https://doi.org/10.1128/MCB.00670-09

Morimoto, R. I. (1998). Regulation of the heat shock transcriptional response: Cross talk between a family of heat shock factors, molecular chaperones, and negative

regulators. *Genes & Development*, *12*(24), 3788–3796. https://doi.org/10.1101/gad.12.24.3788

Morris, D. R., & Geballe, A. P. (2000). Upstream Open Reading Frames as Regulators of mRNA Translation. *Molecular and Cellular Biology*, *20*(23), 8635–8642. https://doi.org/10.1128/MCB.20.23.8635-8642.2000

Murphy, D. J., Hardy, S., & Engel, D. A. (1999). Human SWI-SNF Component BRG1 Represses Transcription of the c-fos Gene. *Molecular and Cellular Biology*, *19*(4), 2724–2733.

Neely, K. E., Hassan, A. H., Brown, C. E., Howe, L., & Workman, J. L. (2002). Transcription Activator Interactions with Multiple SWI/SNF Subunits. *Molecular and Cellular Biology*, *22*(6), 1615–1625. https://doi.org/10.1128/MCB.22.6.1615-1625.2002

Neigeborn, L., & Carlson, M. (1984). Genes affecting the regulation of SUC2 gene expression by glucose repression in Saccharomyces cerevisiae. *Genetics*, *108*(4), 845–858. https://doi.org/10.1093/genetics/108.4.845

Neil, H., Malabat, C., d'Aubenton-Carafa, Y., Xu, Z., Steinmetz, L. M., & Jacquier, A. (2009). Widespread bidirectional promoters are the major source of cryptic transcripts in yeast. *Nature*, *457*(7232), 1038–1042. https://doi.org/10.1038/nature07747

Nevers, A., Doyen, A., Malabat, C., Néron, B., Kergrohen, T., Jacquier, A., & Badis, G. (2018). Antisense transcriptional interference mediates condition-specific gene repression in budding yeast. *Nucleic Acids Research*, *46*(12), 6009–6025. https://doi.org/10.1093/nar/gky342

Olave, I. A., Reck-Peterson, S. L., & Crabtree, G. R. (2002). Nuclear actin and actin-related proteins in chromatin remodeling. *Annual Review of Biochemistry*, *71*, 755–781. https://doi.org/10.1146/annurev.biochem.71.110601.135507

Ottoz, D. S. M., Rudolf, F., & Stelling, J. (2014). Inducible, tightly regulated and growth condition-independent transcription factor in Saccharomyces cerevisiae. *Nucleic Acids Research*, *42*(17), e130. https://doi.org/10.1093/nar/gku616

Peil, K., Värv, S., Ilves, I., Kristjuhan, K., Jürgens, H., & Kristjuhan, A. (2022). Transcriptional regulator Taf14 binds DNA and is required for the function of transcription factor TFIID in the absence of histone H2A.Z. *The Journal of Biological Chemistry*, *298*(9), 102369. https://doi.org/10.1016/j.jbc.2022.102369

Pelechano, V., Wei, W., & Steinmetz, L. M. (2013). Extensive transcriptional heterogeneity revealed by isoform profiling. *Nature*, *497*(7447), 127–131. https://doi.org/10.1038/nature12121

Pertea, M., Pertea, G. M., Antonescu, C. M., Chang, T.-C., Mendell, J. T., & Salzberg, S. L. (2015). StringTie enables improved reconstruction of a transcriptome from RNA-seq reads. *Nature Biotechnology*, *33*(3), 290–295. https://doi.org/10.1038/nbt.3122

Petrenko, N., Jin, Y., Dong, L., Wong, K. H., & Struhl, K. (2019). Requirements for RNA polymerase II preinitiation complex formation in vivo. *ELife*, *8*, e43654. https://doi.org/10.7554/eLife.43654

Prochasson, P., Neely, K. E., Hassan, A. H., Li, B., & Workman, J. L. (2003). Targeting Activity Is Required for SWI/SNF Function In Vivo and Is Accomplished through

Two Partially Redundant Activator-Interaction Domains. *Molecular Cell*, *12*(4), 983–990. https://doi.org/10.1016/S1097-2765(03)00366-6

Proft, M., & Struhl, K. (2002). Hog1 Kinase Converts the Sko1-Cyc8-Tup1 Repressor Complex into an Activator that Recruits SAGA and SWI/SNF in Response to Osmotic Stress. *Molecular Cell*, *9*(6), 1307–1317. https://doi.org/10.1016/S1097-2765(02)00557-9

Pruneski, J. A., Hainer, S. J., Petrov, K. O., & Martens, J. A. (2011). The Paf1 Complex Represses SER3 Transcription in Saccharomyces cerevisiae by Facilitating Intergenic Transcription-Dependent Nucleosome Occupancy of the SER3 Promoter. *Eukaryotic Cell*, *10*(10), 1283–1294. https://doi.org/10.1128/EC.05141-11

Quinlan, A. R., & Hall, I. M. (2010). BEDTools: A flexible suite of utilities for comparing genomic features. *Bioinformatics*, *26*(6), 841–842. https://doi.org/10.1093/bioinformatics/btq033

Ramírez, F., Ryan, D. P., Grüning, B., Bhardwaj, V., Kilpert, F., Richter, A. S., Heyne, S., Dündar, F., & Manke, T. (2016). deepTools2: A next generation web server for deep-sequencing data analysis. *Nucleic Acids Research*, *44*(W1), W160–W165. https://doi.org/10.1093/nar/gkw257

Rando, O. J., & Winston, F. (2012). Chromatin and Transcription in Yeast. *Genetics*, *190*(2), 351–387. https://doi.org/10.1534/genetics.111.132266

Rawal, Y., Chereji, R. V., Qiu, H., Ananthakrishnan, S., Govind, C. K., Clark, D. J., & Hinnebusch, A. G. (2018). SWI/SNF and RSC cooperate to reposition and evict promoter nucleosomes at highly expressed genes in yeast. *Genes & Development*, *32*(9–10), 695–710. https://doi.org/10.1101/gad.312850.118

Richmond, E., & Peterson, C. L. (1996). Functional Analysis of the DNA-Stimulated ATPase Domain of Yeast SWI2/SNF2. *Nucleic Acids Research*, *24*(19), 3685–3692. https://doi.org/10.1093/nar/24.19.3685

Rinn, J. L., & Chang, H. Y. (2012). Genome Regulation by Long Noncoding RNAs. *Annual Review of Biochemistry*, *81*(1), 145–166. https://doi.org/10.1146/annurev-biochem-051410-092902

Romero, O. A., & Sanchez-Cespedes, M. (2014). The SWI/SNF genetic blockade: Effects in cell differentiation, cancer and developmental diseases. *Oncogene*, *33*(21), 2681–2689. https://doi.org/10.1038/onc.2013.227

Rüegsegger, U., Leber, J. H., & Walter, P. (2001). Block of HAC1 mRNA translation by long-range base pairing is released by cytoplasmic splicing upon induction of the unfolded protein response. *Cell*, *107*(1), 103–114. https://doi.org/10.1016/s0092-8674(01)00505-0

Sahu, R. K., Singh, S., & Tomar, R. S. (2021). The ATP-dependent SWI/SNF and RSC chromatin remodelers cooperatively induce unfolded protein response genes during endoplasmic reticulum stress. *Biochimica et Biophysica Acta (BBA) - Gene Regulatory Mechanisms*, *1864*(11–12), 194748. https://doi.org/10.1016/j.bbagrm.2021.194748

Saldanha, A. J. (2004). Java Treeview—Extensible visualization of microarray data. *Bioinformatics*, *20*(17), 3246–3248. https://doi.org/10.1093/bioinformatics/bth349

Schacherer, J., Ruderfer, D. M., Gresham, D., Dolinski, K., Botstein, D., & Kruglyak, L. (2007). Genome-Wide Analysis of Nucleotide-Level Variation in Commonly Used

Saccharomyces cerevisiae Strains. *PLoS ONE*, *2*(3), e322. https://doi.org/10.1371/journal.pone.0000322

Schwabish, M. A., & Struhl, K. (2007). The Swi/Snf Complex Is Important for Histone Eviction during Transcriptional Activation and RNA Polymerase II Elongation In Vivo. *Molecular and Cellular Biology*, *27*(20), 6987–6995. https://doi.org/10.1128/MCB.00717-07

Sehnal, D., Bittrich, S., Deshpande, M., Svobodová, R., Berka, K., Bazgier, V., Velankar, S., Burley, S. K., Koča, J., & Rose, A. S. (2021). Mol* Viewer: Modern web app for 3D visualization and analysis of large biomolecular structures. *Nucleic Acids Research*, *49*(W1), W431–W437. https://doi.org/10.1093/nar/gkab314

Sen, P., Luo, J., Hada, A., Hailu, S. G., Dechassa, M. L., Persinger, J., Brahma, S., Paul, S., Ranish, J., & Bartholomew, B. (2017). Loss of Snf5 Induces Formation of an Aberrant SWI/SNF Complex. *Cell Reports*, *18*(9), 2135–2147. https://doi.org/10.1016/j.celrep.2017.02.017

Shivaswamy, S., & Iyer, V. R. (2008). Stress-Dependent Dynamics of Global Chromatin Remodeling in Yeast: Dual Role for SWI/SNF in the Heat Shock Stress Response. *Molecular and Cellular Biology*, *28*(7), 2221–2234. https://doi.org/10.1128/MCB.01659-07

Shuman, S. (2020). Transcriptional interference at tandem lncRNA and protein-coding genes: An emerging theme in regulation of cellular nutrient homeostasis. *Nucleic Acids Research*, *48*(15), 8243–8254. https://doi.org/10.1093/nar/gkaa630

Silva, J., Fernandes, R., & Romão, L. (2019). Translational Regulation by Upstream Open Reading Frames and Human Diseases. In L. Romão (Ed.), *The mRNA Metabolism in Human Disease* (Vol. 1157, pp. 99–116). Springer International Publishing. https://doi.org/10.1007/978-3-030-19966-1_5

Smith, C. L., & Peterson, C. L. (2005). A conserved Swi2/Snf2 ATPase motif couples ATP hydrolysis to chromatin remodeling. *Molecular and Cellular Biology*, *25*(14), 5880–5892. https://doi.org/10.1128/MCB.25.14.5880-5892.2005

Smolle, M., Venkatesh, S., Gogol, M. M., Li, H., Zhang, Y., Florens, L., Washburn, M. P., & Workman, J. L. (2012). Chromatin remodelers Isw1 and Chd1 maintain chromatin structure during transcription by preventing histone exchange. *Nature Structural & Molecular Biology*, *19*(9), 884–892. https://doi.org/10.1038/nsmb.2312

Stern, M., Jensen, R., & Herskowitz, I. (1984). Five SWI genes are required for expression of the HO gene in yeast. *Journal of Molecular Biology*, *178*(4), 853–868. https://doi.org/10.1016/0022-2836(84)90315-2

Su, A. J., Yendluri, S. C., & Ünal, E. (2023). *Control of meiotic entry by dual inhibition of a key mitotic transcription factor* [Preprint]. Genetics. https://doi.org/10.1101/2023.03.17.533246

Taggart, J., MacDiarmid, C. W., Haws, S., & Eide, D. J. (2017). Zap1-dependent transcription from an alternative upstream promoter controls translation of RTC4 mRNA in zinc-deficient Saccharomyces cerevisiae. *Molecular Microbiology*, *106*(5), 678–689. https://doi.org/10.1111/mmi.13851

Tatip, S., Taggart, J., Wang, Y., MacDiarmid, C. W., & Eide, D. J. (2020). Changes in transcription start sites of Zap1-regulated genes during zinc deficiency:

Implications for HNT1 gene regulation. *Molecular Microbiology*, *113*(1), 285–296. https://doi.org/10.1111/mmi.14416

Traven, A., Jelicic, B., & Sopta, M. (2006). Yeast Gal4: A transcriptional paradigm revisited. *EMBO Reports*, *7*(5), 496–499. https://doi.org/10.1038/sj.embor.7400679

Tresenrider, A., Chia, M., van Werven, F. J., & Ünal, E. (2022). Long undecoded transcript isoform (LUTI) detection in meiotic budding yeast by direct RNA and transcript leader sequencing. *STAR Protocols*, *3*(1), 101145. https://doi.org/10.1016/j.xpro.2022.101145

Tresenrider, A., Morse, K., Jorgensen, V., Chia, M., Liao, H., van Werven, F. J., & Ünal, E. (2021). Integrated genomic analysis reveals key features of long undecoded transcript isoform-based gene repression. *Molecular Cell*, *81*(10), 2231-2245.e11. https://doi.org/10.1016/j.molcel.2021.03.013

Turegun, B., Baker, R. W., Leschziner, A. E., & Dominguez, R. (2018). Actin-related proteins regulate the RSC chromatin remodeler by weakening intramolecular interactions of the Sth1 ATPase. *Communications Biology*, *1*, 1. https://doi.org/10.1038/s42003-017-0002-6

Vale-Silva, L. A., Markowitz, T. E., & Hochwagen, A. (2019). SNP-ChIP: a versatile and tag-free method to quantify changes in protein binding across the genome. In *BMC Genomics* (Vol. 20, Issue 1). https://doi.org/10.1186/s12864-018-5368-4

Van Dalfsen, K. M., Hodapp, S., Keskin, A., Otto, G. M., Berdan, C. A., Higdon, A., Cheunkarndee, T., Nomura, D. K., Jovanovic, M., & Brar, G. A. (2018). Global Proteome Remodeling during ER Stress Involves Hac1-Driven Expression of Long Undecoded Transcript Isoforms. *Developmental Cell*, *46*(2), 219-235.e8. https://doi.org/10.1016/j.devcel.2018.06.016

Vander Wende, H. M., Gopi, M., Onyundo, M., Medrano, C., Adanlawo, T., & Brar, G. A. (2023). Meiotic resetting of the cellular Sod1 pool is driven by protein aggregation, degradation, and transient LUTI-mediated repression. *The Journal of Cell Biology*, *222*(3), e202206058. https://doi.org/10.1083/jcb.202206058

Venkatesh, S., & Workman, J. L. (2015). Histone exchange, chromatin structure and the regulation of transcription. *Nature Reviews. Molecular Cell Biology*, *16*(3), 178–189. https://doi.org/10.1038/nrm3941

Verdone, L. (2006). Histone acetylation in gene regulation. *Briefings in Functional Genomics and Proteomics*, *5*(3), 209–221. https://doi.org/10.1093/bfgp/ell028

Villegas, V., & Zaphiropoulos, P. (2015). Neighboring Gene Regulation by Antisense Long Non-Coding RNAs. *International Journal of Molecular Sciences*, *16*(2), 3251–3266. https://doi.org/10.3390/ijms16023251

Wang, X., Hou, J., Quedenau, C., & Chen, W. (2016). Pervasive isoform-specific translational regulation via alternative transcription start sites in mammals. *Molecular Systems Biology*, *12*(7), 875. https://doi.org/10.15252/msb.20166941

Wang, X., Lee, R. S., Alver, B. H., Haswell, J. R., Wang, S., Mieczkowski, J., Drier, Y., Gillespie, S. M., Archer, T. C., Wu, J. N., Tzvetkov, E. P., Troisi, E. C., Pomeroy, S. L., Biegel, J. A., Tolstorukov, M. Y., Bernstein, B. E., Park, P. J., & Roberts, C. W. M. (2017). SMARCB1-mediated SWI/SNF complex function is essential for enhancer regulation. *Nature Genetics*, *49*(2), 289–295. https://doi.org/10.1038/ng.3746

Wang, X., Wang, S., Troisi, E. C., Howard, T. P., Haswell, J. R., Wolf, B. K., Hawk, W. H., Ramos, P., Oberlick, E. M., Tzvetkov, E. P., Ross, A., Vazquez, F., Hahn, W. C., Park, P. J., & Roberts, C. W. M. (2019). BRD9 defines a SWI/SNF sub-complex and constitutes a specific vulnerability in malignant rhabdoid tumors. *Nature Communications*, *10*(1), 1881. https://doi.org/10.1038/s41467-019-09891-7

Waskom, M. (2021). seaborn: Statistical data visualization. *Journal of Open Source Software*, *6*(60), 3021. https://doi.org/10.21105/joss.03021

Werven, F. J. van, Neuert, G., Hendrick, N., Lardenois, A., Buratowski, S., Oudenaarden, A. van, Primig, M., & Amon, A. (2012). Transcription of Two Long Noncoding RNAs Mediates Mating-Type Control of Gametogenesis in Budding Yeast. *Cell*, *150*(6), 1170–1181. https://doi.org/10.1016/j.cell.2012.06.049

Xia, X. (2019). Translation Control of HAC1 by Regulation of Splicing in Saccharomyces cerevisiae. *International Journal of Molecular Sciences*, *20*(12), 2860. https://doi.org/10.3390/ijms20122860

Yang, X., Zaurin, R., Beato, M., & Peterson, C. L. (2007). Swi3p controls SWI/SNF assembly and ATP-dependent H2A-H2B displacement. *Nature Structural & Molecular Biology*, *14*(6), 540–547. https://doi.org/10.1038/nsmb1238

Yen, K., Vinayachandran, V., Batta, K., Koerber, R. T., & Pugh, B. F. (2012). Genome-wide Nucleosome Specificity and Directionality of Chromatin Remodelers. *Cell*, *149*(7), 1461–1473. https://doi.org/10.1016/j.cell.2012.04.036

Yudkovsky, N., Logie, C., Hahn, S., & Peterson, C. L. (1999). Recruitment of the SWI/SNF chromatin remodeling complex by transcriptional activators. *Genes & Development*, *13*(18), 2369–2374. https://doi.org/10.1101/gad.13.18.2369

Zhang, Y., Liu, T., Meyer, C. A., Eeckhoute, J., Johnson, D. S., Bernstein, B. E., Nusbaum, C., Myers, R. M., Brown, M., Li, W., & Liu, X. S. (2008). Model-based Analysis of ChIP-Seq (MACS). *Genome Biology*, *9*(9), R137. https://doi.org/10.1186/gb-2008-9-9-r137

Zhu, Y., Rowley, M. J., Böhmdorfer, G., & Wierzbicki, A. T. (2013). A SWI/SNF Chromatin-Remodeling Complex Acts in Noncoding RNA-Mediated Transcriptional Silencing. *Molecular Cell*, *49*(2), 298–309. https://doi.org/10.1016/j.molcel.2012.11.011